Syracuse University

SURFACE

Dissertations - ALL   SURFACE

December 2015

Composite Minimization: Proximity Algorithms and Their Applications

Feishe Chen
Syracuse University

Follow this and additional works at: https://surface.syr.edu/etd

Part of the Physical Sciences and Mathematics Commons

Recommended Citation

Chen, Feishe, "Composite Minimization: Proximity Algorithms and Their Applications" (2015).
Dissertations - ALL. 383.
https://surface.syr.edu/etd/383

ABSTRACT

Image and signal processing problems of practical importance, such as incomplete data recovery and compressed sensing, are often modeled as nonsmooth optimization problems whose objective functions are the sum of two terms, each of which is the composition of a prox-friendly function with a matrix. Therefore, there is a practical need to solve such optimization problems. Besides the nondifferentiability of the objective functions of the associated optimization problems and the larger dimension of the underlying images and signals, the sum of the objective functions is not, in general, prox-friendly, which makes solving the problems challenging. Many algorithms have been proposed in literature to attack these problems by making use of the prox-friendly functions in the problems. However, the efficiency of these algorithms relies heavily on the underlying structures of the matrices, particularly for large scale optimization problems. In this dissertation, we propose a novel algorithmic framework that exploits the availability of the prox-friendly functions, without requiring any structural information of the matrices. This makes our algorithms suitable for large scale optimization problems of interest. We also prove the convergence of the developed algorithms.

This dissertation has three main parts. In part 1, we consider the minimization of functions that are the sum of the compositions of prox-friendly functions with matrices. We characterize the solutions to the associated optimization problems as the solutions of fixed point equations that are formulated in terms of the proximity

operators of the dual of the prox-friendly functions. By making use of the flexibility provided by this characterization, we develop a block Gauss-Seidel iterative scheme for finding a solution to the optimization problem and prove its convergence. We discuss the connection of our developed algorithms with some existing ones and point out the advantages of our proposed scheme.

In part 2, we give a comprehensive study on the computation of the proximity operator of the ℓ_p-norm with $0 \leq p < 1$. Nonconvexity and non-smoothness have been recognized as important features of many optimization problems in image and signal processing. The nonconvex, nonsmooth ℓ_p-regularization has been recognized as an efficient tool to identify the sparsity of wavelet coefficients of an image or signal under investigation. To solve an ℓ_p-regularized optimization problem, the proximity operator of the ℓ_p-norm needs to be computed in an accurate and computationally efficient way. We first study the general properties of the proximity operator of the ℓ_p-norm. Then, we derive the explicit form of the proximity operators of the ℓ_p-norm for $p \in \{0, 1/2, 2/3, 1\}$. Using these explicit forms and the properties of the proximity operator of the ℓ_p-norm, we develop an efficient algorithm to compute the proximity operator of the ℓ_p-norm for any p between 0 and 1.

In part 3, the usefulness of the research results developed in the previous two parts is demonstrated in two types of applications, namely, image restoration and compressed sensing. A comparison with the results from some existing algorithms is also presented. For image restoration, the results developed in part 1 are applied

to solve the ℓ_2-TV and ℓ_1-TV models. The resulting restored images have higher peak signal-to-noise ratios and the developed algorithms require less CPU time than state-of-the-art algorithms. In addition, for compressed sensing applications, our algorithm has smaller ℓ_2- and ℓ_∞-errors and shorter computation times than state-of-the-art algorithms. For compressed sensing with the ℓ_p-regularization, our numerical simulations show smaller ℓ_2- and ℓ_∞-errors than that from the ℓ_0-regularization and ℓ_1-regularization. In summary, our numerical simulations indicate that not only can our developed algorithms be applied to a wide variety of important optimization problems, but also they are more accurate and computationally efficient than state-of-the-art algorithms.

Composite Minimization: Proximity Algorithms and Their Applications

By

Feishe Chen

B.S., Sun Yat-sen University, 2007

M.S., Sun Yat-sen University, 2009

Submitted in partial fulfillment of the requirements for the degree of

Doctor of Philosophy in Mathematics

Syracuse University

December 2015

Acknowledgments

First and foremost, I would like to express my sincerest and deepest appreciation to Professor Lixin Shen. He is the most important reason for why I chose Syracuse University. As an advisor, he has led me to the field of numerical optimization and its applications to image processing and compressed sensing. Along the journey of my Ph.D study, he has provided me with guidance, patience, encouragement and other support. I really appreciate that he has spent a lot of time discussing research projects with me, correcting mistakes from my research manuscripts and teaching me how to write a research paper. As a friend, he shares with me his experience in academia or in life and enlightens me when I come across confusion. I would also like to thank Professor Shen and his wife Mrs. Hongling He for the healthy and organic vegetables every summer.

In addition, I am thankful for my other collaborators, Professor Yuesheng Xu and Dr. Bruce Suter. I really appreciate their effort and insightful comments on every paper we have coauthored. Their interest and passion in research are always inspiring. It is my great honor to have had the chance to discuss research with them

their unconditional and endless support and assistance. I am especially thankful to have my wife Shiqi Chen and my son Ryan Chen, to whom this dissertation is dedicated. They make my life in Syracuse more meaningful.

Contents

Chapter 1

Introduction

1.1 Problem Statement

In this dissertation, we consider minimization problems of the form

$$\min\{f_1(A_1 x) + f_2(A_2 x) : x \in \mathbb{R}^n\}, \tag{1.1}$$

where A_i are $m_i \times n$ matrices for $i = 1, 2$. On the other hand, the functions $f_i : \mathbb{R}^{m_i} \to (-\infty, +\infty]$ may be nonsmooth, but prox-friendly. A function Φ is prox-friendly ([6, 28]) if it allows us to solve, relatively easily, a subproblem of the form

$$\min_w \Phi(w) + \lambda\|w\|^2$$

for $\lambda > 0$.

Model (1.1) admits a wide variety of applications of interest. For instance, the total variation (TV) based ROF denoising model [66], the ℓ_2-TV image deblurring [3,

16, 59, 73], the ℓ_1-TV image restoration [25, 41], the framelet based image deblurring [9, 10], image inpainting [10], the basis pursuit problem in compressed sensing [23], medical imaging [51, 52] and the SVM models [27, 71] in machine learning can be identified as special cases of model (1.1). In particular, we briefly mention three applications that are closed related to our research. For ease of exposition, we view the terms $f_1 \circ A_1$ and $f_2 \circ A_2$ in model (1.1) as the fidelity and regularization terms, respectively.

- *Image deblurring with ℓ_2-fidelity term.* The aim of image deblurring is to recover the underlying image from a noisy blurred image. If the observed image is corrupted by noise of Gaussian type, an ℓ_2-type function is favored for forming fidelity term. As a consequence, f_1 can be chosen as the ℓ_2-norm or the indicator function over an ℓ_2-ball whose radius indicates the noise power. The matrix A_1 is determined by the underlying imaging acquisition system. Various choices are available for the regularization term. For instance, if the tight frame regularizer [31, 65] is chosen, the matrix A_2 corresponds to the frame system and f_2 is simply the ℓ_1-norm. If the total variation [66] is adopted, A_2 is the first order difference operator and f_2 is a variant of the ℓ_1-norm.

- *Image deblurring with ℓ_1-fidelity term.* When a blurred image is contaminated by noise of non-Gaussian type, the ℓ_2-type function is not appropriate for forming fidelity term anymore. It is well accepted that the ℓ_1-norm fidelity term can effectively suppress the effect of outliers that may contaminate a given image,

and is therefore particularly suitable for handling impulsive noise [19, 58]. In this case, the ℓ_1-norm is preferred for function f_1 in the fidelity term. The matrix A_1 and the regularization term $f_2 \circ A_2$ can be chosen as those in the image deblurring model with ℓ_2-fidelity term.

- *Compressed sensing.* The goal in compressed sensing is to recover the underlying sparse signal from incomplete measurements that are, possibly, contaminated by Gaussian white noise. As a consequence, f_1 should be an ℓ_2-type function and A_1 is the associated measurement matrix. Further, in compressed sensing the signal of interest is sparsely represented in a suitably chosen transform domain. Hence, A_2 should be chosen as the transformation matrix associated with the transform. The function f_2 can be chosen to be the ℓ_p-norm with $0 \leq p \leq 1$. A discussion on the ℓ_p-norm as a sparse-promoting function will be given in Chapter 3.

1.2 Previous Work

A number of algorithms have been developed for solving the optimization problem (1.1). Depending whether the proximity operators of $f_1 \circ A_1$ and $f_2 \circ A_2$ are prox-friendly or not, the existing algorithms can be roughly categorized in three groups.

- *Both $f_1 \circ A_1$ and $f_2 \circ A_2$ are prox-friendly.* In this case, splitting algorithms such

as Douglas-Rachford algorithm [35, 50] can be adopted for solving problem (1.1).

- *Either $f_1 \circ A_1$ or $f_2 \circ A_2$ is prox-friendly.* Under this circumstance, the first order prima-dual algorithms recently developed in [15, 22, 36, 42] are suitable for solving problem (1.1).

- *Both f_1 and f_2 are prox-friendly while both $f_1 \circ A_1$ and $f_2 \circ A_2$ are not.* In this context, existing algorithms for the optimization problem (1.1) can be roughly classified into two classes. Class 1 collects the algorithms that produce exact solutions to problem (1.1) while Class 2 collects the algorithms that give approximate solutions to problem (1.1). As we know, the coupling of a prox-friendly function with a matrix causes the difficulty in solving the optimization problem (1.1). This difficulty is tackled in different ways in the development of algorithms in Class 1 and Class 2. In the development of algorithms in Class 1, two auxiliary variables are introduced to substitute the multiplications $A_1 x$ and $A_2 x$ in (1.1). As a result, the unconstrained optimization problem (1.1) is converted to a constrained one. The resulting constrained optimization problem can be solved by the split Bregman method [40], the Augmented Lagrangian method (ALM) [39, 43, 60, 63], or the alternating direction method of multipliers (ADMM) [8, 38]. Methods of the split Bregman, ALM and ADMM have been extensively applied in image restoration [1, 10, 40, 59, 70, 74]. In the development of algorithms in Class 2, some auxiliary variables are introduced, but used in a different way. For example, for the term $f_1(A_1 x)$ in (1.1), we use a

variable u to replace $A_1 x$ in the expression $f_1(A_1 x)$ and then enforce u and $A_1 x$ close measured by the ℓ_2-norm of their difference. As a result, the solutions to the resulting optimization problem are no longer the solutions, but approximate ones, to the optimization problem (1.1). Algorithms designed in this line can be found in [21, 25, 32, 41, 55, 72, 76], and the references therein. A potential shortcoming of the algorithms in Class 2 is that the solutions produced by these algorithms may not possess desirable features as expected from the original problem. Therefore, algorithms in Class 1 are preferred for problem (1.1).

1.3 Motivation

Based upon the review presented above, our research will focus on enriching and complementing the existing algorithms in Class 1. To motivate our work, let us state assumptions on problem (1.1) in the following discussion and point out shortcomings of the existing algorithms in Class 1. We assume that

A1. Both f_1 and f_2 are prox-friendly.

A2. Both $f_1 \circ A_1$ and $f_2 \circ A_2$ are not prox-friendly.

Under these assumptions, we briefly review a general procedure in the development of the existing algorithms in Class 1. By introducing two auxiliary variables u and v, problem (1.1) is converted to the following one

$$\min\{f_1(u) + f_2(v) : A_1 x - u = 0, A_2 x - v = 0, x \in \mathbb{R}^n, u \in \mathbb{R}^{m_1}, v \in \mathbb{R}^{m_2}\}, \quad (1.2)$$

which is an optimization problem with linear constraints. The split Bregman method, ALM or ADMM can be adopted for solving the above constrained optimization problem. With any one of these algorithms, three sequences $\{u^k\}$, $\{v^k\}$, and $\{x^k\}$ are generated. We can observe that the updating u and v are independent in the sense that the updated u^{k+1} is not used in updating v^{k+1}, and vise versa. Therefore, the block Gauss-Seidel acceleration technique will not take effect. In addition, updating u and v may require solving large scale systems that could be expensive if the matrices A_1 and A_2 do not have special structures to exploit.

1.4 Contributions

In this dissertation, we propose a novel algorithmic framework that exploits the availability of the prox-friendly functions, without requiring any structural information of the matrices. This makes our proposed algorithms suitable for large scale optimization problems of interest. We also prove the convergence of the developed algorithms.

Our contributions are as follows:

- We characterize the solutions to the optimization problem (1.1) as the solutions of fixed point equations that are formulated in terms of the proximity operators of the dual of the prox-friendly functions f_1 and f_2. By making use of the flexibility provided by this characterization, we develop a block Gauss-Seidel iterative scheme for finding a solution to the optimization problem and prove its convergence. We discuss the connection of our developed algorithms with

some existing ones and point out the advantages of our proposed scheme.

- We give a comprehensive study on the computation of the proximity operator of the ℓ_p-norm with $0 \leq p < 1$. We first study the general properties of the proximity operator of the ℓ_p norm. Then, we derive the explicit form of the proximity operators of the ℓ_p norm for $p \in \{0, 1/2, 2/3, 1\}$. Using these explicit forms and the properties of the proximity operator of the ℓ_p-norm, we develop an efficient algorithm to compute the proximity operator of the ℓ_p-norm for any p between 0 and 1.

- We demonstrate the usefulness of our research results developed in two types of applications, namely, image restoration and compressed sensing. A comparison with the results from some existing algorithms is also presented. Our numerical simulations indicate that not only can our developed algorithms be applied to a wide variety of important optimization problems, but also they are more accurate and computationally efficient than state-of-the-art algorithms.

Chapter 2

Composite Minimization:

Proximity Algorithms

2.1 Introduction

In this chapter, we focus on convex composite minimization problem with form (1.1), that is,

$$\min\{f_1(A_1 x) + f_2(A_2 x) : x \in \mathbb{R}^n\},$$

where f_1, f_2 are proper, lower semi-continuous, convex functions. We assume that both of f_1 and f_2 are prox-friendly functions but neither of $f_1 \circ A_1$ and $f_2 \circ A_2$ are prox-friendly. We characterize the solutions to composite minimization problem (1.1) as the solutions of fixed point equations that are formulated in terms of the proximity operators of the dual of f_1 and f_2. By making use of the flexibility provided

by this characterization, we develop a block Gauss-Seidel iterative scheme for finding a solution to the optimization problem. We show the proposed algorithm can be implemented efficiently when the functions f_1 and f_2 are prox-friendly. Further, convergence analysis on the proposed algorithm is fulfilled using firm non-expansiveness of the proximity operator. Lastly, connection of the proposed algorithm with the Chambolle and Pock's primal-dual method (CP), the augmented lagrangian method (ALM) and the alternating direction method of multipliers (ADMM) will be discussed.

This chapter is organized in the following manner. In section 2.2, we provide characterization of solutions to general problem (1.1) via sub-differentials and fixed point equations based on proximity operators. In section 2.3, we propose a fixed point algorithm in term of proximity operators. The proposed algorithm employs block Gauss-Seidel acceleration. In section 2.4, convergence analysis on the proposed algorithm is provided in this section. In section 2.5, we discuss the connection of the proposed algorithms with CP[15], ALM and ADMM.

2.2 Fixed Point Characterization

In this section, we shall see that a solution of (1.1) can be characterized by fixed point equations in terms of proximity operators. An iterative algorithm based on the fixed-point equations will be proposed to solve model (1.1).

We begin with introducing our notation and reviewing some concepts from convex analysis. For a vector x in the d-dimensional Euclidean space $\mathbb{R}^d$, we use x_i to denote

the ith component of a vector $x \in \mathbb{R}^d$ for $i = 1, 2, \ldots, d$. We define $\langle x, y \rangle := \sum_{i=1}^{d} x_i y_i$, for $x, y \in \mathbb{R}^d$ the standard inner product in $\mathbb{R}^d$. The ℓ_2-norm induced by the inner product in $\mathbb{R}^d$ is defined as $\| \cdot \| := \sqrt{\langle \cdot, \cdot \rangle}$. For a k by d matrix A, its ℓ_2-norm, denoted by $\|A\|$ is defined by $\|A\| = \max\{\|Ax\| : \|x\| = 1, x \in \mathbb{R}^d\}$. By $\mathbb{S}_+^d$, we denote the set of all d by d symmetric, positive definite matrix. Given a matrix $H \in \mathbb{S}_+^d$, the weighted inner product associated with H in $\mathbb{R}^d$ is defined by $\langle x, y \rangle_H = \langle x, Hy \rangle$ and its induced norm is defined by $\|x\|_H := \sqrt{\langle x, Hx \rangle}$. When H is the identity matrix, its associated weighted inner product and induced norm reduce to the standard inner product and ℓ_2-norm in $\mathbb{R}^d$ respectively. For the Hilbert space $\mathbb{R}^d$, the class of all lower semicontinuous convex functions $\psi : \mathbb{R}^d \to \overline{\mathbb{R}} := (-\infty, +\infty]$ such that $\text{dom } \psi := \{x \in \mathbb{R}^d : \psi(x) < +\infty\} \neq \emptyset$ is denoted by $\Gamma_0(\mathbb{R}^d)$.

We shall provide necessary and sufficient conditions for a solution to model (1.1). To this end, we first recall the definitions of sub-differential and Fenchel conjugate. The subdifferential of $\psi \in \Gamma_0(\mathbb{R}^d)$, denoted by $\partial \psi$, is a set-valued operator and is defined at $x \in \mathbb{R}^d$ as follows:

$$\partial \psi(x) := \{y \in \mathbb{R}^d : \psi(z) \geq \psi(x) + \langle y, z - x \rangle \text{ for all } z \in \mathbb{R}^d\}.$$

For a function $\psi \in \Gamma_0(\mathbb{R}^d)$, the sub-differential $\partial \psi(x)$ is a non-empty compact set for any $x \in \text{dom } \psi$ (see. e.g., [64]). For a function $\psi : \mathbb{R}^d \to [-\infty, +\infty]$, the Fenchel conjugate of ψ at $x \in \mathbb{R}^d$ is

$$\psi^*(x) := \sup\{\langle y, x \rangle - \psi(y) : y \in \mathbb{R}^d\}.$$

For a function $\psi \in \Gamma_0(\mathbb{R}^d)$, its sub-differential and Fenchel conjugate are closely

related. Indeed, for a function $\psi \in \Gamma_0(\mathbb{R}^d)$, one has (see, e.g., [64, Proposition 11.3])

$$y \in \partial\psi(x) \iff x \in \partial\psi^*(y). \tag{2.1}$$

The following result provides a characterization to a solution to problem (1.1).

Proposition 2.1. *Assume that the set of solutions to the optimization problem* (1.1) *is nonempty. A vector* $x \in \mathbb{R}^n$ *is a solution to problem* (1.1) *if and only if there exist vectors* $u \in \mathbb{R}^{m_1}$ *and* $v \in \mathbb{R}^{m_2}$ *such that the following relations hold*

$$A_1 x \in \partial f_1^*(u), \tag{2.2}$$

$$A_2 x \in \partial f_2^*(v), \tag{2.3}$$

$$A_1^\top u + A_2^\top v = 0. \tag{2.4}$$

Proof. Suppose x is a solution to problem (1.1). By Fermat's rule, $0 \in A_1^\top \partial f_1(A_1 x) + A_2^\top \partial f_2(A_2 x)$. Therefore, there exist $u \in \partial f_1(A_1 x)$ and $v \in \partial f_2(A_2 x)$ such that $0 = A_1^\top u + A_2^\top v$, that is, (2.4) holds. Further, by (2.1), $u \in \partial f_1(A_1 x)$ and $v \in \partial f_2(A_2 x)$ yield relations (2.2) and (2.3), respectively.

The above reasoning is reversible. That is, if there exist $u \in \mathbb{R}^{m_1}$ and $v \in \mathbb{R}^{m_2}$ such that (2.2)-(2.4) hold, then x is a solution to problem (1.1). $\square$

Based on Proposition 2.1, we shall provide fixed point equations characterization of a solution to model (1.1) in terms of proximity operator. For a function $\psi \in \Gamma_0(\mathbb{R}^d)$, the proximity operator of ψ with respect to $H \in \mathbb{S}_+^d$, denoted by $\text{prox}_{\psi, H}$, is a mapping from $\mathbb{R}^d$ to itself, defined at $x \in \mathbb{R}^d$ by

$$\text{prox}_{\psi, H}(x) := \text{argmin}\left\{\frac{1}{2}\|u - x\|_H^2 + \psi(u) : u \in \mathbb{R}^d\right\}. \tag{2.5}$$

In particular, we use $\text{prox}_{\lambda\psi}$ for $\text{prox}_{\psi,\frac{1}{\lambda}I}$, where $\lambda > 0$ is a scalar.

The proximity operator is firmly non-expansive [2]. An operator $\mathcal{J} : \mathbb{R}^d \rightarrow \mathbb{R}^d$ is called firmly non-expansive with respect to a given matrix $H \in \mathbb{S}_+^d$ if for all $x, y \in \mathbb{R}^d$

$$\|\mathcal{J}y - \mathcal{J}x\|_H^2 \leq \langle \mathcal{J}y - \mathcal{J}x, y - x \rangle_H.$$

It can be observed that a firm non-expansive operator is also Lipschitz continuous with Lipschitz constant 1. For the sake of completeness, the firm non-expansiveness of proximity operator will be shown in the following lemma.

Lemma 2.2. *Given $\psi \in \Gamma_0(\mathbb{R}^d)$ and $H \in \mathbb{S}_+^d$, the proximity operator $\text{prox}_{\psi,H}$ is firmly non-expansive with respect to H.*

Proof. Let $x, y \in \mathbb{R}^d$. By the definition of proximity operator, we have

$$0 \in \partial\psi(\text{prox}_{\psi,H}(x)) + H(\text{prox}_{\psi,H}(x) - x),$$

and

$$0 \in \partial\psi(\text{prox}_{\psi,H}(y)) + H(\text{prox}_{\psi,H}(y) - y),$$

i.e.,

$$H(x - \text{prox}_{\psi,H}(x)) \in \partial\psi(\text{prox}_{\psi,H}(x)),$$

and

$$H(y - \text{prox}_{\psi,H}(y)) \in \partial\psi(\text{prox}_{\psi,H}(y)).$$

The definition of sub-differential yields

$$\begin{cases} \langle \text{prox}_{\psi,H}(y) - \text{prox}_{\psi,H}(x), H(x - \text{prox}_{\psi,H}(x)) \rangle + \psi(\text{prox}_{\psi,H}(x)) \leq \psi(\text{prox}_{\psi,H}(y)) \\[2mm] \langle \text{prox}_{\psi,H}(x) - \text{prox}_{\psi,H}(y), H(y - \text{prox}_{\psi,H}(y)) \rangle + \psi(\text{prox}_{\psi,H}(y)) \leq \psi(\text{prox}_{\psi,H}(x)) \end{cases}.$$

Adding the above two inequalities and rearranging terms yield

$$\langle \text{prox}_{\psi,H}(y) - \text{prox}_{\psi,H}(x), H(\text{prox}_{\psi,H}(y) - \text{prox}_{\psi,H}(x)) \rangle \leq \langle \text{prox}_{\psi,H}(y) - \text{prox}_{\psi,H}(x), H(y - x) \rangle.$$

This completes the proof. $\qquad\qquad\qquad\qquad\qquad\qquad\qquad\qquad\qquad\qquad\square$

The sub-differential and the proximity operator are closely related. This relation is given in the next proposition.

Proposition 2.3. *Let $\psi \in \Gamma_0(\mathbb{R}^d)$, $H \in \mathbb{S}_+^d$ and $x,\ y \in \mathbb{R}^d$. Then $Hy \in \partial\psi(x)$ if and only if $x = \text{prox}_{\psi,H}(x + y)$.*

Proof. Assume $x = \text{prox}_{\psi,H}(x+y)$. By the definition of proximity operator, we have

$$x = \text{argmin}\left\{\frac{1}{2}\|z - (x + y)\|_H^2 + \psi(z) : z \in \mathbb{R}^d\right\}.$$

Being the minimizer of the objective function above, x satisfies the inclusion $0 \in H(x - (x + y)) + \partial\psi(x)$, i.e., $Hy \in \partial\psi(x)$. This shows that $x = \text{prox}_{\psi,H}(x+y)$ implies $Hy \in \partial\psi(x)$.

The above reasoning is reversible. That is, if $Hy \in \partial\psi(x)$, then $x = \text{prox}_{\psi,H}(x+y)$. This completes the proof. $\qquad\qquad\qquad\qquad\qquad\qquad\qquad\qquad\square$

In particular, if $\psi \in \Gamma_0(\mathbb{R}^d)$ and $\lambda > 0$, by choosing $H = \frac{1}{\lambda}I$ we have from Proposition 2.3 that

$$y \in \partial\psi(x) \Leftrightarrow x = \text{prox}_{\lambda\psi}(x + \lambda y). \tag{2.6}$$

With the relationship between the proximity operator and sub-differential given in Proposition 2.3, an inclusion involving sub-differential can be rephrased as an equation in terms of proximity operator. As a consequence, the characterization of a solution to model (1.1) described in Proposition 2.1 can be rewritten as fixed point equations.

Proposition 2.4. *Assume that the set of solutions to the optimization problem* (1.1) *is nonempty. A vector* $x \in \mathbb{R}^n$ *is a solution to model* (1.1) *if and only if for any positive numbers* $\alpha_1 > 0$, $\alpha_2 > 0$, $\gamma > 0$, *there exist* $u \in \mathbb{R}^{m_1}$ *and* $v \in \mathbb{R}^{m_2}$ *such that the following equations hold*

$$\begin{cases} u = \mathrm{prox}_{\alpha_1 f_1^*} (u + \alpha_1 A_1 x) \\ v = \mathrm{prox}_{\alpha_2 f_2^*} (v + \alpha_2 A_2 x) \\ x = x - \gamma(A_1^\top u + A_2^\top v) \end{cases} . \tag{2.7}$$

Proof. It follows immediately from proposition 2.1 and equation (2.6). $\qquad\square$

We show equations in (2.7) can be rewritten in a compact form. To this end, we denote $\mathbb{H} := \mathbb{R}^{m_1} \times \mathbb{R}^{m_2} \times \mathbb{R}^n$ and define an operator $\mathcal{T} : \mathbb{H} \to \mathbb{H}$ at $\rho = (u, v, x) \in \mathbb{H}$ by

$$\mathcal{T}(\rho) := \left(\mathrm{prox}_{\alpha_1 f_1^*}(u), \mathrm{prox}_{\alpha_2 f_2^*}(v), x \right). \tag{2.8}$$

We next show $\mathcal{T}$ defined in the above is the proximity operator of a new function with respect to a matrix in $\mathbb{S}_+^d$. Actually, define $F : \mathbb{H} \to \mathbb{R}$ at $\rho \in \mathbb{H}$ as

$$F(\rho) := f_1^*(u) + f_2^*(v) \tag{2.9}$$

and a diagonal matrix

$$R := \text{diag}\left(\frac{1}{\alpha_1}I, \frac{1}{\alpha_2}I, \frac{1}{\gamma}I\right), \tag{2.10}$$

where $\frac{1}{\alpha_1}I$, $\frac{1}{\alpha_2}I$, $\frac{1}{\gamma}I$ are $m_1 \times m_1$, $m_2 \times m_2$ and $n \times n$ scaled identity matrices respectively. With this notational preparation, we are ready to show that $\mathcal{T}$ is the proximity operator of F with respect to R.

Lemma 2.5. *For $\mathcal{T}$, F and R defined by (2.8), (2.9) and (2.10), respectively, one has $\mathcal{T} = \text{prox}_{F,R}$.*

Proof. For $\rho = (u, v, x) \in \mathbb{R}^{m_1} \times \mathbb{R}^{m_2} \times \mathbb{R}^n$, by the definition of the proximity operator, we have that

$$
\begin{aligned}
\text{prox}_{F,R}(\rho) &= \text{argmin}\left\{\tfrac{1}{2}\|\rho - \tilde{\rho}\|_R^2 + F(\tilde{\rho}) : \tilde{\rho} = (\tilde{u}, \tilde{v}, \tilde{x}) \in \mathbb{R}^{m_1} \times \mathbb{R}^{m_2} \times \mathbb{R}^n\right\} \\
&= \text{argmin}\left\{\tfrac{1}{2}\|u - \tilde{u}\|_{\frac{1}{\alpha_1}I}^2 + f_1^*(\tilde{u}) + \tfrac{1}{2}\|v - \tilde{v}\|_{\frac{1}{\alpha_2}I}^2 + f_2^*(\tilde{v})\right. \\
&\qquad\qquad \left. + \tfrac{1}{2}\|x - \tilde{x}\|_{\frac{1}{\gamma}I}^2 : (\tilde{u}, \tilde{v}, \tilde{x}) \in \mathbb{R}^{m_1} \times \mathbb{R}^{m_2} \times \mathbb{R}^n\right\} \tag{2.11} \\
&= \left(\text{prox}_{\alpha_1 f_1^*}(u), \text{prox}_{\alpha_1 f_2^*}(v), x\right) \\
&= \mathcal{T}(\rho).
\end{aligned}
$$

$\square$

Lemma 2.2 and Lemma 2.5 ensure that the operator $\mathcal{T}$ is firmly non-expansive with respect to matrix R.

Define

$$S_1 := \begin{bmatrix} 0 & 0 & A_1 \\ 0 & 0 & A_2 \\ -A_1 & -A_2 & 0 \end{bmatrix} \tag{2.12}$$

and

$$E_1 := I + R^{-1}S_1. \tag{2.13}$$

Then for $\rho = (u, v, x) \in \mathbb{R}^{m_1} \times \mathbb{R}^{m_2} \times \mathbb{R}^n$, the characterization in (2.7) can be rewritten in a compact form as

$$\rho = \mathcal{T}(E_1\rho). \tag{2.14}$$

By Proposition 2.4 and equation (2.14), a solution to problem (1.1) is essentially a fixed point of the operator $\mathcal{T} \circ E_1$. Although the operator $\mathcal{T}$ is firmly non-expansive, the composition $\mathcal{T} \circ E_1$ might not be due to the expansivity of E_1. We shall show this in the following lemma.

For a $d \times d$ matrix A, the norm $\|A\|_H$ with respect to an $H \in \mathbb{S}_+^d$ is defined as $\|A\|_H := \max\{\|Ax\|_H : x \in \mathbb{R}^d, \|x\|_H = 1\}$.

Lemma 2.6. *Let R and E_1 be defined in (2.10) and (2.12), respectively. Then $\|E_1\|_R > 1$.*

Proof. Given any $\rho \in \mathbb{H}$ with $\|\rho\|_R = 1$. By the definition of E_1, one have

$$
\begin{aligned}
\|E_1\rho\|_R^2 &= \|(I + R^{-1}S_1)\rho\|_R^2 \\
&= \|\rho\|_R^2 + 2\langle \rho, RR^{-1}S_1\rho \rangle + \|R^{-1}S_1\rho\|_R^2 \\
&= 1 + 2\langle \rho, S_1\rho \rangle + \|R^{-1}S_1\rho\|_R^2.
\end{aligned}
$$

Noting that S_1 is a nonzero skew matrix, we have $\langle \rho, S_1\rho \rangle = 0$ and there exists some $\rho \in \mathbb{H}$ with $\|\rho\|_R = 1$ such that $S_1\rho \neq 0$. Hence $\|E_1\|_R > 1$. $\square$

As a consequence of Lemma 2.6, the sequence $\{\rho_k\}$ generated by $\rho^{k+1} = \mathcal{T}(E_1\rho^k)$ with a given initial guess ρ^0, may not converge. Actually, it was already observed numerically in the application of the L1/TV model for impulsive noise removal [55].

2.3 Fixed Point Algorithm

Our goal is to develop an algorithm that can be used for finding a solution to equation (2.7) (i.e., (2.14)). It was pointed out in the previous section that a simple iterative scheme would not be enough to yield a solution to equation (2.14). Since any solution to problem (1.1) is also a solution to equation (2.7), this motivates us to derive from (2.7) a mathematically equivalent characterization with which an iterative scheme derived from the new characterization will lead to a solution to problem (1.1).

Proposition 2.7. *Assume that the set of solutions to the optimization problem (1.1) is nonempty. A vector $x \in \mathbb{R}^n$ is a solution to (1.1) if and only if for any positive numbers $\alpha_1 > 0$, $\alpha_2 > 0$, $\beta > 0$, $\gamma > 0$, there exist $u \in \mathbb{R}^{m_1}, v \in \mathbb{R}^{m_2}$ such that the following hold*

$$\begin{cases} u = \mathrm{prox}_{\alpha_1 f_1^*}\left(u + \alpha_1 A_1(x - \beta(A_1^\top u + A_2^\top v))\right), \\ v = \mathrm{prox}_{\alpha_2 f_2^*}\left(v + \alpha_2 A_2(x - \beta(A_1^\top u + A_2^\top v))\right), \\ x = x - \gamma(A_1^\top u + A_2^\top v). \end{cases} \tag{2.15}$$

Proof. This follows from Proposition 2.4 and the fact that $A_1^\top u + A_2^\top v = 0$. □

Next, we present an iterative scheme for finding solutions to (2.15). For purposes of comparison, we first include an iterative scheme arising from the characterization

given in (2.7). Beginning with an initial estimate $(u^0, v^0, x^0) \in \mathbb{R}^{m_1} \times \mathbb{R}^{m_2} \times \mathbb{R}^n$, this scheme updates its variables as follows:

$$
\begin{cases}
u^{k+1} = \text{prox}_{\alpha_1 f_1^*} \left(u^k + \alpha_1 A_1 x^k \right) \\
v^{k+1} = \text{prox}_{\alpha_2 f_2^*} \left(v^k + \alpha_2 A_2 x^k \right) \\
x^{k+1} = x^k - \gamma(A_1^\top u^{k+1} + A_2^\top v^{k+1})
\end{cases}
\quad . \tag{2.16}
$$

From the above scheme, we can see that updating u^{k+1} and v^{k+1} can be parallelized in the sense that the computation of v^{k+1} is independent of the update of u^{k+1}. We then turn to the characterization given in Proposition 2.15. Beginning with an initial estimate $(u^0, v^0, x^0) \in \mathbb{R}^{m_1} \times \mathbb{R}^{m_2} \times \mathbb{R}^n$, we propose an iterative scheme arising from (2.15) that iterates as

$$
\begin{cases}
u^{k+1} = \text{prox}_{\alpha_1 f_1^*} \left(u^k + \alpha_1 A_1 \left(x^k - \beta(A_1^\top u^k + A_2^\top v^k) \right) \right) \\
v^{k+1} = \text{prox}_{\alpha_2 f_2^*} \left(v^k + \alpha_2 A_2 \left(x^k - \beta(A_1^\top u^{k+1} + A_2^\top v^k) \right) \right) \\
x^{k+1} = x^k - \gamma(A_1^\top u^{k+1} + A_2^\top v^{k+1})
\end{cases} \tag{2.17}
$$

The above scheme (2.17) shows that the update u^{k+1} can be immediately used in computing v^{k+1}. Algorithm 1 describes an entire procedure for finding a solution to problem (1.1) based on the characterization in Proposition 2.7.

Algorithm 1: Gauss-Seidel Method for Model (1.1)

Input: Initialization: $u^0 \in \mathbb{R}^{m_1}$, $v^0 \in \mathbb{R}^{m_2}$, $x^0 \in \mathbb{R}^n$; α_1, α_2, β, $\gamma > 0$.

Result: x^∞

while *it is not convergent* **do**
  $\quad$ Computing $(u^{k+1}, v^{k+1}, x^{k+1})$ via the iterative scheme (2.17).

In the following section, convergence analysis of Algorithm 1 will be given.

2.4   Convergence Analysis

In this section, our effort will be devoted to the convergence analysis of Algorithm 1.

For easy of exposition, let us introduce the following notation:

$$
S_1 = \begin{bmatrix} 0 & 0 & A_1 \\ 0 & 0 & A_2 \\ -A_1^\top & -A_2^\top & 0 \end{bmatrix},
$$

$$
S_2 = \begin{bmatrix} 0 & -\beta A_1 A_2^\top & 0 \\ -\beta A_2 A_1^\top & 0 & 0 \\ 0 & 0 & 0 \end{bmatrix},
$$

$$
P = \begin{bmatrix} \frac{1}{\alpha_1}I - \beta A_1 A_1^\top & 0 & 0 \\ 0 & \frac{1}{\alpha_2}I - \beta A_2 A_2^\top & 0 \\ 0 & 0 & \frac{1}{\gamma}I \end{bmatrix},
$$

$$
E = R^{-1}(P + S_1 + S_2).
$$

$$(2.18)$$

Then the fixed point equations (2.15) can be rewritten in the compact form

$$
\rho = \mathcal{T}(E\rho), \tag{2.19}
$$

where $\rho = (u, v, x)$ and $\mathcal{T}$ is defined by (2.8).

One useful property of the operator $\mathcal{T} \circ E$ is as follows.

Lemma 2.8. *Let $\mathcal{T}$, R, and E be defined in (2.8), (2.10), and (2.18), respectively. If pairs $(\rho_i, a_i) \in \mathbb{H} \times \mathbb{H}$ with $\rho_i = (u_i, v_i, x_i) \in \mathbb{R}^{m_1} \times \mathbb{R}^{m_1} \times \mathbb{R}^n$, $i = 1, 2$, satisfy*

$$
\rho_i = \mathcal{T}(E\rho_i + R^{-1}a_i), \tag{2.20}
$$

then

$$\langle \rho_2 - \rho_1, a_2 - a_1 \rangle \geq \beta \| A_1^\top (u_2 - u_1) + A_2^\top (v_2 - v_1) \|^2. \qquad (2.21)$$

Proof.   By Lemma 2.5 and the firm non-expansiveness of $\mathcal{T}$,

$$
\begin{aligned}
\| \rho_2 - \rho_1 \|_R^2 \; &= \; \| \mathcal{T}(E\rho_2 + R^{-1} a_2) - \mathcal{T}(E\rho_1 + R^{-1} a_1) \|_R^2 \\[2mm]
&\leq \; \langle \rho_2 - \rho_1, RE(\rho_2 - \rho_1) + a_2 - a_1 \rangle \\[2mm]
&= \; \langle \rho_2 - \rho_1, (P + S_1 + S_2)(\rho_2 - \rho_1) \rangle + \langle \rho_2 - \rho_1, a_2 - a_1 \rangle \\[2mm]
&= \; \langle \rho_2 - \rho_1, P(\rho_2 - \rho_1) \rangle + \langle \rho_2 - \rho_1, S_1(\rho_2 - \rho_1) \rangle \\[2mm]
&\quad + \langle \rho_2 - \rho_1, S_2(\rho_2 - \rho_1) \rangle + \langle \rho_2 - \rho_1, a_2 - a_1 \rangle.
\end{aligned}
$$

Noting that S_1 is a skewed matrix, we have that $\langle \rho_2 - \rho_1, S_1(\rho_2 - \rho_1) \rangle = 0$. Thus,

$$\langle \rho_2 - \rho_1, a_2 - a_1 \rangle \geq \langle \rho_2 - \rho_1, (R - P)(\rho_2 - \rho_1) \rangle - \langle \rho_2 - \rho_1, S_2(\rho_2 - \rho_1) \rangle. \qquad (2.22)$$

By the definitions of P and S_2 given in (2.18), we have that

$$\langle \rho_2 - \rho_1, (R - P)(\rho_2 - \rho_1) \rangle = \beta \| A_1^\top (u_2 - u_1) \|^2 + \beta \| A_2^\top (v_2 - v_1) \|^2$$

and

$$-\langle \rho_2 - \rho_1, S_2(\rho_2 - \rho_1) \rangle = 2\beta \langle A_1^\top (u_2 - u_1), A_2^\top (v_2 - v_1) \rangle.$$

Hence,

$$
\begin{aligned}
\langle \rho_2 - \rho_1, a_2 - a_1 \rangle \; &\geq \; \beta \| A_1^\top (u_2 - u_1) \|^2 + \beta \| A_2^\top (v_2 - v_1) \|^2 \\[2mm]
&\quad + 2\beta \langle A_1^\top (u_2 - u_1), A_2^\top (v_2 - v_1) \rangle \\[2mm]
&= \; \beta \| A_1^\top (u_2 - u_1) + A_2^\top (v_2 - v_1) \|^2
\end{aligned}
$$

This completes the proof. $\square$

For a given $a \in \mathbb{H}$, we define $\mathcal{M} : \mathbb{H} \to \mathbb{H}$ by $\rho = \mathcal{M}(a)$ if (ρ, a) satisfies (2.20).

Lemma 2.8 actually implies the monotonicity of the operator $\mathcal{M}$. We next will discuss

the relation between two consecutive iterations from the iterative scheme (2.17). For

ease of exposition, we introduce the following notation:

$$
L = \begin{bmatrix} 0 & 0 & 0 \\ -\beta A_2 A_1^\top & 0 & 0 \\ -A_1^\top & -A_2^\top & 0 \end{bmatrix},
$$

$$
U = \begin{bmatrix} 0 & -\beta A_1 A_2^\top & A_1 \\ 0 & 0 & A_2 \\ 0 & 0 & 0 \end{bmatrix}.
\tag{2.23}
$$

Then the matrix E defined in (2.18) can be also written as

$$
E = R^{-1}(L + P + U).
$$

As a result, the iterative scheme in (2.17) can be rephrased as

$$
\rho^{k+1} = \mathcal{T}(R^{-1} L \rho^{k+1} + R^{-1}(P + U)\rho^k),
\tag{2.24}
$$

where $\rho^k = (u^k, v^k, x^k)$. One can notice from equation (2.24) that ρ^{k+1} is expressed

in an implicit way, but can be computed explicitly as shown in (2.17).

Lemma 2.9. *Let $\mathcal{T}$, R be defined in (2.8), (2.10) and let L, U be defined in (2.23),*

respectively. For $\rho_i = (u_i, v_i, x_i)$ and $\tilde{\rho}_i = (\tilde{u}_i, \tilde{v}_i, \tilde{x}_i)$, $i = 1, 2$, if the pairs $(\rho_i, \tilde{\rho}_i) \in$

$\mathbb{H} \times \mathbb{H}$ *satisfy*

$$
\rho_i = \mathcal{T}(R^{-1} L \rho_i + R^{-1}(P + U)\tilde{\rho}_i),
\tag{2.25}
$$

then

$$\langle \rho_2 - \rho_1, P[(\rho_2 - \tilde{\rho}_2) - (\rho_1 - \tilde{\rho}_1)] \rangle \leq (\gamma - \beta)\|A_1^\top(u_2 - u_1) + A_2^\top(v_2 - v_1)\|^2$$

$$+ \beta \langle A_1^\top(u_2 - u_1), A_2^\top[(v_2 - \tilde{v}_2) - (v_1 - \tilde{v}_1)] \rangle.$$

Proof. Notice that $\rho_i = \mathcal{T}(E\rho_i + R^{-1}(P+U)(\tilde{\rho}_i - \rho_i))$. By identifying $(P+U)(\tilde{\rho}_i - \rho_i)$ as a_i in Lemma 2.8, we obtain the following

$$\langle \rho_2 - \rho_1, P[(\rho_2 - \tilde{\rho}_2) - (\rho_1 - \tilde{\rho}_1)] \rangle \leq \langle \rho_2 - \rho_1, U[(\tilde{\rho}_2 - \rho_2) - (\tilde{\rho}_1 - \rho_1)] \rangle \tag{2.26}$$

$$- \beta\|A_1^\top(u_2 - u_1) + A_2^\top(v_2 - v_1)\|^2.$$

Substituting U defined in (2.23) back to (2.26) and rearranging the terms yield

$$\langle \rho_2 - \rho_1, P[(\rho_2 - \tilde{\rho}_2) - (\rho_1 - \tilde{\rho}_1)] \rangle \leq \langle A_1^\top(u_2 - u_1), (\tilde{x}_2 - x_2) - (\tilde{x}_1 - x_1) \rangle$$

$$+ \langle A_2^\top(v_2 - v_1), (\tilde{x}_2 - x_2) - (\tilde{x}_1 - x_1) \rangle \tag{2.27}$$

$$- \beta\|A_1^\top(u_2 - u_1) + A_2^\top(v_2 - v_1)\|^2$$

$$+ \beta \langle A_1^\top(u_2 - u_1), A_2^\top[(v_2 - \tilde{v}_2) - (v_1 - \tilde{v}_1)] \rangle$$

Further, equation (2.25) implies $\tilde{x}_i - x_i = \gamma(A_1^\top u_i + A_2^\top v_i)$. Substituting this back in (2.27), we have

$$\langle \rho_2 - \rho_1, P[(\rho_2 - \tilde{\rho}_2) - (\rho_1 - \tilde{\rho}_1)] \rangle \leq \gamma\|A_1^\top(u_2 - u_1) + A_2^\top(v_2 - v_1)\|^2$$

$$- \beta\|A_1^\top(u_2 - u_1) + A_2^\top(v_2 - v_1)\|^2 \tag{2.28}$$

$$+ \beta \langle A_1^\top(u_2 - u_1), A_2^\top[(v_2 - \tilde{v}_2) - (v_1 - \tilde{v}_1)] \rangle$$

which completes the proof. $\qquad\square$

Based on the result in Lemma 2.9, we shall establish a relationship between the sequence $\{(u^k, v^k, x^k) : k \in \mathbb{N}\}$ generated by the iterative scheme (2.17) and $\hat{\rho} =$

$(\hat{u}, \hat{v}, \hat{x})$ that satisfies fixed point equations (2.15). To this end, we introduce

$$
\begin{aligned}
P_1 &= \tfrac{1}{\alpha_1} I - \beta A_1 A_1^\top \\
P_2 &= \tfrac{1}{\alpha_2} I - \beta A_2 A_2^\top
\end{aligned}
\tag{2.29}
$$

Lemma 2.10. *Let $\alpha_1, \alpha_2, \beta, \gamma$ be positive, let $\hat{\rho} = (\hat{u}, \hat{v}, \hat{x}) \in \mathbb{H}$ be a solution to the fixed point equation (2.15), and let $\{\rho^k = (u^k, v^k, x^k) : k \in \mathbb{N}\}$ be the sequence generated by (2.17). If $\|A_1\|^2 < \frac{1}{\alpha_1 \beta}$, $\|A_2\|^2 < \frac{1}{\alpha_2 \beta}$, then the following equation holds:*

$$
(\|\rho^{k+1} - \hat{\rho}\|_P^2 + \beta\|A_2^\top(v^{k+1} - \hat{v})\|^2) - (\|\rho^k - \hat{\rho}\|_P^2 + \beta\|A_2^\top(v^k - \hat{v})\|^2) \le y^k, \tag{2.30}
$$

where

$$
\begin{aligned}
y^k &= -\|u^{k+1} - u^k\|_{P_1}^2 - \|v^{k+1} - v^k\|_{P_2}^2 - (\beta - \gamma)\|A_1^\top u^{k+1} + A_2^\top v^{k+1}\|^2 \\
&\quad - \beta\|A_1^\top u^{k+1} + A_2^\top v^k\|^2.
\end{aligned}
$$

Proof. Since the positive parameters α_1, α_2, β and γ satisfy $\|A_1\|^2 < \frac{1}{\alpha_1 \beta}$, $\|A_2\|^2 < \frac{1}{\alpha_2 \beta}$, the matrices P_1, P_2 in (2.29) and P in (2.18) are symmetric and positive definite. Notice that ρ^{k+1}, ρ^k and $\hat{\rho}$ satisfy

$$
\rho^{k+1} = \mathcal{T}(R^{-1} L \rho^{k+1} + R^{-1}(P + U)\rho^k),
$$

and

$$
\hat{\rho} = \mathcal{T}(R^{-1} L \hat{\rho} + R^{-1}(P + U)\hat{\rho}).
$$

Identifying ρ^{k+1}, ρ^k, and $\hat{\rho}$, respectively, as ρ_2, $\tilde{\rho}_2$, ρ_1 in Lemma 2.9 together with $A_1^\top \hat{u} + A_2 \top \hat{v} = 0$ leads to

$$
\langle \rho^{k+1} - \hat{\rho}, P(\rho^{k+1} - \rho^k) \rangle \le (\gamma - \beta)\|A_1^\top u^{k+1} + A_2^\top v^{k+1}\|^2 + \beta\langle A_1^\top(u^{k+1} - \hat{u}), A_2^\top(v^{k+1} - v^k) \rangle.
$$

Using the identity $2\langle \rho^{k+1} - \hat\rho, P(\rho^{k+1} - \rho^k)\rangle = \|\rho^{k+1} - \hat\rho\|_P^2 - \|\rho^k - \hat\rho\|_P^2 + \|\rho^{k+1} - \rho^k\|_P^2$

and noticing that $\|\rho^{k+1} - \rho^k\|_P^2 = \|u^{k+1} - u^k\|_{P_1}^2 + \|v^{k+1} - v^k\|_{P_2}^2 + \frac{1}{\gamma}\|x^{k+1} - x^k\|^2$ and

$x^{k+1} - x^k = -\gamma(A_1^\top u^{k+1} + A_2^\top v^{k+1})$, we obtain

$$
\begin{aligned}
\|\rho^{k+1} - \hat\rho\|_P^2 - \|\rho^k - \hat\rho\|_P^2 \leq\ & -\|u^{k+1} - u^k\|_{P_1}^2 - \|v^{k+1} - v^k\|_{P_2}^2 \\
& -\tfrac{1}{\gamma}\|x^{k+1} - x^k\|^2 \\
& +2(\gamma - \beta)\|A_1^\top u^{k+1} + A_2^\top v^{k+1}\|^2 \\
& +2\beta\langle A_1^\top(u^{k+1} - \hat u), A_2^\top(v^{k+1} - v^k)\rangle. \\
=\ & -\|u^{k+1} - u^k\|_{P_1}^2 - \|v^{k+1} - v^k\|_{P_2}^2 \\
& +(\gamma - \beta)\|A_1^\top u^{k+1} + A_2^\top v^{k+1}\|^2 \\
& -\beta\|A_1^\top u^{k+1} + A_2^\top v^{k+1}\|^2 \\
& +2\beta\langle A_1^\top(u^{k+1} - \hat u), A_2^\top(v^{k+1} - v^k)\rangle.
\end{aligned}
\tag{2.31}
$$

It can be verified by using $A_1^\top \hat u + A_2^\top \hat v = 0$ that the sum of the last two terms in (2.31)

equals to $-\beta\|A_1^\top u^{k+1} + A_2^\top v^k\|^2 - \beta\|A_2^\top(v^{k+1} - \hat v)\|^2 + \beta\|A_2^\top(v^k - \hat v)\|^2$. Therefore,

$$
(\|\rho^{k+1} - \hat\rho\|_P^2 + \beta\|A_2^\top(v^{k+1} - \hat v)\|^2) - (\|\rho^k - \beta\hat\rho\|_P^2 + \|A_2^\top(v^k - \hat v)\|^2) \leq y^k. \tag{2.32}
$$

This completes the proof of the result. $\qquad\square$

We are ready to prove the convergence of the sequence $\{(u^k, v^k, x^k) : k \in \mathbb{N}\}$

generated by the iterative scheme (2.17).

Theorem 2.11. *Let α_1 , α_2, β, γ be positive numbers and let $\{\rho^k = (u^k, v^k, x^k) : k \in \mathbb{N}\}$ be the sequence generated by scheme (2.17). If $\|A_1\|^2 < \frac{1}{\alpha_1\beta}$, $\|A_2\|^2 < \frac{1}{\alpha_2\beta}$, and $0 < \gamma \leq \beta$, then the sequence $\{(u^k, v^k, x^k) : k \in \mathbb{N}\}$ converges to a triple $\hat\rho = (\hat u, \hat v, \hat x)$, a solution of (2.15).*

Proof. We will show $\{(u^k, v^k, x^k) : k \in \mathbb{N}\}$ converges to a triple $(\hat{u}, \hat{v}, \hat{x})$ satisfying (2.15) by three steps. Firstly, by Lemma 2.10 we show $\{\rho^k = (u^k, v^k, x^k) : k \in \mathbb{N}\}$ is bounded and therefore the sequence has a convergent subsequence. Next, we show that this convergent subsequence converges to a triple $\hat{\rho} = (\hat{u}, \hat{v}, \hat{x})$ satisfying (2.15). Finally, we show the entire sequence $\{(u^k, v^k, x^k) : k \in \mathbb{N}\}$ converges to this triple.

If $\|A_1\|^2 < \frac{1}{\alpha_1 \beta}$, $\|A_2\|^2 < \frac{1}{\alpha_2 \beta}$, then P_1, P_2, P are symmetric and positive definite. If $0 < \gamma \leq \beta$, the values of y^k in Lemma 2.10 is non-positive. Thus, from (2.30) we know that the sequence $\{\|\rho^k - \hat{\rho}\|_P^2 + \|A_2^\top(v^k - \hat{v})\|^2 : k \in \mathbb{N}\}$ is nonincreasing and convergent. This implies the boundedness of the sequence $\{\|\rho^k - \rho\|_P : k \in \mathbb{N}\}$. Therefore, the sequence $\{(u^k, v^k, x^k) : k \in \mathbb{N}\}$ is bounded. Hence, there exists a convergent subsequence $\{(u^{k_i}, v^{k_i}, x^{k_i}) : i \in \mathbb{N}\}$ such that for some vector $(\widetilde{u}, \widetilde{v}, \widetilde{x}) \in \mathbb{R}^{m_1} \times \mathbb{R}^{m_2} \times \mathbb{R}^n$

$$\lim_{i \to \infty}(u^{k_i}, v^{k_i}, x^{k_i}) = (\widetilde{u}, \widetilde{v}, \widetilde{x}) \tag{2.33}$$

We shall show that $(\widetilde{u}, \widetilde{v}, \widetilde{x})$ satisfies the fixed point equations (2.15). Summing (2.30) for k from 1 to infinity, we conclude that

$$\begin{aligned}
\|\rho^1 - \hat{\rho}\|_P^2 + \beta\|A_2^\top v^1 - \hat{v}\|^2 \;\geq\; & \sum_{k=1}^{\infty}\|u^{k+1} - u^k\|_{P_1}^2 + \sum_{k=1}^{\infty}\|v^{k+1} - v^k\|_{P_2}^2 \\
& + \sum_{k=1}^{\infty}(\beta - \gamma)\|A_1^\top u^{k+1} + A_2^\top v^{k+1}\|_2^2
\end{aligned}$$

The convergence of three series in the above inequality yield that

$$
\begin{cases}
\lim_{k \to \infty} u^{k+1} - u^k = 0 \\[2mm]
\lim_{k \to \infty} v^{k+1} - v^k = 0 \\[2mm]
\lim_{k \to \infty} A_1^\top u^{k+1} + A_2^\top v^{k+1} = 0 \\[2mm]
\lim_{k \to \infty} x^{k+1} - x^k = \lim_{k \to \infty} -\gamma (A_1^\top u^{k+1} + A_2^\top v^{k+1}) = 0
\end{cases}
,
$$

which particularly indicates

$$
\begin{cases}
\lim_{i \to \infty} u^{k_i+1} - u^{k_i} = 0 \\[2mm]
\lim_{i \to \infty} v^{k_i+1} - v^{k_i} = 0 \\[2mm]
\lim_{i \to \infty} A_1^\top u^{k_i+1} + A_2^\top v^{k_i+1} = 0 \\[2mm]
\lim_{i \to \infty} x^{k_i+1} - x^{k_i} = 0
\end{cases}
. \tag{2.34}
$$

By (2.33) and (2.34), we have that

$$
\begin{cases}
\lim_{i \to \infty} u^{k_i+1} = \widetilde{u} \\[2mm]
\lim_{i \to \infty} v^{k_i+1} = \widetilde{v} \\[2mm]
\lim_{i \to \infty} x^{k_i+1} = \widetilde{x}
\end{cases}
\tag{2.35}
$$

In (2.17), the involved proximity operators and matrices are continuous operators.

Equations (2.33) and (2.35) imply that $(\widetilde{u}, \widetilde{v}, \widetilde{x})$ satisfies (2.15).

Now, let us take $(\hat{u}, \hat{v}, \hat{x}) = (\widetilde{u}, \widetilde{v}, \widetilde{x})$. Then from (2.33) we have that

$$
\lim_{i \to \infty} \left(\|\rho^{k_i} - \hat{\rho}\|_P^2 + \beta \|A_2^\top (v^{k_i} - \hat{v})\|^2 \right) = 0.
$$

The monotonicity and convergence of the sequence $\{\|\rho^k - \hat{\rho}\|_P^2 + \beta \|A_2^\top (v^k - \hat{v})\|^2 :$ $k \in \mathbb{N}\}$ imply that

$$
\lim_{k \to \infty} \left(\|\rho^k - \hat{\rho}\|_P^2 + \beta \|A_2^\top (v^k - \hat{v})\|^2 \right) = 0.
$$

Thus, the sequence $\{\rho^k = (u^k, v^k, x^k) : k \in \mathbb{N}\}$ converges to a triple $\hat{\rho} = (\hat{u}, \hat{v}, \hat{x})$ satisfying (2.15). This completes the proof of this theorem. $\qquad\square$

2.5 Connections with Existing Algorithms

In this section, we point out the connections of our proposed algorithm with several well-known methods. Specifically, we would explore the connection of the proposed algorithm with Chambolle and Pock's (CP) Primal-Dual method, Augmented Lagrangian Method (ALM) and Alternating Direction Method of Multipliers (ADMM).

To this end, we first consider a degenerated form of Algorithm 1 without Gauss-Seidel acceleration between u and v and with equal parameters $\alpha_1 = \alpha_2 = \alpha$. This degenerated form is presented in Algorithm 2.

Algorithm 2: Degenerated form of Algorithm 1

Input: Initialization: $u^0 \in \mathbb{R}^{m_1}$, $v^0 \in \mathbb{R}^{m_2}$, $x^0 \in \mathbb{R}^n$; parameters α, β, γ.

Result: x^∞

while *it is not convergent* **do**

$$
\begin{cases}
u^{k+1} = \text{prox}_{\alpha f_1^*}\Big(u^k + \alpha A_1\big(x^k - \beta(A_1^\top u^k + A_2^\top v^k)\big)\Big) \\
v^{k+1} = \text{prox}_{\alpha f_2^*}\Big(v^k + \alpha A_2\big(x^k - \beta(A_1^\top u^k + A_2^\top v^k)\big)\Big) \\
x^{k+1} = x^k - \gamma(A_1^\top u^{k+1} + A_2^\top v^{k+1})
\end{cases}
\tag{2.36}
$$

By letting

$$w^k := (u^k; v^k), \quad A := \begin{bmatrix} A_1 \\ A_2 \end{bmatrix}, \quad \text{and} \quad f^*(w) := f_1^*(u) + f_2^*(v),$$

we can rewrite (2.36) in a more compact form

$$\begin{cases} w^{k+1} = \text{prox}_{\alpha f^*}\left(w^k + \alpha A(x^k - \beta A^\top w^k)\right) \\ x^{k+1} = x^k - \gamma A^\top w^{k+1} \end{cases}. \tag{2.37}$$

In the meantime, the fixed point equations corresponding to scheme (2.37) have the following form

$$\begin{cases} w = \text{prox}_{\alpha f^*}\left(w + \alpha A(x - \beta A^\top w)\right) \\ x = x - \gamma A^\top w \end{cases}. \tag{2.38}$$

The fixed point equations (2.38) characterize a solution x to the following minimization problem

$$\min\{f(Ax) : x \in \mathbb{R}^n\}, \tag{2.39}$$

where $f(w)$ is defined by $f(w) := f_1(u) + f_2(v)$.

Next, we will show that we can specify scheme (2.37) as a special case of scheme (2.17) and therefore the convergence of scheme (2.37) follows automatically. To cast scheme (2.37) into scheme (2.17), we let

$$u = w, \ f_1^* = f^*, \ f_2^* = 0, \ A_1 = A, \ A_2 = 0, \ \alpha_1 = \alpha \tag{2.40}$$

in scheme (2.17). For such the choice of those quantities, we are able to rewrite

scheme (2.17) as

$$
\begin{cases}
w^{k+1} = \text{prox}_{\alpha f^*}\Big(w^k + \alpha A\big(x^k - \beta(A^\top w^k)\big)\Big) \\[2mm]
v^{k+1} = v^k \\[2mm]
x^{k+1} = x^k - \gamma(A^\top w^{k+1})
\end{cases}
, \qquad (2.41)
$$

from which one can notice that sequence $\{v^k : k \in \mathbb{N}\}$ is a constant vector sequence. By ignoring the trivial step involving v^{k+1}, scheme (2.41) becomes scheme (2.37).

Lemma 2.12. *Let α, β, γ be positive, let $\hat{\rho} = (\hat{w}, \hat{x}) \in \mathbb{H}$ satisfy the fixed point equations (2.38), and let $\{\rho^k = (w^k, x^k) : k \in \mathbb{N}\}$ be the sequence generated by (2.37). Set*

$$
Q := \frac{1}{\alpha} I - \beta A A^\top, \ \ P := \begin{bmatrix} Q & \\ & \frac{1}{\gamma} I \end{bmatrix}.
$$

If $\|A\|^2 < \frac{1}{\alpha\beta}$, then

$$
\|\rho^{k+1} - \hat{\rho}\|_P^2 - \|\rho^k - \hat{\rho}\|_P^2 \le -\|w^{k+1} - w^k\|_Q - (2\beta - \gamma)\|A^\top(w^{k+1} - \hat{w})\|^2. \quad (2.42)
$$

Proof. This is an immediate result of Lemma 2.10 by specifying corresponding quantities as in (2.40) and noticing that $v^{k+1} = v^k$ for such the choice of those quantities. $\square$

With Lemma 2.12, we can prove our result on the convergence of the sequence $\{(w^k, x^k) : k \in \mathbb{N}\}$ generated by scheme (2.37).

Theorem 2.13. *Let α, β, γ be positive, let $\hat{\rho} = (\hat{w}, \hat{x}) \in \mathbb{H}$ satisfy the fixed point equations (2.38), and let $\{\rho^k = (w^k, x^k) : k \in \mathbb{N}\}$ be the sequence generated by (2.37). If $\|A\|^2 < \frac{1}{\alpha\beta}$ and $0 < \gamma \le 2\beta$ then the sequence $\{(w^k, x^k) : k \in \mathbb{N}\}$ converges to a pair $(\hat{w}, \hat{x})$ satisfying (2.38).*

Proof. It follows the proof of Theorem 2.11 by specifying corresponding quantities in scheme (2.17) as in (2.40) and using Lemma 2.12. $\qquad\square$

To guarantee convergence, it is necessary for Algorithm 1 that $0 < \alpha_1\beta < \frac{1}{\|A_1\|^2}$ and $0 < \alpha_2\beta < \frac{1}{\|A_2\|^2}$, for Algorithm 2 that $0 < \alpha\beta < \frac{1}{\|[A_1;A_2]\|^2}$. It can be noticed that $\max\{\|A_1\|^2, \|A_2\|^2\} \leq \|[A_1;A_2]\|^2$, which implies $\min\{\frac{1}{\|A_1\|^2}, \frac{1}{\|A_2\|^2}\} \geq \frac{1}{\|[A_1;A_2]\|^2}$. Hence, more flexibility exhibits for the choice of α_1, α_2, β in Algorithm 1 than for the choice of α, β in Algorithm 2.

2.5.1   Connection with Chambolle and Pock's Algorithm

First of all, let us review Chambolle and Pock's (CP) algorithm [15] for solving the following optimization problem

$$\min\{f(Ax) + g(x) : x \in \mathbb{R}^n\}, \tag{2.43}$$

where $f \in \Gamma_0(\mathbb{R}^m)$, $g \in \Gamma_0(\mathbb{R}^n)$, and A is a matrix of size $m \times n$. We assume that model (2.43) has a minimizer. The CP algorithm proposed in [15] for model (2.43) can be written as

$$\begin{cases} w^{k+1} = \text{prox}_{\sigma f^*}(w^k + \sigma A\bar{x}^k), \\ x^{k+1} = \text{prox}_{\tau g}(x^k - \tau A^\top w^{k+1}), \\ \bar{x}^{k+1} = 2x^{k+1} - x^k. \end{cases} \tag{2.44}$$

For any initial guess $(x^0, \bar{x}^0, w^0) \in \mathbb{R}^n \times \mathbb{R}^n \times \mathbb{R}^m$, the sequence $\{(x^k, w^k) : k \in \mathbb{N}\}$ converges as long as $0 < \sigma\tau < \|A\|^{-2}$.

In particular, when we set $g = 0$, a direct computation shows that $\text{prox}_{\tau g}$ is the identity operator for any $\tau > 0$. Set $\alpha = \sigma$ and $\beta = 2\tau$. Accordingly, the general CP method in (2.44) becomes

$$
\begin{cases}
w^{k+1} = \text{prox}_{\alpha f^*} \left(w^k + \alpha A \left(x^{k-1} - \beta A^\top w^k \right) \right), \\
x^{k+1} = x^k - \frac{\beta}{2} A^\top w^{k+1}.
\end{cases}
\tag{2.45}
$$

On the other hand, when we set $g = 0$, model (2.43) reduces to model (2.39). Our algorithm for model (2.39) is presented in scheme (2.37).

Therefore, by comparing the CP algorithm and the scheme (2.37) for model (2.39), we can see that the CP algorithm uses x^{k-1} while the scheme (2.37) uses x^k in the computation of w^{k+1}. Further, the step size of the CP algorithm for updating x^{k+1} is fixed as $\frac{\beta}{2}$ while it can be any number in $(0, 2\beta]$ for the scheme (2.37). Although, the relation $0 < \alpha\beta < 2\|A\|^{-2}$ is required for the CP algorithm while the relation $0 < \alpha\beta < \|A\|^{-2}$ is needed for the scheme (2.37), for a fixed α, we can choose the step size for the scheme (2.37) twice bigger than that for the CP algorithm.

2.5.2 Connection with Augmented Lagrangian Methods

As discussed earlier, a reduced iterative scheme (2.36) from Algorithm 1 can be written in a compact form of (2.37). Notice that the first step involving the proximity operator $\text{prox}_{\alpha f^*}$ is equivalent to find the minimizer of a minimization problem. One

can verify that (2.37) is equivalent to the following iterative scheme

$$
\begin{cases}
w^{k+1} = \operatorname{argmin}\left\{f^*(w) - \langle x^k, A^\top w\rangle + \frac{\beta}{2}\|A^\top w\|^2 + \frac{1}{2}\|w - w^k\|_Q^2 : w \in \mathbb{R}^m\right\} \\[2mm]
x^{k+1} = x^k - \gamma A^\top w^{k+1}
\end{cases}
\tag{2.46}
$$

where $Q = \frac{1}{\alpha}I - \beta AA^\top$ is a positive definite matrix. The condition $\alpha\beta < \frac{1}{\|A\|_2^2}$ ensures the positive definiteness of Q. In the literature of nonlinear programming [5], augmented Lagrangian methods (ALMs) are often used to convert a constrained optimization problem to an unconstrained one by adding the objective function a penalty term associated with the constraints. If we choose $Q = 0$ and $\gamma = \beta$ in (2.46), it reduces to the augmented Lagrangian method:

$$
\begin{cases}
w^{k+1} = \operatorname{argmin}\{f^*(w) - \langle x^k, A^\top w\rangle + \frac{\beta}{2}\|A^\top w\|^2 : w \in \mathbb{R}^m\} \\[2mm]
x^{k+1} = x^k - \beta A^\top w^{k+1}
\end{cases}
\tag{2.47}
$$

Even though we can assume that the proximity operator of f has a closed form, there is lack of an effective way to update w^{k+1} in (2.47) when A is not the identity matrix. However, the vector w^{k+1} in the scheme (2.46) can be effectively updated once a proper Q is chosen. This essentially illustrates that Algorithm 2 is superior to the ALM from the numerical implementation point of view.

2.5.3 Connection with Alternating Direction Method of Multipliers

Similarly, the iterative scheme (2.17) in Algorithm 1 can be cast as a special case of the following scheme

$$\begin{cases} u^{k+1} = \operatorname{argmin}\{f_1^*(u) + f_2^*(v^k) - \langle x^k, A_1^\top u + A_2^\top v^k \rangle \\ \qquad\qquad + \frac{\beta}{2}\|A_1^\top u + A_2^\top v^k\|^2 + \frac{1}{2}\|u - u^k\|_{Q_1}^2 : u \in \mathbb{R}^{m_1}\} \\ v^{k+1} = \operatorname{argmin}\{f_1^*(u^{k+1}) + f_2^*(v) - \langle x^k, A_1^\top u^{k+1} + A_2^\top v \rangle \\ \qquad\qquad + \frac{\beta}{2}\|A_1^\top u^{k+1} + A_2^\top v\|^2 + \frac{1}{2}\|v - v^k\|_{Q_2}^2 : v \in \mathbb{R}^{m_2}\} \\ x^{k+1} = x^k - \gamma(A_1^\top u^{k+1} + A_2^\top v^{k+1}) \end{cases} \qquad (2.48)$$

where $Q_1 = \frac{1}{\alpha_1}I - \beta A_1 A_1^\top$, $Q_2 = \frac{1}{\alpha_2}I - \beta A_2 A_2^\top$ are positive definite matrices. The positive definiteness of Q_1 and Q_2 will be guaranteed under the conditions $0 < \alpha_1\beta < \frac{1}{\|A_1\|^2}$ and $0 < \alpha_2\beta < \frac{1}{\|A_2\|^2}$. If Q_1 and Q_2 are taken as zero matrices and $\gamma = \beta$, the scheme (2.48) reduces to the alternating direction method of multipliers (ADMM):

$$\begin{cases} u^{k+1} = \operatorname{argmin}\{f_1^*(u) + f_2^*(v^k) - \langle x^k, A_1^\top u + A_2^\top v^k \rangle \\ \qquad\qquad + \frac{\beta}{2}\|A_1^\top u + A_2^\top v^k\|^2 : u \in \mathbb{R}^{m_1}\} \\ v^{k+1} = \operatorname{argmin}\{f_1^*(u^{k+1}) + f_2^*(v) - \langle x^k, A_1^\top u^{k+1} + A_2^\top v \rangle \cdot \\ \qquad\qquad + \frac{\beta}{2}\|A_1^\top u^{k+1} + A_2^\top v\|^2 : v \in \mathbb{R}^{m_2}\} \\ x^{k+1} = x^k - \beta(A_1^\top u^{k+1} + A_2^\top v^{k+1}) \end{cases} \qquad (2.49)$$

Similar to what we have observed for the ALM, solving the two optimization problems in (2.49) is still challenging in general when both A_1 and A_2 are not the identity matrix. However, the vectors u^{k+1} and v^{k+1} in the scheme (2.48) can be effectively

updated once Q_1 and Q_2 are properly chosen. Hence our Algorithm 1 is superior to the ADMM from the numerical implementation point of view.

Chapter 3

Computing the Proximity

Operator of the ℓ_p-Norm

3.1 Introduction

The notion of sparsity has been widely explored recently in compressed sensing, matrix completion, machine learning, and image recovery. Typically, the sparsity of a signal is characterized by the ℓ_0-norm of the signal that is essentially the number of non-zero components in the signal. Due to the non-convexity, it is often relaxed to the ℓ_1-norm which is convex and can promote sparsity as well. Seeking a solution to a problem via the ℓ_1-regularization has become the focus of attention of a massive volume of research in the context of compressed sensing. The usefulness of the ℓ_0- and ℓ_1-norm in sparsity-aware applications comes from the fact that their proximity

operators have explicit forms and can be implemented easily. The concrete forms of the proximity operators of the ℓ_0- and ℓ_1-norm will be given in the next section. The proximity operator, introduced early in [56], is a useful and convenient tool in characterizing the solutions of optimization problems and developing iterative algorithms for finding them. Some recent applications of the proximity operator in signal and image processing can be found in [21, 29, 47, 45, 48, 49, 54, 61, 62, 67, 68] and the references therein.

Our main interest is to study the proximity operator of the ℓ_p-norm with $0 < p < 1$. The ℓ_p-regularization has been introduced in existing work. In [7], the ℓ_p-regularization was introduced for image reconstruction. In [53, 57, 69], the ℓ_p-norm is naturally involved in statistically modeling the wavelet coefficients of an image. Particularly, a popular generalized Gaussian distribution (GGD) of the form $P(x) \sim \exp(-|x/s|^p)$ is often adopted with the value for p typically being in the range of $[1/2, 1]$. Therefore, it is highly needed to compute the proximity operator of the ℓ_p-norm with $0 < p < 1$.

Unfortunately, the proximity operator of the ℓ_p-norm with $0 < p < 1$ does not have an explicit form except a few of p values. In [44], finding the proximity operator of the ℓ_p-norm for $p = 1/2$ (or $2/3$) is formulated as finding a root of a corresponding cubic (or quartic) polynomial. In the approach proposed in [44], all the roots of the polynomial should be computed and then compared to select a proper root by some discriminate conditions. Recently, the closed-form of the proximity operator of the ℓ_p-

norm was reported in [75] for $p = 1/2$ and in [14] for $p = 2/3$. Applications in image deconvolution with ℓ_p-regularization ($p = 1/2, 2/3$) were also reported in [14, 44, 75].

For our contribution, we have a systematic study on the computation of the proximity operator of the ℓ_p norm with $0 < p < 1$. The properties of the proximity operator of the ℓ_p norm are presented by analyzing the objective function of optimization problem associated with the proximity operator. By using these properties, the closed-form of the proximity operator of the ℓ_p ($p = 1/2, 2/3$) norm is given accompanying with an alternative, but simple, proof in comparison with that given in [14, 75]. For computing the proximity operator of the ℓ_p norm with p not being 0, 1/2, 2/3, or 1, we need to solve a nonlinear equation associated with the proximity operator. We propose to use Newton's method to solve this equation. To make Newton's method efficiently, the initial estimate for Newton's method requires to be very close to the true solution of the equation. We suggest a way to locate this initial estimate by exploiting the availability of the proximity operators of the ℓ_0-, $\ell_{1/2}$-, $\ell_{2/3}$-, and ℓ_1-norm.

The outline of this part is as follows. In section 3.2 we present the properties of the proximity operator of the ℓ_p-norm with $0 < p < 1$. In section 3.3, we give the explicit forms of the proximity operator of the ℓ_p-norm for $p = 1/2$ and $p = 2/3$. In section 3.4, we apply Newton's method to develop a numerical algorithm to compute the proximity operator of the ℓ_p-norm for $0 < p < 1$.

3.2 Properties of the Proximity Operator of the ℓ_p-Norm

For a vector $x = (x_1, \ldots, x_d)^\top$ in $\mathbb{R}^d$, its ℓ_0-norm $\|x\|_0$ is simply the number of nonzero entries in x and its ℓ_p-norm for $p > 0$ is defined by $\|x\|_p := \left(\sum_{i=1}^d |x_i|^p \right)^{1/p}$. Note that $\|\cdot\|_p$ is only a quasi-norm for $0 < p < 1$. The proximity operator of the ℓ_p-norm with index $\mu > 0$ at $x \in \mathbb{R}^d$ is a set-valued operator from $\mathbb{R}^d \to 2^{\mathbb{R}^d}$, with $2^{\mathbb{R}^d}$ denoting the collection of all sets of vectors in $\mathbb{R}^d$, and is defined as

$$\text{prox}_{\mu\|\cdot\|_p^p}(x) := \underset{u \in \mathbb{R}^d}{\text{argmin}} \left\{ \mu\|u\|_p^p + \frac{1}{2}\|u - x\|_2^2 \right\}. \tag{3.1}$$

Here, $\|\cdot\|_0^0$ should be understood as $\|\cdot\|_0$ when $p = 0$. By the definition of the proximity operator, we have that

$$\text{prox}_{\mu\|\cdot\|_p^p}(x) = \text{prox}_{\mu|\cdot|^p}(x_1) \times \cdots \times \text{prox}_{\mu|\cdot|^p}(x_d), \tag{3.2}$$

for $x \in \mathbb{R}^d$. Therefore, in order to compute the proximity operator of the ℓ_p-norm we only need to compute $\text{prox}_{\mu|\cdot|^p}$ the proximity operator of the function $|\cdot|^p$ in $\mathbb{R}$. To simplify our notation in the rest of discussion, we set

$$\mathcal{T}_{\mu,p} := \text{prox}_{\mu|\cdot|^p}.$$

The proximity operators $\mathcal{T}_{\mu,0}$ and $\mathcal{T}_{\mu,1}$ are the well-known hard- and soft-thresholding

operators, respectively. Both have closed forms at $x \in \mathbb{R}$ as follows:

$$\mathcal{T}_{\mu,0}(x) \;=\; \begin{cases} \{0\}, & \text{if } |x| < \sqrt{2\mu}; \\[2mm] \{0, x\}, & \text{if } |x| = \sqrt{2\mu}; \\[2mm] \{x\}, & \text{otherwise.} \end{cases} \tag{3.3}$$

$$\mathcal{T}_{\mu,1}(x) \;=\; \text{sign}(x) \cdot \max\{|x| - \mu, 0\}. \tag{3.4}$$

Explicit forms of $\mathcal{T}_{\mu,p}$ for $p = 1/2$ and $2/3$ were discussed in [44]. The proximity operator $\mathcal{T}_{\mu,p}$ was also studied in [75].

For arbitrary $p \geq 0$ and $\mu > 0$, the operator $\mathcal{T}_{\mu,p}$ at $x \in \mathbb{R}$ is the collection of the minimizers of the function

$$J_{\mu,p,x}(u) := \mu |u|^p + \frac{1}{2}(u - x)^2 \tag{3.5}$$

over $\mathbb{R}$. That is,

$$\mathcal{T}_{\mu,p}(x) := \text{argmin}\{J_{\mu,p,x}(u) : u \in \mathbb{R}\}. \tag{3.6}$$

Since the function $J_{\mu,p,x}$ is continuous for $p > 0$ and lower semi-continuous for $p = 0$ on $\mathbb{R}$ and $\lim_{|u| \to +\infty} J_{\mu,p,x}(u) = +\infty$, then there exists $u_\star$ such that $J_{\mu,p,x}(u_\star) \leq J_{\mu,p,x}(u)$ for all $u \in \mathbb{R}$. That is, $u_\star \in \mathcal{T}_{\mu,p}(x)$, equivalently, the set $\mathcal{T}_{\mu,p}(x)$ is non-empty for any x.

In the rest of this section, we will present the properties of the proximity operator $\mathcal{T}_{\mu,p}$ for $p \geq 0$.

Lemma 3.1. *For any $p \geq 0$ and $\mu > 0$, it holds that $\mathcal{T}_{\mu,p}(-x) = -\mathcal{T}_{\mu,p}(x)$ for all $x \in \mathbb{R}$.*

Proof. We first prove that $\mathcal{T}_{\mu,p}(-x) \subseteq -\mathcal{T}_{\mu,p}(x)$. By definition (3.5), the relation $J_{\mu,p,-x}(u) = J_{\mu,p,x}(-u)$ holds for $u \in \mathbb{R}$. Now, suppose that $u_\star \in \mathcal{T}_{\mu,p}(-x)$. Thus $J_{\mu,p,-x}(u_\star) \leq J_{\mu,p,-x}(u)$ for all $u \in \mathbb{R}$. With the help of the above relation, this inequality is equivalent to $J_{\mu,p,x}(-u_\star) \leq J_{\mu,p,x}(-u)$ which implies $-u_\star \in \mathcal{T}_{\mu,p}(x)$. That is, $u_\star \in -\mathcal{T}_{\mu,p}(x)$. All above arguments are reversible, therefore we can show that $-\mathcal{T}_{\mu,p}(x) \subseteq \mathcal{T}_{\mu,p}(-x)$. This completes the proof. $\qquad \square$

With Lemma 3.1, it will be sufficient to study the set $\mathcal{T}_{\mu,p}(x)$ for all non-negative x. Specifically, for $x = 0$, we can straightforwardly derive that for all $p \geq 0$ and $\mu > 0$

$$\mathcal{T}_{\mu,p}(0) = \{0\}. \tag{3.7}$$

For x being positive, the following lemma characterizes the elements in the set $\mathcal{T}_{\mu,p}(x)$.

Lemma 3.2. *For $p \geq 0$, $\mu > 0$ and $x > 0$, then every non-zero element in $\mathcal{T}_{\mu,p}(x)$ is positive and its value is less or equal to x. Moreover, assume that the set $\mathcal{T}_{\mu,p}(x)$ has a non-zero element, say, $u_\star$, then $u_\star = x$ if $p = 0$; and $u_\star < x$ if $p > 0$.*

Proof. Suppose that $u_\star$ is in $\mathcal{T}_{\mu,p}(x)$ and is non-zero. If $u_\star$ is negative, then $|-u_\star - x| < |u_\star - x|$ which yields $J_{\mu,p,x}(-u_\star) < J_{\mu,p,x}(u_\star)$. Thus, $u_\star$ is not in $\mathcal{T}_{\mu,p}(x)$, which contradicts our assumption. Hence, $u_\star$ must be positive. We further show that $u_\star \leq x$. If it is not true, that is $u_\star > x$. We then define $\widetilde{u} := 2x - u_\star$. It can be verified directly that $|\widetilde{u}| < u_\star$ and $|\widetilde{u} - x| = |u_\star - x|$. Therefore, we have $J_{\mu,p,x}(\widetilde{u}) < J_{\mu,p,x}(u_\star)$. This implies that $u_\star$ is not in $\mathcal{T}_{\mu,p}(x)$, thus, contradicts our assumption again. Hence, $u_\star \leq x$.

As we know that $\mathcal{T}_{\mu,0}$ is the hard-thresholding operator, by equation (3.3), every non-zero element $u_\star$ in the set $\mathcal{T}_{\mu,0}(x)$ is identical to x.

Finally, we prove that $u_\star < x$ for $p > 0$. Since $u_\star \leq x$, we only need to show that x is not in the set $\mathcal{T}_{\mu,p}(x)$. Actually it follows from the fact that $J'_{\mu,p,x}(x) = \mu p x^{p-1} > 0$ for any positive number x. $\qquad\square$

We remark that for $p > 1$, the set $\mathcal{T}_{\mu,p}(x)$ contains only one element and this element is non-zero if and only if x is non-zero. By Lemma 3.1 and equation (3.7), we consider the case of x being positive. Since the function $J_{\mu,p,x}$ is strictly convex and coercive, the set $\mathcal{T}_{\mu,p}(x)$ has a unique element. We further notice that $J'_{\mu,p,x}(0) = -x < 0$. Hence, the element cannot be zero. Hence, we can view $\mathcal{T}_{\mu,p}$ as an operator from $\mathbb{R}$ to $\mathbb{R}$. This is a shrinkage, but not sparse-promoting, operator in the sense that $0 \neq |\mathcal{T}_{\mu,p}(x)| < |x|$ for any non-zero number x.

The situation, however, is completely different for $p = 0$ and $p = 1$ as indicated by the hard- and soft-thresholding operators, respectively. Therefore, we turn our attention for the operator $\mathcal{T}_{\mu,p}$ with $0 < p < 1$.

For convenience, given any $\mu > 0$ and $0 < p < 1$, we define

$$\varpi_{\mu,p} := (\mu p(1-p))^{\frac{1}{2-p}}, \quad \widetilde{\tau}_{\mu,p} := (2-p)(\mu p)^{\frac{1}{2-p}}(1-p)^{\frac{p-1}{2-p}}. \qquad (3.8)$$

and

$$\tau_{\mu,p} := \frac{2-p}{2(1-p)}(2\mu(1-p))^{\frac{1}{2-p}}, \quad \varrho_{\mu,p} := (2\mu(1-p))^{\frac{1}{2-p}}. \qquad (3.9)$$

We first study the convexity of the function $J_{\mu,p,x}$ on the interval $[0, +\infty)$ for positive x. For our convenience, the first and the second derivatives of $J_{\mu,p,x}$ at $u > 0$

are given as follows:

$$J'_{\mu,p,x}(u) = u + \mu p u^{p-1} - x \quad \text{and} \quad J''_{\mu,p,x}(u) = 1 + \mu p(p-1)u^{p-2}.$$

Lemma 3.3. *For any fixed $0 < p < 1$, $\mu > 0$, and $x > 0$, the following statements hold for the function $J_{\mu,p,x}$.*

(i) *$J_{\mu,p,x}(u)$ is concave on $[0, \varpi_{\mu,p}]$ and convex on $[\varpi_{\mu,p}, +\infty)$;*

(ii) *If $x \le \tilde{\tau}_{\mu,p}$, then $J_{\mu,p,x}$ is increasing on $[0, +\infty)$;*

(iii) *If $x > \tilde{\tau}_{\mu,p}$, then $J'_{\mu,p,x}(\cdot)$ has exactly two roots, namely, u_- and u_+, on the interval $(0, +\infty)$. Moreover, the roots satisfy the inequality $u_- < \varpi_{\mu,p} < u_+$, the function $J_{\mu,p,x}(u)$ has a local maximum at $u = u_-$ and a local minimum at $u = u_+$.*

Proof. Item (i): The function $J_{\mu,p,x}$ is continuous on $[0, \infty)$. One can directly verify that $J''_{\mu,p,x}(\varpi_{\mu,p}) = 0$, $J''_{\mu,p,x}(u) < 0$ for $u \in (0, \varpi_{\mu,p})$, and $J''_{\mu,p,x}(u) > 0$ for $u \in (\varpi_{\mu,p}, +\infty)$. Hence, the function $J_{\mu,p,x}(u)$ having the inflation point at $u = \varpi_{\mu,p}$, is concave on $[0, \varpi_{\mu,p}]$ and convex on $[\varpi_{\mu,p}, +\infty)$.

Item (ii): It suffices to show $J'_{\mu,p,x}(u) \ge 0$ on $(0, \infty)$. Define $h(u) := J'_{\mu,p,x}(u)$. One can check that h is convex on $(0, \infty)$ and has unique global minimizer at $u = \varpi_{\mu,p}$ with the minimal value $h(\varpi_{\mu,p}) = \tilde{\tau}_{\mu,p} - x$. Hence, $h(u) \ge h(\varpi_{\mu,p}) \ge 0$.

Item (iii): With the function h defined in the above, one can verify that $\lim_{u \to 0+} h(u) = +\infty$, $\lim_{u \to +\infty} h(u) = +\infty$, and $h(\varpi_{\mu,p}) = \tilde{\tau}_{\mu,p} - x < 0$. Further, it can be verified that $h'(u) < 0$ for $u \in (0, \varpi_{\mu,p})$ and $h'(u) > 0$ for $u \in (\varpi_{\mu,p}, +\infty)$, that is, h is decreasing

on $(0, \varpi_{\mu,p})$ and increasing on $(\varpi_{\mu,p}, +\infty)$. Putting all above together and using the mean value theorem, there exist a unique number $u_- \in (0, \varpi_{\mu,p})$ and a unique number $u_+ \in (\varpi_{\mu,p}, +\infty)$ such that $h(u_-) = h(u_+) = 0$. From item (i), one gets that $J_{\mu,p,x}(u)$ has a local maximum at $u = u_-$ and a local minimum at $u = u_+$. $\qquad\square$

In what follows, we will focus on the relationship between x and $\mathcal{T}_{\mu,p}(x)$.

Proposition 3.4. *Let x be a positive number. For any fixed $0 < p < 1$ and $\mu > 0$, $J_{\mu,p,x}(u)$ defined on $[0, +\infty)$ attains its global minimum at $u = 0$ if and only if $x \leq \tau_{\mu,p}$. In particular, $u = 0$ is the unique minimizer of $J_{\mu,p,x}(u)$ on $[0, \infty)$ if and only if $x < \tau_{\mu,p}$.*

Proof.   Assume $J_{\mu,p,x}(0) \leq J_{\mu,p,x}(u)$ for all $u > 0$, that is, $0 \leq \mu u^p + \frac{1}{2}u^2 - ux$ which is the same as $0 \leq \mu u^{p-1} + \frac{1}{2}u - x$. Define $g(u) := \mu u^{p-1} + \frac{1}{2}u$. Clearly the function g is strictly convex on $(0, +\infty)$ and achieves its minimum value at $u = \varrho_{\mu,p}$ over this interval. The minimum value $g(\varrho_{\mu,p})$ is equal to $\tau_{\mu,p}$ which should be greater than or equal to x.

Conversely, $x \leq \tau_{\mu,p}$ implies that $u = 0$ is a minimizer of $J_{\mu,p,x}(u)$ since the above arguments are reversible.

The equivalence between the uniqueness and the strict inequality follows in the same manner by replacing "$\leq$" with "$<$" in the proof.

$\qquad\square$

Note that $\widetilde{\tau}_{\mu,p} < \tau_{\mu,p}$ for any $0 < p < 1$ and $\mu > 0$. One knows from item (ii) of

Lemma 3.3 that $J_{\mu,p,x}(u)$ achieves its global minimum only at $u = 0$ when $x \leq \widetilde{\tau}_{\mu,p}$. This observation is further confirmed by Proposition 3.4.

For $x > \widetilde{\tau}_{\mu,p}$, from item (iii) of Lemma 3.3 we know that $J_{\mu,p,x}(u)$ has its local minimums at $u = 0$ and $u = u_+$. We will then determine which one provides the global minimum of $J_{\mu,p,x}$. It turns out from Proposition 3.4 that if $\widetilde{\tau}_{\mu,p} < x < \tau_{\mu,p}$, then the global minimum of $J_{\mu,p,x}$ achieves only at $u = 0$, i.e., $\mathcal{T}_{\mu,p}(x) = \{0\}$. The cases of $x = \tau_{\mu,p}$ and $x > \tau_{\mu,p}$ will be studied in the following results.

Proposition 3.5. *For any $0 < p < 1$, $\mu > 0$, if $x = \tau_{\mu,p}$ then $u_+ = \varrho_{\mu,p}$ and the function $J_{\mu,p,x}$ attains its global minimizers at both $u = 0$ and $u = u_+$. That is,* $\mathcal{T}_{\mu,p}(x) = \{0, u_+\}.$

Proof. It can be directly seen that $\varpi_{\mu,p} < \varrho_{\mu,p}$ and $J'_{\mu,p,x}(\varrho_{\mu,p}) = 0$. By Lemma 3.3, one has $u_+ = \varrho_{\mu,p}$. Further, one computes $J_{\mu,p,x}(u_+) = J_{\mu,p,x}(0) = \frac{1}{2}\tau_{\mu,p}^2$. Hence, $J_{\mu,p,x}$ achieves its minima at both $u = 0$ and $u = u_+$. $\square$

Proposition 3.6. *For any $0 < p < 1$, $\mu > 0$, if $x > \tau_{\mu,p}$ then the function $J_{\mu,p,x}$ attains its global minimum at $u = u_+$. That is, $\mathcal{T}_{\mu,p}(x) = \{u_+\}$.*

Proof. By Lemma 3.3, the function $J_{\mu,p,x}$ has local minima at both $u = 0$ and $u = u_+$. By Proposition 3.4, one can conclude that $J_{\mu,p,x}$ has its global minimum at $u = u_+$. This completes the proof. $\square$

Table 3.1 presents the properties of the function $J_{\mu,p,x}$ for $\mu > 0$, $0 < p < 1$, and $x \geq 0$. Figure 3.1 provides plots of the objective functions $J_{\mu,p,x}$ for various values

of x. More precisely, Figure 3.1(a) presents an instance of item (ii) in Lemma 3.3; Figure 3.1(b) presents an instance of item (iii) in Lemma 3.3 and Proposition 3.4; Figure 3.1(c) reflects the situation of Proposition 3.5; and Figure 3.1(d) gives an example of Proposition 3.6.

Table 3.1: The properties of the function $J_{\mu,p,x}$ for $\mu > 0$, $0 < p < 1$, and $x \geq 0$. "l-min" and "g-min" stand for the local minimum and global minimum, respectively.

	$u \in [0, \varpi_{\mu,p}]$	$u \in [\varpi_{\mu,p}, +\infty)$	$u = 0$	$u = u_-$	$u = u_+$
$x \in [0, \widetilde{\tau}_{\mu,p})$	concave	convex	g-min	–	–
$x \in [\widetilde{\tau}_{\mu,p}, \tau_{\mu,p})$	concave	convex	g-min	l-max	l-min
$x = \tau_{\mu,p}$	concave	convex	g-min	l-max	g-min
$x \in (\tau_{\mu,p}, +\infty)$	concave	convex	l-min	l-max	g-min

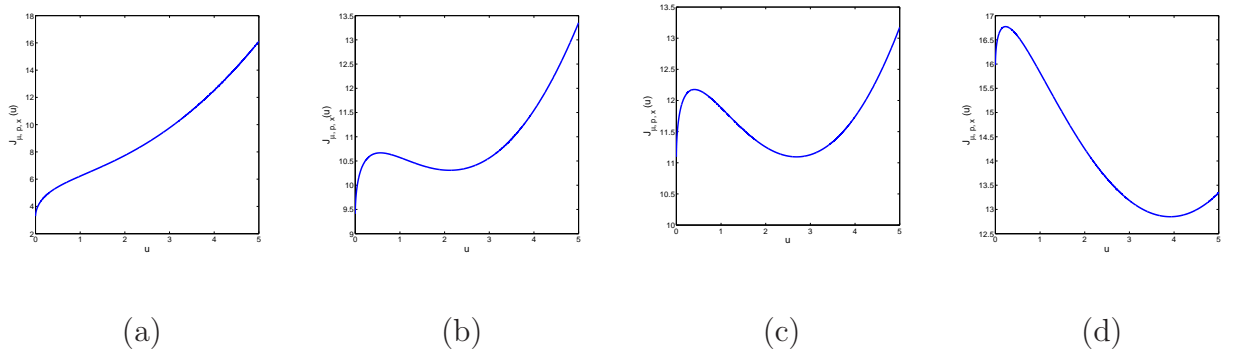(a)   (b)   (c)   (d)

Figure 3.1: The curves of $J_{\mu,p,x}$ for different choices of x: (a) $x \leq \tilde{\tau}_{\mu,p}$ ($x = 0.9\tilde{\tau}_{\mu,p}$); (b) $\tilde{\tau}_{\mu,p} < x < \tau_{\mu,p}$ ($x = \tilde{\tau}_{\mu,p} + 0.8(\tau_{\mu,p} - \tilde{\tau}_{\mu,p})$); (c) $x = \tau_{\mu,p}$; and (d) $x > \tau_{\mu,p}$ ($x = 1.2\tau_{\mu,p}$).

From Table 3.1, Lemma 3.1, Propositions 3.4, 3.5, and 3.6, we conclude that

$$
\mathcal{T}_{\mu,p}(x) = \begin{cases} \{0\}, & \text{if } |x| < \tau_{\mu,p}; \\[2mm] \{0, \operatorname{sign}(x) \cdot \varrho_{\mu,p}\}, & \text{if } |x| = \tau_{\mu,p}; \\[2mm] \{\operatorname{sign}(x) \cdot u_+\}, & \text{otherwise,} \end{cases}
\tag{3.10}
$$

where u_+ is the largest zero of the first derivative function $J'_{\mu,p,|x|}$.

From equation (3.10) one can see that $\mathcal{T}_{\mu,p}$ is a sparse-promoting thresholding operator with threshold $\tau_{\mu,p}$. The monotonicity of the threshold $\tau_{\mu,p}$ with respect to p is described in the following.

Proposition 3.7. *If $0 < \mu \leq \frac{1}{2}$, $\tau_{\mu,p}$ as a function of p for a fixed μ is decreasing on the interval $(0,1)$; if $\mu > \frac{1}{2}$, it is increasing on the interval $(0, 1 - \frac{1}{2\mu})$ and decreasing on the interval $(1 - \frac{1}{2\mu}, 1)$.*

Proof. Let us define $f(p) := \ln(\tau_{\mu,p})$. Then the monotonicity of $f(p)$ is consistent with that of $\tau_{\mu,p}$ as a function of p. By the definition of $\tau_{\mu,p}$ in (3.9), we have that $f'(p) = \frac{1}{(2-p)^2} \ln[2\mu(1-p)]$. If $\mu \leq \frac{1}{2}$, then $f'(p) < 0$ on $(0,1)$. Therefore $\tau_{\mu,p}$ is decreasing on $(0,1)$ with respect to p. If $\mu > \frac{1}{2}$, we have that $f'(p) > 0$ on $(0, 1 - \frac{1}{2\mu})$ and $f'(p) < 0$ on $(1 - \frac{1}{2\mu}, 1)$. Therefore, $\tau_{\mu,p}$ is increasing on $(0, 1 - \frac{1}{2\mu})$ and decreasing on $(1 - \frac{1}{2\mu}, 1)$ with respect to p. $\qquad\square$

Figure 3.2 and Figure 3.3 display the proximity operators $\mathcal{T}_{\mu,p}$ for various values of p and μ. Figure 3.2 depicts the proximity operators $\mathcal{T}_{1/3,p}$ for $p = 0, \frac{1}{2}, \frac{2}{3}, \frac{4}{5}, 1$ while Figure 3.3 depicts the proximity operators $\mathcal{T}_{3,p}$ for $p = 0, \frac{1}{2}, \frac{2}{3}, \frac{4}{5}, \frac{9}{10}, 1$. The blue curves

connecting point $(\tau_{\mu,p}, \varrho_{\mu,p})$ (or $(-\tau_{\mu,p}, -\varrho_{\mu,p})$) on black curve and point $(\tau_{\mu,p}, 0)$ (or $(-\tau_{\mu,p}, 0)$) on red curve in both Figure 3.2 and Figure 3.3 capture the evolution of the $(\tau_{\mu,p}, \varrho_{\mu,p})$ as p changes from 0 to 1. The evolution curve of $(\tau_{\mu,p}, \varrho_{\mu,p})$ also validates the statements in Proposition 3.7. Therefore, the main issue is to compute $\mathcal{T}_{\mu,p}(x)$
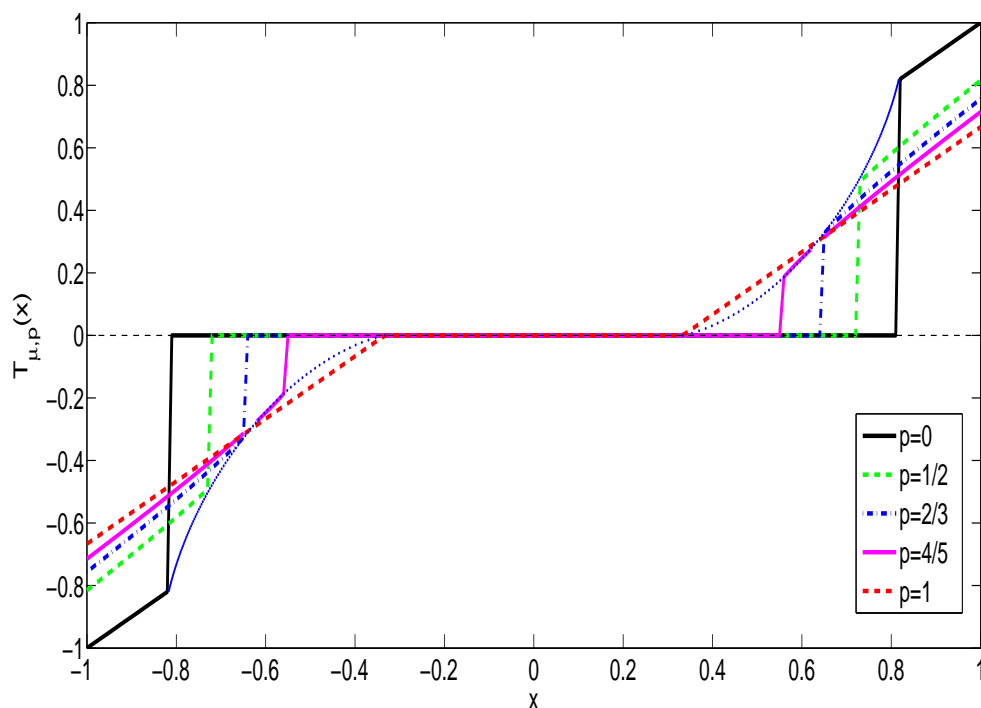

Figure 3.2: The proximity operators $\mathcal{T}_{\mu,p}$ for $\mu = \frac{1}{3}$ and $p = 0, \frac{1}{2}, \frac{2}{3}, \frac{4}{5}, 1$.

for $x > \tau_{\mu,p}$. That is, we need to find u_+ at which the function $J_{\mu,p,x}$ attains its global minimum. Actually, by Proposition 3.6, u_+ is the largest root of the equation

$$u + \mu p u^{p-1} - x = 0. \tag{3.11}$$

In section 3.3, we shall show that equation (3.11) can be converted to a polynomial when p is an rational number. In section 3.4, we shall numerically compute u_+ as a
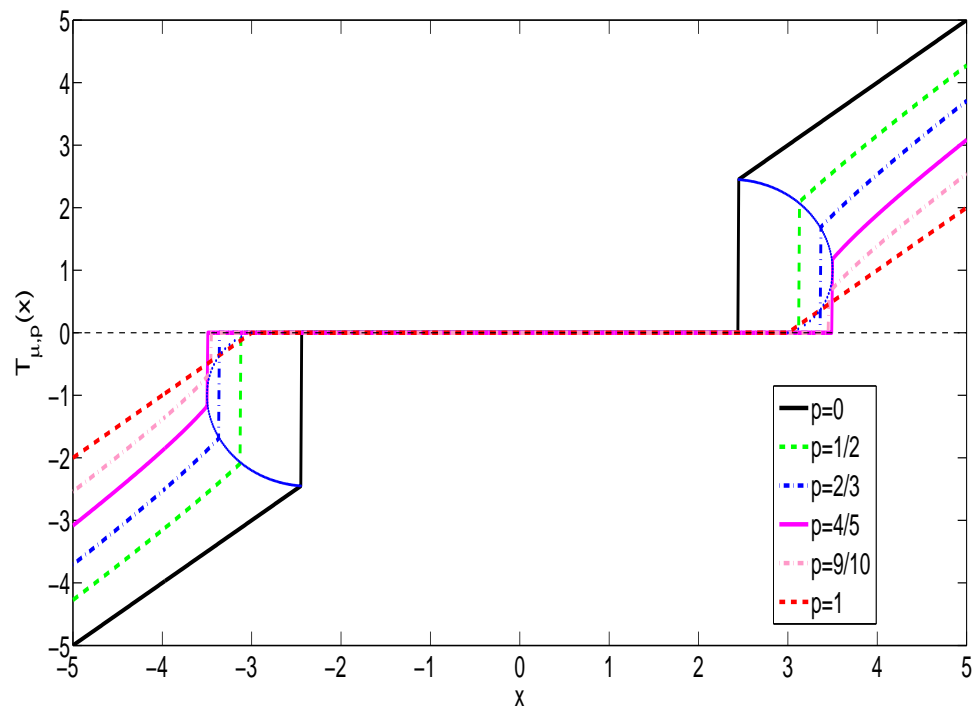
Figure 3.3: The proximity operators $\mathcal{T}_{\mu,p}$ for $\mu = 3$ and $p = 0, \frac{1}{2}, \frac{2}{3}, \frac{4}{5}, \frac{9}{10}, 1$.

solution of equation (3.11) via Newton's method when p is not 0, 1/2, 2/3, or 1.

To close this section, we will show that the proximity operator $\mathcal{T}_{\mu,p}$ for $0 < p <$ 1 is not non-expansive. Recall that an operator $Q : \mathbb{R} \rightarrow \mathbb{R}$ is non-expansive if $|Q(x) - Q(y)| \le |x - y|$ for all $x, y \in \mathbb{R}$.

Lemma 3.8. *Let $0 < p < 1$ and $\mu > 0$, and let x_1 and x_2 be two real numbers satisfying $x_1 < x_2$. Then for any $u_i \in \mathcal{T}_{\mu,p}(x_i)$, for $i = 1, 2$, it holds that $u_1 \le u_2$. Furthermore, if $x_1 < -\tau_{\mu,p}$ or $x_2 > \tau_{\mu,p}$, then u_1 is strictly less than u_2.*

Proof. By Lemma 3.1 and equation (3.10), it is sufficient to consider the case of both x_1 and x_2 positive. By the definition of the proximity operator, one has that

$$J_{\mu,p,x_1}(u_1) \le J_{\mu,p,x_1}(u_2)$$

$$J_{\mu,p,x_2}(u_2) \le J_{\mu,p,x_2}(u_1).$$

Adding the above two inequations leads to $(u_2 - u_1)(x_2 - x_1) \ge 0$. Since $x_1 < x_2$ one obtains $u_1 \le u_2$.

Next, we show that if $x_2 > \tau_{\mu,p}$ then $u_1 < u_2$. In fact, if $x_1 < \tau_{\mu,p}$, then $u_1 = 0$ from equation (3.10) and $u_2 > \varpi_{\mu,p} > 0$ by Lemma 3.3. Hence, $u_1 < u_2$. If $x_1 = \tau_{\mu,p}$ and $u_1 = 0$, $u_1 < u_2$ holds. Therefore, we assume that $x_1 \ge \tau_{\mu,p}$ and $u_1 \ne 0$. Then by item (iii) of Lemma 3.3 or equation (3.11) the pairs (x_i, u_i), $i = 1, 2$, satisfy the following equations $\mu p u_i^{p-1} + u_i - x_i = 0$. It indicates that $u_1 \ne u_2$. Hence, $u_1 < u_2$. This completes the proof. □

Proposition 3.9. *Let $0 < p < 1$ and $\mu > 0$, and let x_1 and x_2 be two real numbers such that $x_1 < x_2$. Then for any $u_i \in \mathcal{T}_{\mu,p}(x_i)$, $i = 1, 2$, the following statements hold:*

(i) if x_1 and x_2 have different signs or both them lie in the interval $(-\tau_{\mu,p}, \tau_{\mu,p})$, then $u_2 - u_1 < x_2 - x_1$.

(ii) if both x_1 and x_2 lie in the interval $(\tau_{\mu,p}, +\infty)$ or $(-\infty, -\tau_{\mu,p})$, then $u_2 - u_1 > x_2 - x_1$.

Proof. If x_1 and x_2 have different signs, then Item (i) follows immediately from Lemma 3.1 and Lemma 3.2. If both them lie in the interval $(-\tau_{\mu,p}, \tau_{\mu,p})$, then item (i) follows from equation (3.10).

Now, we turn to prove item (ii). We first assume that both x_1 and x_2 lie in the interval $(\tau_{\mu,p}, +\infty)$. By Lemma 3.3, u_1 is the critical point of J_{μ,p,x_1} while u_2 is the critical point of J_{μ,p,x_2}. Therefore, one has $x_i = u_i + \mu p u_i^{p-1}$, for $i = 1, 2$. It follows that

$$x_2 - x_1 = u_2 - u_1 + \mu p(u_2^{p-1} - u_1^{p-1}).$$

Since $x_1 < x_2$, one has $u_1 < u_2$ by Lemma 3.8. Hence, the difference $u_2^{p-1} - u_1^{p-1}$ in the above equation is strictly less than zero. It yields that $u_2 - u_1 > x_2 - x_1$. By Lemma 3.1, the result of item (ii) is also true for x_1 and x_2 lie in the interval $(-\infty, -\tau_{\mu,p})$. The proof is complete. $\qquad\square$

We conclude from item (ii) in Proposition 3.9 that $\mathcal{T}_{\mu,p}$ is not non-expansive.

3.3 The Proximity Operators of the $\ell_{1/2}$- and $\ell_{2/3}$-Norm

As we mentioned in section 3.2 that the proximity operators $\mathcal{T}_{\mu,1/2}$ and $\mathcal{T}_{\mu,2/3}$ have been discussed in [14], based on the properties presented in section 3.2 we will provide the explicit forms of $\mathcal{T}_{\mu,1/2}$ and $\mathcal{T}_{\mu,2/3}$ with alternative, but much simple, proofs for them.

We begin to show that for a rational number $0 < p < 1$ and $x > \tau_{\mu,p}$ the computation of $\mathcal{T}_{\mu,p}(x)$ can be reduced to finding the largest zero of a polynomial. More precisely, let us write $p = \frac{l}{k}$, where k, l are relatively prime integers. Actually, set $t = u^{\frac{1}{k}}$. Substituting u in (3.11) by t^k and simplifying the resulting equation lead to the following polynomial equation

$$t^{2k-l} - xt^{k-l} + \frac{l}{k}\mu = 0, \ t > 0. \tag{3.12}$$

Since k and l are relatively prime integers and $k > l$, the least degree of the polynomial in (3.12) is 3 only when $k = 2$ and $l = 1$, that is, $p = 1/2$. The second least degree of the polynomial is 4 only when $k = 3$ and $l = 2$, that is, $p = 2/3$. In the following, we shall present the closed-form formulas for the proximity operators $\mathcal{T}_{\mu,p}$ with $p = 1/2$ and $p = 2/3$. For other choices of the rational number p, we need to find the solutions of equation (3.12) where the degree of the polynomial is higher than 4, therefore, it is hardly to have a closed-form formula for representing the roots of the polynomial.

The closed-form formula for the proximity operators $\mathcal{T}_{\mu,1/2}$ is given as follows.

Proposition 3.10. *Let $\mu > 0$. Then for $x \in \mathbb{R}$*

$$
\mathcal{T}_{\mu,1/2}(x) = \begin{cases}
\{0\}, & \text{if } |x| < \frac{3}{2}\mu^{\frac{2}{3}}; \\
\{0, \text{sign}(x) \cdot \mu^{\frac{2}{3}}\}, & \text{if } |x| = \frac{3}{2}\mu^{\frac{2}{3}}; \\
\left\{\frac{2}{3}x\left(1 + \cos\left(\frac{2}{3}\cos^{-1}\left(-\frac{3^{3/2}}{4}\mu|x|^{-3/2}\right)\right)\right)\right\}, & \text{otherwise.}
\end{cases}
\tag{3.13}
$$

Proof. One can check that $\tau_{\mu,1/2} = \frac{3}{2}\mu^{\frac{2}{3}}$ and $\varrho_{\mu,1/2} = \mu^{\frac{2}{3}}$. By equation (3.10) and the fact of $\text{sign}(x)|x| = x$, one just needs to show that for $x > \frac{3}{2}\mu^{\frac{2}{3}}$,

$$
u_+ = \frac{2}{3}x\left(1 + \cos\left(\frac{2}{3}\cos^{-1}\left(-\frac{3^{3/2}}{4}\mu x^{-3/2}\right)\right)\right).
\tag{3.14}
$$

When $p = 1/2$, equation (3.12) becomes

$$
t^3 - xt + \frac{\mu}{2} = 0.
$$

By item (iii) of Lemma 3.3, the above cubic equation has three real roots with two positive roots and one negative root. Furthermore, u_+ is the square of the largest root of the cubic equation. Fortunately, using a formula in [?] this largest root is

$$
t = 2\sqrt{\frac{x}{3}}\cos\left(\frac{1}{3}\cos^{-1}\left(-\frac{3\mu}{4x}\sqrt{\frac{3}{x}}\right)\right).
$$

Hence $u_+ = t^2$. Using the formula $\cos^2\theta = \frac{1}{2}(1 + \cos(2\theta))$, we know that t^2 exactly equals to the right-hand side of equation (3.14). This completes the proof of the result. $\square$

Next, we present the closed-form formula for the proximity operators $\mathcal{T}_{\mu,2/3}$.

Proposition 3.11. *Let $\mu > 0$. Then for $x \in \mathbb{R}$*

$$\mathcal{T}_{\mu,2/3}(x) = \begin{cases} \{0\}, & \text{if } |x| < 2(\frac{2}{3}\mu)^{\frac{3}{4}}; \\ \{0, \text{sign}(x) \cdot (\frac{2}{3}\mu)^{\frac{3}{4}}\}, & \text{if } |x| = 2(\frac{2}{3}\mu)^{\frac{3}{4}}; \\ \left\{\text{sign}(x) \cdot \frac{1}{8}\left(\sqrt{2z} + \sqrt{\frac{2|x|}{\sqrt{2z}} - 2z}\right)^3\right\}, & \text{otherwise,} \end{cases} \tag{3.15}$$

where

$$z = \left(\frac{1}{16}x^2 + \sqrt{\frac{x^4}{256} - \frac{8\mu^3}{729}}\right)^{\frac{1}{3}} + \left(\frac{1}{16}x^2 - \sqrt{\frac{x^4}{256} - \frac{8\mu^3}{729}}\right)^{\frac{1}{3}}. \tag{3.16}$$

Proof. One can check that $\tau_{\mu,2/3} = 2(\frac{2}{3}\mu)^{\frac{3}{4}}$ and $\varrho_{\mu,2/3} = (\frac{2}{3}\mu)^{\frac{3}{4}}$. By equation (3.10) and Lemma 3.1 we only need to compute the proximity operator $\mathcal{T}_{\mu,2/3}(x)$ for $x > 2(\frac{2}{3}\mu)^{\frac{3}{4}}$.

When $p = 2/3$, equation (3.12) becomes

$$t^4 - xt + \frac{2\mu}{3} = 0, \tag{3.17}$$

which also has two and only two positive roots and whose largest root can lead to u_+. We now find the largest positive root of equation (3.17). For any real number w, equation (3.17) is identical to the following one

$$(t^2 + w)^2 = 2wt^2 + xt + (w^2 - \frac{2}{3}\mu). \tag{3.18}$$

In particular, we can choose a specific w so that the expression of the right-hand side of the above equation can be completed in square with respect to the variable t. This requires that w satisfies the following equation

$$w^3 - \frac{2}{3}\mu w - \frac{1}{8}x^2 = 0,$$

which has at least one real solution. Actually, $w = z$ with z given by (3.16) is the solution of this cubic equation. With this choice, equation (3.18) is equivalent to the following two equations

$$t^2 + \sqrt{2z}t + (z + \frac{\sqrt{2}x}{4}z^{-1/2}) = 0 \quad \text{and} \quad t^2 - \sqrt{2z}t + (z - \frac{\sqrt{2}x}{4}z^{-1/2}) = 0$$

The first quadratic equation has two complex roots while the second one has two real roots. We therefore only need to find the largest root of the second quadratic equation. Actually, this root is

$$t = \frac{1}{2}\left(\sqrt{2z} + \sqrt{\frac{2x}{\sqrt{2z}} - 2z} \right).$$

This completes the proof. □

3.4   Computing the Proximity Operator of the ℓ_p-Norm $(0 < p < 1)$

In the previous sections, we have already presented the closed-form formulas for the proximity operator $\mathcal{T}_{\mu,p}$ with p being 0, 1/2, 2/3 and 1. For other choice of p, we shall develop in this section a numerical algorithm for computing the proximity operator $\mathcal{T}_{\mu,p}$.

According to (3.10), it is essential to develop a numerical scheme that can compute $\mathcal{T}_{\mu,p}(x)$ for all $x > \tau_{\mu,p}$. Note that in this case the set $\mathcal{T}_{\mu,p}(x)$ only contains one element and we simply use $\mathcal{T}_{\mu,p}(x)$ to denote this element. We further know that $\mathcal{T}_{\mu,p}(x)$ with

$x > \tau_{\mu,p}$ is the largest solution of equation (3.11). To locate this solution, we propose

to approximate it by Newton's method. For fixed $\mu > 0$, $0 < p < 1$, and $x > \tau_{\mu,p}$,

define

$$H(u) := u - \frac{h(u)}{h'(u)} \tag{3.19}$$

where $h(u) := u + \mu p u^{p-1} - x$. Newton's method begins with an estimate u_0 of $\mathcal{T}_{\mu,p}(x)$

and then defines inductively

$$u_{n+1} = H(u_n), \tag{3.20}$$

where $n \geq 0$.

Proposition 3.12. *For $p \in (0,1)$, $\mu > 0$, and $x > \tau_{\mu,p}$, if an initial estimate $u_0 >$*

$\mathcal{T}_{\mu,p}(x)$ then the sequence generated by (3.20) is decreasing and bounded below by

$\mathcal{T}_{\mu,p}(x)$. Moreover, the sequence converges to $\mathcal{T}_{\mu,p}(x)$.

Proof. Let us prove the sequence $\{u_n : n \in \mathbb{N}\}$ is decreasing and bounded below by

$\mathcal{T}_{\mu,p}(x)$ first. We proceed inductively. For $n = 0$, it is true by the assumption that

$u_0 > \mathcal{T}_{\mu,p}(x)$. Now suppose that $\mathcal{T}_{\mu,p}(x) \leq u_{k+1} \leq u_k$ for all $0 \leq k \leq n-1$. We show

that $\mathcal{T}_{\mu,p}(x) \leq u_{n+1} \leq u_n$. By Lemma 3.3, the function h is increasing and convex

on $[\mathcal{T}_{\mu,p}(x), +\infty)$. Hence, $h(u_n) > 0$ and $h'(u_n) > 0$. We obtain that $u_{n+1} < u_n$ from

the identity $0 = h(u_n) + h'(u_n)(u_{n+1} - u_n)$. By the convexity of h, we have that

$h(u) > h(u_n) + h'(u_n)(u - u_n)$ for all $u \in [\mathcal{T}_{\mu,p}(x), +\infty)$ and $u \neq u_n$. In particular,

taking $u = \mathcal{T}_{\mu,p}(x)$ in this inequality, we have that $0 > h(u_n) + h'(u_n)(\mathcal{T}_{\mu,p}(x) - u_n)$.

This yields $\mathcal{T}_{\mu,p}(x) \leq u_{n+1}$. Therefore, the sequence converges, says, $\lim_{n \to +\infty} u_n =$

$u_\star \geq \mathcal{T}_{\mu,p}(x)$. Taking the limit on both sides of equation (3.20) leads to $h(u_\star) = 0$. Using Lemma 3.3 again, we know that $u_\star = \mathcal{T}_{\mu,p}(x)$. $\qquad\square$

By Lemma 3.2, we can choose $u_0 = x$ as our initial estimator in Newton's method (3.20). A better initial estimator can be chosen as well. To this end, we need the following technical lemma.

Lemma 3.13. *Let $\mu > 0$ and $x > 0$. Let p_1 and p_2 be two numbers in $[0,1]$ with $p_1 < p_2$. Define $p_{12} := (p_1/p_2)^{1/(p_2-p_1)}$. Then for any $u_i \in \mathcal{T}_{\mu,p_i}(x)$, $i = 1, 2$, we have that $u_1 \leq u_2$ if $\max\{u_1, u_2\} \leq p_{12}$; $u_1 \geq u_2$ if $\min\{u_1, u_2\} \geq p_{12}$.*

Proof. Since $x > 0$ and $u_i \in \mathcal{T}_{\mu,p_i}(x)$, then both u_1 and u_2 are non-negative from Lemma 3.2. By the definition of the proximity operator, from $u_i \in \mathcal{T}_{\mu,p_i}(x)$, we have that $J_{\mu,p_1,x}(u_1) \leq J_{\mu,p_1,x}(u_2)$ and $J_{\mu,p_2,x}(u_2) \leq J_{\mu,p_2,x}(u_1)$. Adding these two inequalities together yields

$$u_1^{p_1} - u_1^{p_2} \leq u_2^{p_1} - u_2^{p_2}. \tag{3.21}$$

Define $g(u) := u^{p_1} - u^{p_2}$ on the interval $[0, +\infty)$. We can check directly that g is continuous, is increasing on $[0, p_{12}]$, and decreasing on $[p_{12}, +\infty)$. Then, the results of this theorem follows from inequality (3.21). $\qquad\square$

For any $p \in (0, 1)$, but not $1/2$ and $2/3$, we define p_- to be the largest element in

the set $\{0, 1/2, 2/3, 1\}$ that is smaller than p. That is,

$$p_- = \begin{cases} 0, & \text{if } p \in (0, 1/2); \\[2mm] 1/2, & \text{if } p \in (1/2, 2/3); \\[2mm] 2/3, & \text{if } p \in (2/3, 1). \end{cases}$$

Proposition 3.14. *For $p \in (0, 1) \setminus \{1/2, 2/3\}$, $\mu > 0$, and $x > \max\{\tau_{\mu,p}, \tau_{\mu,p_-}\}$, if*

$$x > \max\{\tau_{\mu,p} - \varrho_{\mu,p}, \tau_{\mu,p_-} - \varrho_{\mu,p_-}\} + \left(\frac{p_-}{p}\right)^{1/(p-p_-)}, \tag{3.22}$$

then

$$\mathcal{T}_{\mu,p}(x) \leq \mathcal{T}_{\mu,p_-}(x).$$

Proof. By Item (ii) in Proposition 3.9, we have that $\mathcal{T}_{\mu,p}(x) > x - (\tau_{\mu,p} - \varrho_{\mu,p})$ and $\mathcal{T}_{\mu,p_-}(x) > x - (\tau_{\mu,p_-} - \varrho_{\mu,p_-})$. By the assumption (3.22) together the proceeding two inequalities, both $\mathcal{T}_{\mu,p}(x)$ and $\mathcal{T}_{\mu,p_-}(x)$ are bigger than $(p_-/p)^{1/(p-p_-)}$. Our result follows from Lemma 3.13. $\qquad\square$

To summarize the above discussions, a detailed pseudocode for computing the proximity operator $\mathcal{T}_{\mu,p}(x)$ including stopping criteria is given in Algorithm 3. We point it out that the proximity operator $\mathcal{T}_{\frac{1}{3}, \frac{4}{5}}$ showing in Figure **??**(a) and the proximity operators $\mathcal{T}_{3, \frac{4}{5}}$ and $\mathcal{T}_{3, \frac{9}{10}}$ showing in Figure **??**(b) are computed numerically through Algorithm 3.

Algorithm 3: (Computing $\mathcal{T}_{\mu,p}(x)$ for $0 < p < 1$)

Input: $p \in [0,1]$, $\mu > 0$, $\epsilon > 0$, and $x \in \mathbb{R}$

Result: $\mathcal{T}_{\mu,p}(x)$

begin

    if $p = 0,\ 1/2,\ 2/3,\ or\ 1$ **then**

        $\mathcal{T}_{\mu,p}(x)$ is given by the formula (3.3), (3.13), (3.15), or (3.4).

    else

        if $|x| \leq \tau_{\mu,p}$ **then**

$$\mathcal{T}_{\mu,p}(x) = \begin{cases} \{0\}, & \text{if } |x| < \tau_{\mu,p}; \\ \{0, \text{sign}(x) \cdot \varrho_{\mu,p}\}, & \text{if } |x| = \tau_{\mu,p}; \end{cases}$$

        else

            Determine an initial estimator u_0 for the Newton iteration;

            if $|x| > \max\{\tau_{\mu,p} - \varrho_{\mu,p}, \tau_{\mu,p_-} - \varrho_{\mu,p_-}\} + \left(\frac{p_-}{p}\right)^{1/(p-p_-)}$ *and* $|x| > \tau_{\mu,p_-}$

            then

                $u_0 = \mathcal{T}_{\mu,p_-}(|x|)$

            else $u_0 = |x|$

            Newton's iteration;

            while $|u_n - u_{n-1}| > \epsilon$ *or* $h(u_n) > \epsilon$ **do**

                $u_{n+1} = H(u_n)$

            the final iterate is denoted by u_∞ ;

            $\mathcal{T}_{\mu,p}(x) = \text{sign}(x)u_\infty$;

Chapter 4

Applications and Numerical

Experiments

In this chapter, we formulate application problems in image processing and compressed sensing as composite minimization problems. For convex composite minimization problems arising from image deblurring and compressed sensing, proposed algorithms from chapter 2 will be applied and comparisons of proposed algorithms with other algorithms will be performed. Also, an algorithm using the proximity operator of the ℓ_p-norm will be developed to solve the ℓ_p-regularized compressed sensing problem.

4.1   Applications

In the field of engineering, many application problems including image processing, compressed sensing are aiming to recover underlying image or signal from a degraded version. A degraded image or signal y can be modeled as

$$y = Mx + \eta, \tag{4.1}$$

where $x \in \mathbb{R}^n$ is the image or signal to be reconstructed, M is a $d \times n$ matrix that models the measurement process, and $\eta \in \mathbb{R}^d$ is an additive noise. In linear inverse problem (4.1), the goal is to recover image x when y and M are given. For different choices of M, recovering x becomes different application problems. For instance, it becomes the deblurring problem if M represents a blurring matrix; it becomes the inpainting problem if M represents a projection of an image onto some known pixels domain. If M is the identity matrix, it reduces to the denoising problem. If matrix M models incomplete measurement and x has (approximately) sparse representation, recovering x becomes a problem in compressed sensing. But linear inverse problem (4.1) is usually ill-posed in image processing or compressed sensing. For instance, in image deblurring, linear inverse problem (4.1) is ill-posed in the sense that the blurring matrix A is ill-conditioned and solution could be sensitive to the additive noise. With incomplete measurement in compressed sensing, linear inverse problem (4.1) has infinite number of solutions.

To recover the underlying image or signal x in (4.1), one powerful method is regularization method. A regularized model for model (4.1) can be derived from

Bayesian rule depending on the prior information of image or signal x to be recovered

and the type of the additive noise. In Bayesian approach, we assume that the degraded

image or signal y is a realization from a random vector Y and the underlying image

or signal x is a realization of another random vector X. By Bayesian formula, the

conditional *a posteriori* probability $p(x|y)$, the probability that x occurs when y is

observed, is given by

$$p(x|y) = \frac{p(y|x)p_X(x)}{p_Y(y)}. \tag{4.2}$$

To find an estimate of x, A maximum *a posteriori* expectation maximization could

be used by maximizing the conditional *a posteriori* probability $p(x|y)$. By taking

the negative logarithm of equation (4.2) and ignoring the constant term $\log p_Y(y)$, an

estimate of x is equivalent to a solution to the following minimization problem

$$\min_x \{-\log p(y|x) - \log p_X(x)\}. \tag{4.3}$$

The term $\log p_X(x)$ is used to regularize a solution from the assumption on prior

information of x. Gibbs prior is usually assigned to the random vector X in practice.

Hence, the prior $p_X(x)$ has form

$$p_X(x) = \frac{1}{T} e^{-\gamma \mathcal{E}(x)}, \tag{4.4}$$

where T is a normalization factor, γ is a positive number and $\mathcal{E}(x)$ is a given energy

function of x. The choice of the energy function varies from application to applica-

tion. In image processing, as one choice of energy function $\mathcal{E}(x)$, the total variation

$\|x\|_{\text{TV}}$ [66] has been extensively used due to the fact that the total variation is sensitive

to geometric features of images, such as edges. Another alternative is $\mathcal{E}(x) = \|Wx\|_1$, where W is a matrix representation of wavelet or framelet since natural images tend to be sparse in the wavelet or framlet domain[26, 30, 31, 65]. In compressed sensing, if the underlying signal itself is sparse, the ℓ_p-function $\|x\|_p^p$ with $0 \le p \le 1$ is appropriate for the energy function $\mathcal{E}(x)$ due to the fact that ℓ_p-norm is sparsity-promoting. While if the signal is not sparse itself but is sparse in the transformation domain associated with a linear transform T, then $\mathcal{E}(x) = \|Tx\|_p$ is suitable.

The expression $\log p(y|x)$ in (4.3) is viewed as a fidelity term measuring the discrepancy between the noisy observation y and an ideal one. The fidelity term $\log p(y|x)$ depends on the property of the additive noise η. For convenience, we assume the noise η is d-dimensional. When the noise η is of Gaussian type, it is assumed that the components η_i of η are independently and identically distributed(i.i.d.) from a Gaussian distribution $\mathcal{N}(0, \sigma^2)$. It follows that the likelihood $p(y|x) = (2\pi)^{-\frac{d}{2}} \sigma^{-d} e^{-\frac{\|y-Mx\|^2}{2\sigma^2}}$. Putting the expression $p_X(x)$ and $p(y|x)$ into (4.3) and ignoring the constant, we obtain an equivalent model of (4.3) when Gaussian noise is involved

$$\min_x \{\frac{1}{2}\|y - Mx\|^2 + \mu\mathcal{E}(x)\}, \tag{4.5}$$

where μ is a positive parameter related to the noise standard deviation σ and parameter γ in the Gibbs prior. As shown by model (4.5), an ℓ_2-fidelity term is appropriate for Gaussian noise corrupted data from statistics point of view. However, if the observation involves impulse noise rather than Gaussian noise, an ℓ_2-fidelity term is not suitable anymore. If the observation y is corrupted by salt-and-pepper noise (a

special type of impulse noise) with a noise level $0 < r < 1$, y can be modeled as

$$y_i = \begin{cases} 0, & \text{with probability } \frac{r}{2}, \\ 255, & \text{with probability } \frac{r}{2}, \\ (Mx)_i & \text{with probability } 1 - r, \end{cases} \tag{4.6}$$

where y_i is the i-th component of y. For observation corrupted by salt-pepper noise

given in (4.6), we have that

$$p(y|x) = (\frac{r}{2})^{|\{i:y_i \neq (Mx)_i\}|} \cdot (1-r)^{|\{i:y_i = (Mx)_i\}|}, \tag{4.7}$$

where $|S|$ denotes the number of elements in the set S. Note that $|\{i : y_i \neq (Mx)_i\}| = \|Mx - y\|_0$, where $\|\cdot\|_0$ denotes the number of non-zero elements in a vector. Then

the equation (4.7) becomes

$$p(y|x) = (1-r)^d (\frac{2}{r} - 2)^{-\|Mx-y\|_0}. \tag{4.8}$$

Putting the expression $p_X(x)$ and $p(y|x)$ into (4.3) and ignoring the constant, we

obtain an equivalent model of (4.3) when salt-and-pepper noise is involved

$$\min_x \{\|y - Mx\|_0 + \mu\mathcal{E}(x)\}, \tag{4.9}$$

where μ is a positive parameter related to the corruption percentage r and parameter

γ in the Gibbs prior. The non-convexity of the fidelity term $\|y - Mx\|_0$ introduces

numerical difficulties in solving the minimization problem (4.9). To overcome the

numerical difficulty resulted from the non-convexity of the term $\|y - Mx\|_0$, one way

is to relax the non-convex term $\|y - Mx\|_0$ to a convex function $\|y - Mx\|_1$. With

such a relaxation, model (4.9) becomes

$$\min_x\{\|y - Mx\|_1 + \mu\mathcal{E}(x)\}. \tag{4.10}$$

In fact, the ℓ_1-norm fidelity term was first proposed by Nikolova for the total variation regularization of images corrupted by impulse noise[58]. Its effectiveness in handling impulse noise can be also found in [19]. The suitability of replacing the ℓ_0-norm by the ℓ_1-norm was also addressed in compressed sensing[12].

The parameter μ in both (4.5) and (4.10) is called the regularization parameter and need be predetermined. This regularization parameter balances the fitness of observed data and preservation of prior information of underlying solution. If noise power is less, more weight should be placed on the fidelity(fitting) term and therefore smaller value of μ should be chosen; while bigger value of μ is desired if noise power is more. But it is still challenging to choose an appropriate regularization parameter in practice. If an estimated upper bound of the noise power is available, an unconstrained model can be substituted by a constrained model without introducing regularization parameter. In particular, if the involved noise is Gaussian type, a variant model of (4.5) has the form

$$\min_x\{\mathcal{E}(x) : \|y - Mx\| \le \epsilon\}, \tag{4.11}$$

where ϵ^2 is an estimated upper bound on the noise power of Gaussian noise. Between models (4.5) and (4.11), another difference is on the differentiability of the fidelity term. As a quadratic function, the fidelity term in (4.5) is differentiable, while the fidelity term in (4.11) that can be written as an indicator function is non-smooth.

The exact form of models (4.5), (4.10) and (4.11) is highly related to the type of noise in (4.1), the choice of regularization term and the matrix M. In the following, the ℓ_2-TV and ℓ_1-TV models and models in compressed sensing will be reviewed accordingly.

4.1.1   Applications to Image Deblurring

In this section, we first identify two well-known image deblurring models, namely the ℓ_2-TV and ℓ_1-TV models, as special cases of the general model (1.1). We then give details on how Algorithms 1 and 2 are applied. In particular, we present the explicit expressions of the proximity operators of f_1^* and f_2^*. Since the total variation (TV) is involved in both image deblurring models, we begin with presenting the discrete setting for total variation.

For convenience of exposition, we assume that an image considered has a size of $\sqrt{n} \times \sqrt{n}$. The image is treated as a vector in $\mathbb{R}^n$ in such a way that the ij-th pixel of the image corresponds to the $(i + (j-1)\sqrt{n})$-th component of the vector in $\mathbb{R}^n$. The total variation of the image x can be expressed as the composite function of a convex function $\psi : \mathbb{R}^{2n} \to \mathbb{R}$ and a $2n \times n$ matrix B. To define the matrix B, we

need a $\sqrt{n} \times \sqrt{n}$ difference matrix D as follows:

$$D := \begin{bmatrix} 0 & & & \\ -1 & 1 & & \\ & \ddots & \ddots & \\ & & -1 & 1 \end{bmatrix}.$$

The matrix D will be used to "differentiate" pixel values along rows or along columns

of an image matrix. Through the matrix Kronecker product $\otimes$, we define the $2n \times n$

matrix B by

$$B := \begin{bmatrix} I \otimes D \\ D \otimes I \end{bmatrix}, \tag{4.12}$$

where I is the $\sqrt{n} \times \sqrt{n}$ identity matrix. The matrix B will be used to "differentiate"

the entire image matrix. The norm of B is $\|B\|^2 = 8 \sin^2 \frac{(\sqrt{n}-1)\pi}{2\sqrt{n}}$ (see [54]).

We define $\psi : \mathbb{R}^{2n} \to \mathbb{R}$ at $v \in \mathbb{R}^{2n}$ as

$$\psi(v) := \sum_{i=1}^{n} \left\| [v_i, v_{n+i}]^\top \right\|. \tag{4.13}$$

Based on the definition of the $2n \times n$ matrix B and the convex function ψ, the

(isotropic) total variation of an image x can be denoted by $\psi(Bx)$, i.e.

$$\|x\|_{\mathrm{TV}} := \psi(Bx). \tag{4.14}$$

The ℓ_2-TV Image Deblurring Model

If the additive noise is Gaussian type, model (4.5) can be adopted. Using the total

variation as the energy function yields the ℓ_2-TV image deblurring model. The ℓ_2-TV

image deblurring model has the form of

$$\min\left\{\frac{1}{2}\|Mx - y\|^2 + \mu\|x\|_{\mathrm{TV}} : x \in \mathbb{R}^n\right\}, \tag{4.15}$$

where μ is a regularization parameter.

Now, let us set

$$m_1 = n, \quad m_2 = 2n, \quad f_1 := \frac{1}{2}\|\cdot - y\|^2, \quad f_2 := \mu\psi, \quad A_1 := M, \quad \text{and} \quad A_2 := B,$$

where ψ is given by (4.13) and B is defined by (4.12). Then the ℓ_2-TV image deblurring mode (4.15) can be viewed as a special case of model (1.1). In addition, $f_1 \in \Gamma_0(\mathbb{R}^n)$ and $f_2 \in \Gamma_0(\mathbb{R}^{2n})$. Therefore, both Algorithms 1 and 2 can be applied for the ℓ_2-TV model. Furthermore, we give the explicit forms of the proximity operators $\mathrm{prox}_{\alpha f_1^*}$ and $\mathrm{prox}_{\alpha f_2^*}$ for any positive number α. Actually, by the definition of Fenchel conjugate, we have

$$f_1^*(u) = \frac{1}{2}\|u\|^2 + \langle u, y\rangle.$$

By the definition of proximity operator, we have that for $u \in \mathbb{R}^n$

$$\mathrm{prox}_{\alpha f_1^*}(u) = \frac{1}{1+\alpha}u - \frac{\alpha}{1+\alpha}y.$$

By introducing the ℓ_2-ball $B = \{p \in \mathbb{R}^2 : \|p\| \leq \mu\}$, for $v \in \mathbb{R}^{2n}$ we have

$$f_2^*(v) = \sum_{i=1}^{n} \iota_B\bigl([v_i, v_{n+i}]^\top\bigr),$$

where the indicator function ι_B over the non-empty set B is defined by

$$\iota_B(p) = \begin{cases} 0 & \text{if } p \in B, \\ \infty & \text{otherwise} \end{cases}.$$

For $v \in \mathbb{R}^{2n}$, we write $z = \text{prox}_{\alpha f_2^*}(v)$. Then for $i = 1, 2, \ldots, n$, we have that

$$[z_i, z_{n+i}]^\top = \min\{\|[v_i, v_{n+i}]^\top\|, \mu\} \frac{[v_i, v_{n+i}]^\top}{\|[v_i, v_{n+i}]^\top\|}. \tag{4.16}$$

The ℓ_1-TV Image Deblurring Model

The ℓ_1-TV image deblurring model is usually used for the recovery of an unknown

image $x \in \mathbb{R}^n$ from an impulse noise corrupted observable data $y \in \mathbb{R}^n$ modeled by

(4.6), where M represents a blurring matrix and η is an impulse noise. To recover

the underlying image x from an observed data with impulse noise corruption, we

adopt model (4.10) with the ℓ_1-norm fidelity term. Replacing the energy function by

total variation yields the ℓ_1-TV image deblurring model. The ℓ_1-TV image deblurring

model has the form of

$$\min\{\|Mx - y\|_1 + \mu\|x\|_{TV} : x \in \mathbb{R}^n\}, \tag{4.17}$$

where μ is again the regularization parameter.

Now, let us set

$$m_1 = n, \quad m_2 = 2n, \quad f_1 := \|\cdot - y\|_1, \quad f_2 := \mu\psi, \quad A_1 := M, \quad \text{and} \quad A_2 := B,$$

where ψ is given by (4.13) and B is defined by (4.12). Then the ℓ_1-TV image de-

blurring mode (4.17) can be viewed as a special case of model (1.1). In addition,

$f_1 \in \Gamma_0(\mathbb{R}^n)$ and $f_2 \in \Gamma_0(\mathbb{R}^{2n})$. Therefore, both Algorithms 1 and 2 can be applied

for the ℓ_1-TV model. Further, the proximity operator $\text{prox}_{\alpha f_2^*}$ has been given via

(4.16). We jus need to present the proximity operator $\text{prox}_{\alpha f_1^*}$. Actually, we have

that for $u \in \mathbb{R}^n$

$$
(\mathrm{prox}_{\lambda f_1}(u))_i = \begin{cases} y_i + \mathrm{sign}(u_i - y_i)(|u_i - y_i| - \lambda), & \text{if } |u_i - y_i| \geq \lambda; \\ \\ y_i, & \text{otherwise,} \end{cases}
$$

where $i = 1, 2, \ldots, n$. Using the Moreau's identity $\mathrm{prox}_{\alpha f_1^*}(u) = u - \alpha \mathrm{prox}_{\frac{1}{\alpha} f_2}(\frac{u}{\alpha})$, we have that for $u \in \mathbb{R}^n$

$$
(\mathrm{prox}_{\alpha f_1^*}(u))_i = \begin{cases} \mathrm{sign}(u_i - \alpha y_i), & \text{if } |u_i - \alpha y_i| \geq 1; \\ \\ u_i - \alpha y_i, & \text{otherwise,} \end{cases}
$$

where $i = 1, 2, \ldots, n$.

In summary, for both the ℓ_2-TV and ℓ_1-TV image deblurring models, the associated proximity operators $\mathrm{prox}_{\alpha f_1^*}$ and $\mathrm{prox}_{\alpha f_2^*}$ have closed forms. As a consequence, the sequence $\{(u^k, v^k, x^k) : k \in \mathbb{N}\}$ generated by Algorithms 1 and 2 can be efficiently computed.

4.1.2 Application to Compressed Sensing

In this section, we consider the problems from compressed sensing. The breakthrough of the compressed sensing theory is that one can represent a signal at a rate significantly below the Nyquist sampling frequency [13]. The basic principle in compressed sensing is that a sparse or compressible signal can be reconstructed from a small number of measurements, measured through appropriate linear combinations of signal values, via an optimization approach. An essential goal in compressed sensing is to reconstruct the ideal signal from a small number of measurements. A key to this goal

is the notion of sparsity. It was shown mathematically in [13] that under the sparsity assumption, the signal can be exactly reconstructed from the given measurements and the chance of its being wrong is infinitesimally small. The sparsity of the signal can be captured by using regularization with the ℓ_1-norm or ℓ_p-norm with $0 \leq p < 1$. In the seminal work [11, 33], the compressed sensing problem was described as solving the ℓ_1-minimization problem subject to linear constrains that involve measurements and a measurement matrix. In the work[17, 18], an exact recovery of a sparse signal was described by solving the ℓ_p-minimization problem.

We identify the ℓ_1-minimization or ℓ_p-minimization problems in compressed sensing as special cases of the general composite minimization model (1.1). If the ℓ_1-norm is adopted for regularization, the composite minimization problem has convex objective function and proposed algorithms from chapter 2 can be applied. If the ℓ_p-regularization $(0 \leq q < 1)$is chosen, existing algorithms arising from convex minimization may be extended to solve the non-convex ℓ_p-minimization problem.

The ℓ_1-Regularization for Compressed Sensing

In this section, we consider the ℓ_1-regularized minimization problem from compressed sensing and identify it as a special case of the convex composite minimization model (1.1). The proposed algorithms from chapter 2 can be applied by providing explicit form of the proximity operators $\text{prox}_{\alpha f_1^*}$ and $\text{prox}_{\alpha f_2^*}$ for the specific functions f_1^* and f_2^*.

In compressed sensing, the signal of interest $x \in \mathbb{R}^n$ is assumed to have (approximately) sparse representation in some linear transform domain. A collected signal $y \in \mathbb{R}^{m_1}$ is modeled by (4.1), where M is an $m_1 \times n$ ($m_1 < n$) matrix and models the incomplete measurement. By convention, $\eta \in \mathbb{R}^{m_1}$ in (4.1) represents an additive Gaussian noise. The underlying signal x can be restored by solving the unconstrained model (4.5) or the constrained model (4.11) with an appropriate energy function $\mathcal{E}(x)$. If an upper bound of noise power is available and x has a sparse representation under a linear transform T (an $m_2 \times n$ matrix), restoring the underlying signal x can be formulated as solving the following ℓ_1-minimization problem

$$\min\{\|Tx\|_1 : x \in \mathbb{R}^n\}, \text{ subject to} \|Mx - y\| \leq \epsilon, \tag{4.18}$$

where ϵ^2 indicates the upper bound of noise power. Let $C := \{u \in \mathbb{R}^{m_1} : \|u-y\| \leq \epsilon\}$ and $f_1 := \iota_C$, $f_2 := \| \cdot \|_1$, $A_1 := M$, $A_2 := T$, then the minimization problem (4.18) can be viewed as a special case of the general problem (1.1). The conjugate function f_2^* of $f_2 = \| \cdot \|_1$ is the indicator function ι_B, where $B = \{v \in \mathbb{R}^{m_2} : \|v\|_\infty \leq 1\}$ represents the unit l_∞-ball. As a result, the proximity operator $\text{prox}_{\alpha f_2^*}(v)$ is the projection of v onto the set B. Indeed, we have for $v \in \mathbb{R}^{m_2}$

$$(\text{prox}_{\alpha f_2^*}(v))_i = \begin{cases} v_i, & \text{if } |u_i| \leq 1, \\ \text{sign}(u_i), & otherwise \end{cases},$$

for $i = 1, \cdots, m_2$. Since the function f_1 is an indicator function over the ℓ_2-ball C with center y and radius ϵ, the proximity operator $\text{prox}_{\lambda f_1}(u)$ is the projection of v

onto C, i.e.,

$$\text{prox}_{\lambda f_1}(u) = \begin{cases} u, & \text{if } \|u - y\| \leq \epsilon, \\ y + \frac{\epsilon}{\|u-y\|}(u - y), & \text{otherwise} \end{cases}.$$

Using the Moreau's identity $\text{prox}_{\alpha f_1^*}(u) = u - \alpha \text{prox}_{\frac{1}{\alpha}f_1}(\frac{u}{\alpha})$, we can get

$$\text{prox}_{\alpha f_1^*}(u) = \begin{cases} 0, & \text{if } \|u - \alpha y\| \leq \alpha\epsilon, \\ (1 - \frac{\alpha\epsilon}{\|u-\alpha y\|})(u - \alpha y), & \text{otherwise} \end{cases}.$$

As displayed above, the proximity operators $\text{prox}_{\alpha f_1^*}$ and $\text{prox}_{\alpha f_2^*}$ associated to model (4.18) have closed form. As a consequence, the sequence $\{(u^k, v^k, x^k) : k \in \mathbb{N}\}$ generated by Algorithms 1 and 2 can be efficiently computed as well for problem (4.18).

The ℓ_p-Regularization for Compressed Sensing

In this section, we consider the non-convex composite minimization problem with the ℓ_p-regularization ($0 < p < 1$) in compressed sensing. For the ℓ_p-regularization, researchers have shown their interest and considerable effort has been devoted to its study[7, 17, 18, 24, 37, 46, 53, 57, 69, 75]. It has been shown from numerical experiment that using the ℓ_p-norm promotes sparser solutions and lower prediction errors for model selection when compared to the use of the ℓ_1-norm[75]. Moreover, It has also been proven that fewer measurements as well as weaker conditions are required for sparse signal recovery[18, 46, 75]. For simplicity, it is assumed that the signal itself is sparse, i.e., the matrix T is the identity matrix. Replacing the ℓ_1-norm

in model (4.18) by the ℓ_p-norm yields the following variant model

$$\min_x \{\|x\|_p^p : \|Mx - y\| \leq \epsilon\}. \tag{4.19}$$

When $p = 1$, model (4.19) reduces to the constrained basis pursuit denoising model in [23], which is convex and has been solved by many algorithms, see, for example, [4, 34] and references therein. We also developed an accurate and efficient algorithm for solving the optimization problem with $p = 1$ in [20].

However, replacing the ℓ_1-norm by the ℓ_p-norm with $0 < p < 1$ results in a non-convex model in (4.19). Desirable properties involving Fenchel conjugate that are seen in proper semi-continuous convex function, would not be seen in the ℓ_p-norm. The proposed algorithms in chapter 2 would not work appropriately for the ℓ_p-minimization problem (4.19). In the numerical experiment for the non-convex ℓ_p-regularized compressed sensing, we will extend the algorithm for basis pursuit denoising model in our recent work[20] to solve the ℓ_p-minimization problem (4.19).

4.2 Numerical Experiments

In this section, numerical experiments are carried out to demonstrate the performance of our proposed Algorithms 1 and 2 for the image deblurring and the ℓ_1-regularized compressed sensing. Numerical performance of the ℓ_p-regularization for compressed sensing is also presented. For convex composite minimization problem, the Chambolle-Pock (CP) algorithm and ZBO algorithm[77] for (1.2) are compared

to the proposed algorithms from chapter 2 for the ℓ_2-TV, ℓ_1-TV image deblurring and the ℓ_1-regularized compressed sensing model (4.18). The ZBO algorithm proposed in [77] solves model (1.2) via the following scheme

$$
\begin{cases}
w^{k+1} = \operatorname{argmin}\left\{ f(w) - \langle \lambda^k, Ax^k - w\rangle + \frac{\beta}{2}\|Ax^k - w\|_2^2 \right. \\
\qquad\qquad \left. + \frac{1}{2}\|w - w^k\|_{Q_1}^2 : w \in \mathbb{R}^m \right\} \\
x^{k+1} = \operatorname{argmin}\left\{ -\langle \lambda^k, Ax - w^{k+1}\rangle + \frac{\beta}{2}\|Ax - w^{k+1}\|_2^2 \right. \qquad , \\
\qquad\qquad \left. + \frac{1}{2}\|x - x^k\|_{Q_2}^2 : x \in \mathbb{R}^n \right\} \\
\lambda^{k+1} = \lambda^k - \gamma(Ax^{k+1} - w^{k+1})
\end{cases}
\tag{4.20}
$$

where Q_1, Q_2 are positive definite matrices, and β, $\gamma > 0$. When Q_1 and Q_2 are chosen as $Q_1 = (\frac{1}{\alpha_1} - \beta)I$ and $Q_2 = \frac{1}{\alpha_2}I - \beta A^\top A$ respectively, scheme (4.20) has closed form. The positive definiteness of Q_1 and Q_2 ensures that $\alpha_1\beta < 1$ and $\alpha_2\beta < \frac{1}{\|A\|^2}$. Each algorithm is carried out until the stopping criterion $\|x^{k+1} - x^k\|^2/\|x^k\|^2 \le Tol$ is satisfied, where Tol representing the tolerance, will be specified differently in different applications.

4.2.1 Parameter Settings

Prior to applying Algorithms 1 and 2, the CP algorithm and the ZBO algorithm to the ℓ_2-TV model and the ℓ_1-TV model and the ℓ_1-regularized compressed sensing model, the parameters arising from those algorithms need to be determined. Convergence analysis of the algorithms specifies the relation between these parameters. Under the conditions on parameters that guarantee convergence, we notice that larger product

of the parameters results in faster convergence[20]. Therefore, once one parameter is fixed, the others can be described by this fixed one. To this end, we fix the value of the parameter β in each above algorithm and then figure out the values of the others. The setting of parameters is described as follow.

For Algorithm 1, the positive parameters α_1, α_2, and γ satisfy

$$\alpha_1 < \frac{1}{\beta\|A_1\|^2}, \quad \alpha_2 < \frac{1}{\beta\|A_2\|^2}, \quad \text{and} \quad \gamma \leq \beta. \tag{4.21}$$

For Algorithm 2, the parameters α and γ satisfy

$$\alpha < \frac{1}{\beta\|[A_1; A_2]\|^2} \quad \text{and} \quad \gamma \leq 2\beta. \tag{4.22}$$

For the CP algorithm (see (2.45)), we set

$$\alpha < \frac{2}{\beta\|[A_1; A_2]\|^2}. \tag{4.23}$$

For the ZBO algorithm, the parameters α_1, α_2, and γ satisfy

$$\alpha_1 < \frac{1}{\beta}, \quad \alpha_2 < \frac{1}{\beta\|[A_1; A_2]\|^2}, \quad \text{and} \quad \gamma \leq \beta. \tag{4.24}$$

With such settings on the parameters for the algorithms , the convergence of Algorithm 1, Algorithm 2, and the CP method are guaranteed by Theorem 2.13, Theorem 2.11, and a result from [15], respectively. With the given stopping criterion, the parameter β in each algorithm is chosen in a way that it would produce better recovered images in terms of PSNR value for image deblurring and β is chosen to produce better recovered signal in terms of ℓ_2-error for compressed sensing.

4.2.2 Numerical Results for Image Deblurring

In this section, numerical experiments for image deblurring are carried out to demonstrate the performance of our proposed Algorithms 1 and 2 for the 256×256 test images "Cameraman", "Peppers", "Goldhill" and 512×512 test image "Lena"'. The tolerance Tol in the stopping criterion is chosen to be 10^{-6}. The quality of the recovered images from each algorithm is evaluated by the peak-signal-to-noise ratio (PSNR), which is defined as PSNR $:= 20 \log_{10} \left(\frac{255n}{\|\tilde{x}-x\|} \right)$, where $x \in \mathbb{R}^n$ is the original image and $\tilde{x}$ represents the recovered image. The evolution curve of the function values with respect to iteration will be also adopted to evaluate the performance of algorithms.

In our simulations, blurring matrices M in model (4.1) for image deblurring are generated by a rotationally symmetric Gaussian lowpass filter of size "hsize" with standard deviation "sigma" from the MATLAB script `fspecial('gaussian',hsize,sigma)`. Such matrix M is referred to as the $(hsize, sigma)$-GBM. We remark that the norm of M is always 1, i.e.,

$$\|M\| = 1. \tag{4.25}$$

The $(15, 10)$-GBM and $(21, 10)$-GBM are used to generate blurred images in our experiments. To compute the pixel values under the operation of M and B near the boundary of images, we choose to use "symmetric" type for the boundary extension. Let B be the difference matrix defined by (4.12). We know $\|B\| < \sqrt{8}$. As a result, the parameters are set in the following way.

For Algorithm 1, we set the parameters α_1, α_2, and γ as follows:

$$\alpha_1 := \frac{0.999}{\beta}, \quad \alpha_2 := \frac{1}{8\beta}, \quad \text{and} \quad \gamma := \beta. \tag{4.26}$$

For Algorithm 2, we set the parameters α and γ as follows:

$$\alpha := \frac{1}{8\beta} \quad \text{and} \quad \gamma := 2\beta. \tag{4.27}$$

For the CP algorithm(see (2.45)), we set

$$\alpha := \frac{1}{4\beta}. \tag{4.28}$$

For the ZBO algorithm, we set the parameters α_1, α_2, and γ as follows:

$$\alpha_1 := \frac{0.999}{\beta}, \quad \alpha_2 := \frac{1}{8\beta}, \quad \text{and} \quad \gamma := \beta. \tag{4.29}$$

Numerical Results for the ℓ_2-TV Image Deblurring

In problems of image deblurring with the ℓ_2-TV model, a noisy image is obtained by blurring an ideal image with a $(hsize, sigma)$-GBM followed by adding white Gaussian noise. Two blurring matrices, namely $(21, 10)$-GBM and $(15, 10)$-GBM, are used in our experiments.

For blurring matrix $(21, 10)$-GBM, the white noise with mean zero and standard deviation 1 is added to blurred images while for blurring matrix $(15, 10)$-GBM, the additive white noise has mean zero and standard deviation 5. The regularization parameter in the ℓ_2-TV model (4.15) is set as $\mu = 0.02$ for blurring matrices $(21, 10)$-GBM and as $\mu = 0.2$ for blurring matrices $(15, 10)$-GBM. With these settings, numerical results for four test images "Cameraman", "Lena", "Peppers", and "Goldhill" are

reported in Table 4.1 for $(21, 10)$-GBM and in Table 4.2 for $(15, 10)$-GBM in terms of numbers of iterations, the CPU times, and the PSNR values. As shown in the Tables, Algorithm 1 performs best in terms of computational cost (total iterations and CPU time). The quality of the recovered images from Algorithm 1 is better than or comparable to the quality of recovered images from other algorithms in terms of PSNR values. The evolution curves of function values for each images are shown in Figures 4.1, 4.2, 4.3, and 4.4 for $(21, 10)$-GBM, and in Figures 4.5, 4.6, 4.7, and 4.8 for $(15, 10)$-GBM. Also, as shown in the Figures, the sequence of function values at $\{x^k : k \in \mathbb{N}\}$ generated by Algorithm 1 approaches the minimum value fastest, followed by sequences from Algorithm 2 and then by that from CP and ZBO algorithms. The performance of CP and ZBO algorithms is quite similar in terms of iterations, CPU time, PSNR and evolution of function values.

Method	Cameraman			Lena			Peppers			Goldhill		
	Itrs	CPU(s)	PSNR	Itrs	CPU(s)	PSNR	Itrs	CPU(s)	PSNR	Itrs	CPU(s)	PSNR
CP	177	18.82	23.09	157	107.57	26.45	205	21.10	25.38	166	16.64	24.80
ZBO	177	19.90	23.09	157	109.51	26.45	205	22.96	25.38	166	18.43	24.80
Alg. 2	151	15.98	23.35	140	93.92	26.66	171	17.17	25.61	152	15.48	24.87
Alg. 1	93	11.34	23.45	84	45.60	26.79	98	10.73	25.75	91	10.01	25.13

Table 4.1: Numerical results for the ℓ_2-TV model for images blurred by the $(21, 10)$-GBM.

Method	Cameraman			Lena			Peppers			Goldhill		
	Itrs	CPU(s)	PSNR	Itrs	CPU(s)	PSNR	Itrs	CPU(s)	PSNR	Itrs	CPU(s)	PSNR
CP	88	8.00	22.88	77	51.82	26.12	89	8.64	23.98	76	7.42	24.27
ZBO	84	8.95	22.88	77	54.50	26.12	89	9.42	23.98	76	8.06	24.27
Alg. 2	81	7.76	23.11	76	50.59	26.17	86	8.45	24.19	75	7.53	24.26
Alg. 1	50	5.18	23.00	46	23.75	26.12	50	5.15	24.13	44	4.68	24.29

Table 4.2: Numerical results for the ℓ_2-TV model for images blurred by the $(15, 10)$-GBM.

Numerical Results for the ℓ_1-TV Image Deblurring

In problems of image deblurring with the ℓ_1-TV model, a noisy image is obtained by blurring an ideal image with a $(hsize, sigma)$-GBM followed by adding impulse noise. Two blurring matrices, namely $(21, 10)$-GBM and $(15, 10)$-GBM, are used again in our experiments.

For the blurring matrix $(21, 10)$-GBM, the impulse noise with noise level $p = 0.3$ is added to blurred images while the additive impulsive noise has noise level $p = 0.5$ for the blurring matrix $(15, 10)$-GBM. We set the regularization parameter $\mu = 0.01$ for $(21, 10)$-GBM and $\mu = 0.02$ for $(15, 10)$-GBM in the ℓ_1-TV model (4.17). With these settings, numerical results for four test images "Cameraman", "Lena", "Peppers", and "Goldhill" are reported in Table 4.3 for $(21, 10)$-GBM and in Table 4.4 for $(15, 10)$-GBM in terms of numbers of iterations, the CPU times, and the PSNR values. One can observed from the Tables that Algorithm 1 yields higher PSNR value and consumes less CPU time than Algorithm 2, CP and ZBO algorithms. The evolution curves of function values with respect to iteration are shown in Figure
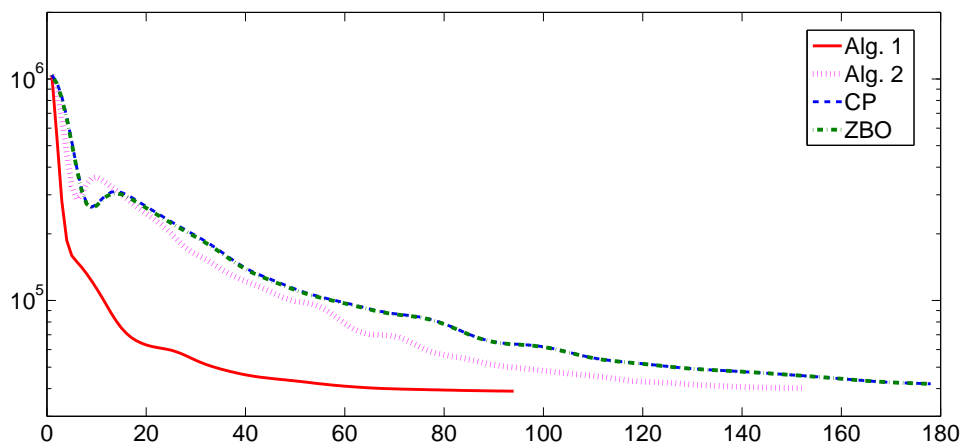
Figure 4.1: Evolution of function values for the ℓ_2-TV model for image "Cameraman" blurred by the $(21, 10)$-GBM.

4.9, 4.10, 4.11 and 4.12 for $(21, 10)$-GBM, and in Figure 4.13, 4.14, 4.15 and 4.16 for $(15, 10)$-GBM. It can be noticed that sequence of function values generated from Algorithm 1 approaches the minimum value fastest. Further, visual quality of the deblurred images is shown in Figure 4.17 and Figure 4.18 for each algorithm. The visual improvement by Algorithm 1 over CP and the ZBO algorithm can be seen by the deblurred images.

Method	Cameraman			Lena			Peppers			Goldhill		
	Itrs	CPU(s)	PSNR	Itrs	CPU(s)	PSNR	Itrs	CPU(s)	PSNR	Itrs	CPU(s)	PSNR
CP	367	44.39	23.47	354	241.09	26.53	414	45.57	25.73	381	42.07	25.05
ZBO	368	45.09	23.48	355	251.43	26.53	415	47.70	25.74	382	44.28	25.04
Alg. 2	275	29.92	23.57	272	194.29	26.69	315	34.68	25.82	312	34.56	25.16
Alg. 1	192	21.34	24.22	189	136.42	27.38	207	22.79	26.66	208	23.09	25.74

Table 4.3: Numerical results for the ℓ_1-TV model for images blurred by the $(21, 10)$-GBM.
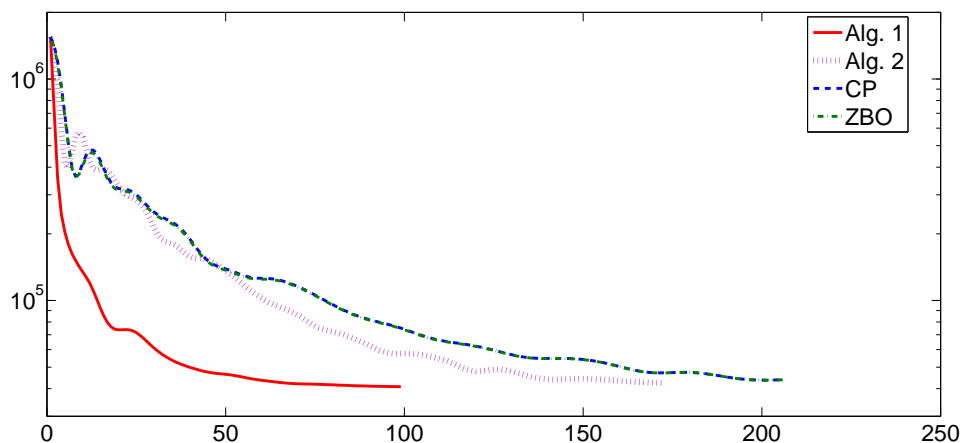
Figure 4.2: Evolution of function values for the ℓ_2-TV model for image "Peppers" blurred by the $(21, 10)$-GBM.

4.2.3 Numerical Results for the ℓ_1-Regularized Compressed Sensing

This section will be devoted to the comparison of Algorithm 1 to CP and ZBO for the ℓ_1-regularized compressed sensing problem (4.18). we assume that the underlying signal is not necessarily sparse itself, but is sparse when mapped to another domain via linear transform.

First of all, we describe how the signals are generated. The underlying signal we
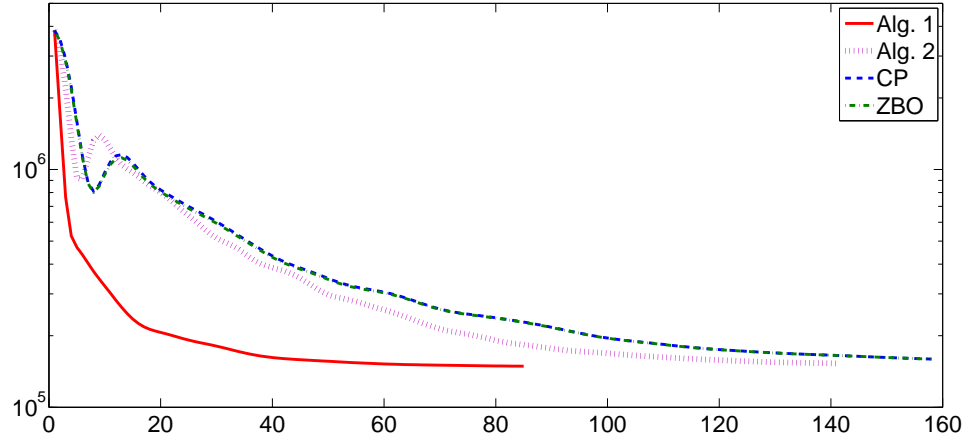
Figure 4.3: Evolution of function values for the ℓ_2-TV model for image "Lena" blurred by the $(21, 10)$-GBM.

consider is obtained by sampling the piecewise linear function

$$
s(t) = \begin{cases}
1 + 2t, & 0 \leq t \leq 1 \\
3, & 0 < t \leq 2 \\
5 - t, & 2 < t \leq 3 \\
2, & 3 < t \leq 4 \\
6 - t, & 4 < t \leq 5
\end{cases} \cdot \tag{4.30}
$$

To obtain the original test signal, we take 512 sample points with equal width from the function (4.30).The original test signal is shown in Figure 4.19. The $m_1 \times n$ random matrix M whose entries are i.i.d. from standard normal distribution $\mathcal{N}(0, 1)$ is given in advance. The norm of M denoted by $\|M\|$ can be calculated by MATLAB script `norm(M)`. The observed signal is acquired after the underlying signal passes by the measurement matrix M and is contaminated by Gaussian noise, which is modeled
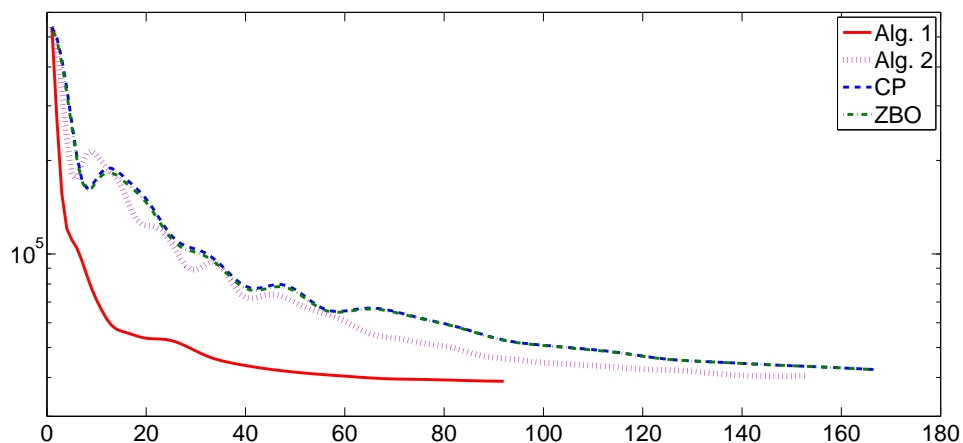
Figure 4.4: Evolution of function values for the ℓ_2-TV model for image "Goldhill" blurred by the $(21, 10)$-GBM.

by equation (4.1).

Further, to use model (4.18), an appropriate matrix T by which the original signal is mapped to a sparse signal, and the parameter ϵ indicating the noise power need be determined. With the given original signal as in Figure 4.19, a good choice of T will be a matrix that represents the high-pass filters of a framelet. Specifically, the high-pass filters associated with T are chosen as $h_1 = \frac{\sqrt{2}}{4}[1, 0, -1]$ and $h_2 = \frac{1}{4}[-1, 2, -1]$. With symmetric extension on the boundary of the signal, the matrix T of size $2n \times n$

Figure 4.5: Evolution of function values for the ℓ_2-TV model for image "Cameraman" blurred by the $(15, 10)$-GBM.

associated with those two high-pass filters has explicit form

$$
T =
\left[
\begin{array}{c|c}
\begin{array}{ccccc}
\sqrt{2}/4 & -\sqrt{2}/4 & & & \\
\sqrt{2}/4 & 0 & -\sqrt{2}/4 & & \\
& \ddots & \ddots & \ddots & \\
& & \sqrt{2}/4 & 0 & -\sqrt{2}/4 \\
& & & \sqrt{2}/4 & -\sqrt{2}/4
\end{array} \\
\hline
\begin{array}{ccccc}
1/4 & -1/4 & & & \\
-1/4 & 2/4 & -1/4 & & \\
& \ddots & \ddots & \ddots & \\
& & -1/4 & 2/4 & -1/4 \\
& & & -1/4 & 1/4
\end{array}
\end{array}
\right],
\tag{4.31}
$$

where the upper half corresponds to the high-pass filter h_1 and the lower half corre-
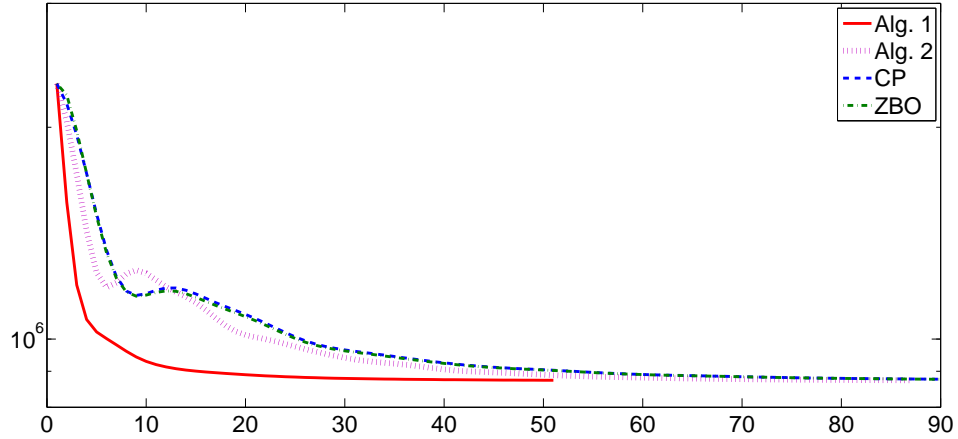
Figure 4.6: Evolution of function values for the ℓ_2-TV model for image "Peppers" blurred by the $(15, 10)$-GBM.

sponds to the other high-pass filter h_2. The norm $\|T\| \leq 1$ since T only contains the part of high-pass filters of a tight frame system. The parameter of noise power is set as $\epsilon = \sqrt{m_1}\sigma$, where σ represents the variance of the Gaussian noise. Regarding the variance of the noise, we will choose $\sigma = 0.05$ and $\sigma = 0$ in our experiment. In the case $\sigma = 0$, it implies that the observed signal is noise free. For different noise level, we set Tol differently. When $\sigma = 0.05$ Tol is set to be 10^{-4}, while it is set to be 10^{-6} when $\sigma = 0$. The maximal number of iterations allowed for each algorithm is set to 5,000.

To solve model (4.18), Algorithm 1, CP and ZBO will be applied. The setup of parameters α introduced in those algorithms are chosen in the similar manner as in image deblurring discussed earlier. That is, if β is assumed to be predetermined, α's and γ's are set to be as large as possible under the condition that the convergence
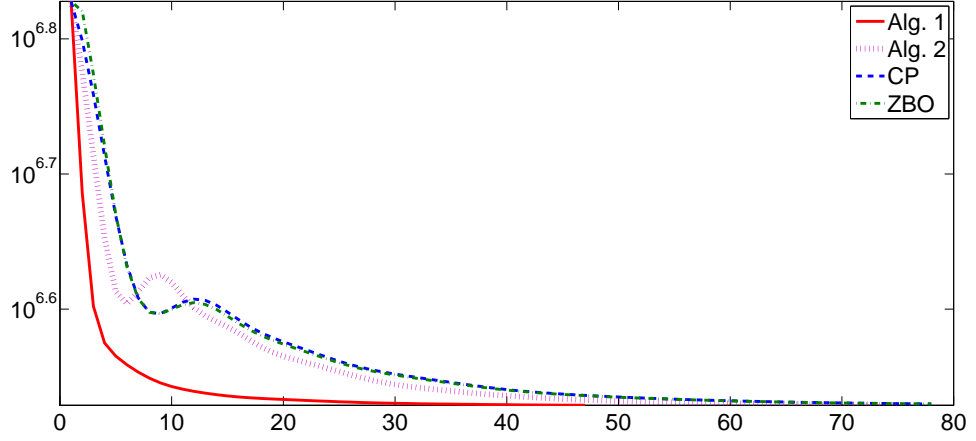
Figure 4.7: Evolution of function values for the ℓ_2-TV model for image "Lena" blurred by the $(15, 10)$-GBM.

is guaranteed. The parameter β for each algorithm is chosen such that it will yield smaller relative ℓ_2-error. The setting of parameters is described as follow.

For Algorithm 1, the positive parameters α_1, α_2, and γ satisfy

$$\alpha_1 := \frac{0.999}{\beta \|M\|^2}, \quad \alpha_2 := \frac{0.999}{\beta}, \quad \text{and} \quad \gamma := \beta. \tag{4.32}$$

For the CP algorithm (see (2.45)), we set

$$\alpha := 2 \frac{0.999}{\beta \|[M; T]\|^2}. \tag{4.33}$$

For the ZBO algorithm, the parameters α_1, α_2, and γ satisfy

$$\alpha_1 := \frac{0.999}{\beta}, \quad \alpha_2 := \frac{0.999}{\beta \|[M; T]\|^2}, \quad \text{and} \quad \gamma := \beta. \tag{4.34}$$

Numerical experiment is conducted on different settings on the $m_1 \times n$ measurement matrix M and on the variance σ of the Gaussian noise. With the given original
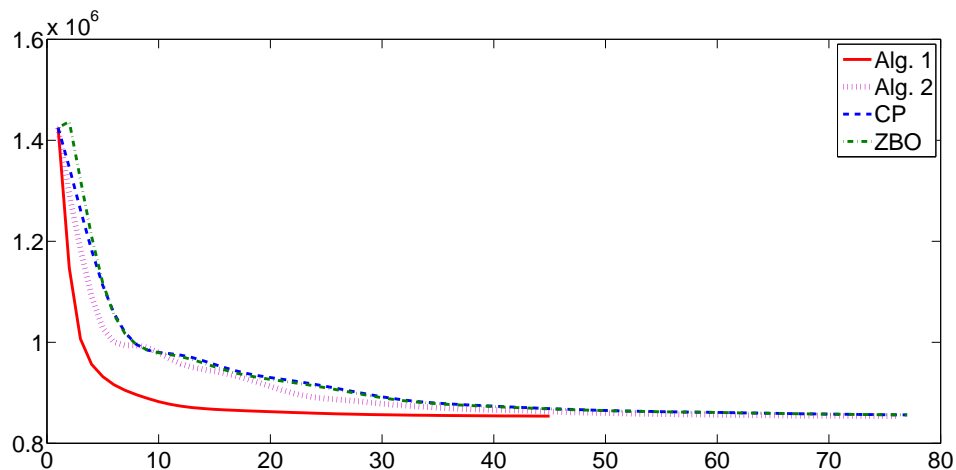
Figure 4.8: Evolution of function values for the ℓ_2-TV model for image "Goldhill" blurred by the $(15, 10)$-GBM.

signal shown in Figure 4.19, one should notice that $n = 512$. For each setting of m_1 and σ, Table 4.5 reports the performance of each algorithms in terms of iteration, CPU time consumed, relative ℓ_2-error and absolute error under the same stopping criterions. Figures 4.20, 4.21, 4.22 and 4.23 show the evolution curves of function values with respect to iteration. Figures 4.24, 4.25, 4.26 and 4.27 show the relative ℓ_2-error respectively with respect to iteration. One can easily observe that Algorithm 1 outperforms CP and ZBO algorithms dramatically for all of the metrics. Smaller relative ℓ_2-error and function values can be achieved much faster from Algorithm 1.

Method	Cameraman			Lena			Peppers			Goldhill		
	Itrs	CPU(s)	PSNR	Itrs	CPU(s)	PSNR	Itrs	CPU(s)	PSNR	Itrs	CPU(s)	PSNR
CP	280	29.78	23.77	289	200.71	27.15	300	31.85	25.75	294	32.01	25.15
ZBO	281	31.51	23.77	290	209.85	27.15	300	35.82	25.74	295	32.82	25.15
Alg. 2	228	24.14	24.20	235	170.57	27.55	250	26.59	26.28	247	26.56	25.52
Alg. 1	147	16.10	24.42	149	108.95	27.89	153	16.37	26.61	151	16.06	25.76

Table 4.4: Numerical results for the ℓ_1-TV model for images blurred by the $(15, 10)$-GBM.

		Alg. 1				CP				ZBO			
m_1	σ	Itrs	CPU(s)	ℓ_2-err	ℓ_∞-err	Itrs	CPU(s)	ℓ_2-err	ℓ_∞-err	Itrs	CPU(s)	ℓ_2-err	ℓ_∞-err
$n/2$	0.05	195	0.3750	1.38e-3	1.77e-2	3455	3.3281	5.73e-3	3.80e-2	4052	3.6718	5.28e-3	3.76e-2
$n/4$	0.05	313	0.1718	1.87e-3	4.27e-2	4740	1.7031	8.29e-3	6.21e-2	4345	1.8281	8.57e-3	6.83e-2
$n/2$	0.0	613	0.7344	6.46e-6	5.35e-5	5000	4.2343	3.51e-3	3.10e-2	5000	4.4375	3.95e-3	2.89e-2
$n/4$	0	1840	0.7500	1.99e-5	1.55e-4	5000	1.8125	6.30e-3	5.16e-2	5000	2.28125	6.57e-3	5.65e-2

Table 4.5: Numerical results for the ℓ_1-regularized compressed sensing.

4.2.4 Numerical Results for the ℓ_p-Regularized Compressed Sensing

This section is devoted to showing the numerical performance of the ℓ_p-regularization for compressed sensing. We demonstrate numerically that the ℓ_p-regularization with $0 < p < 1$ often performs better than the ℓ_1-regularization for compressed sensing in terms of the quality of recovered sparse signals.

We begin with a description on the sensing matrix and sparse signals. In our experiments, the sensing matrix M of size $m \times n$ $(m < n)$ is a random matrix whose elements are generated independently from standard normal distribution $\mathcal{N}(0, 1)$. According to [4], a length-n, s-sparse signal (a signal having exactly s nonzero com-
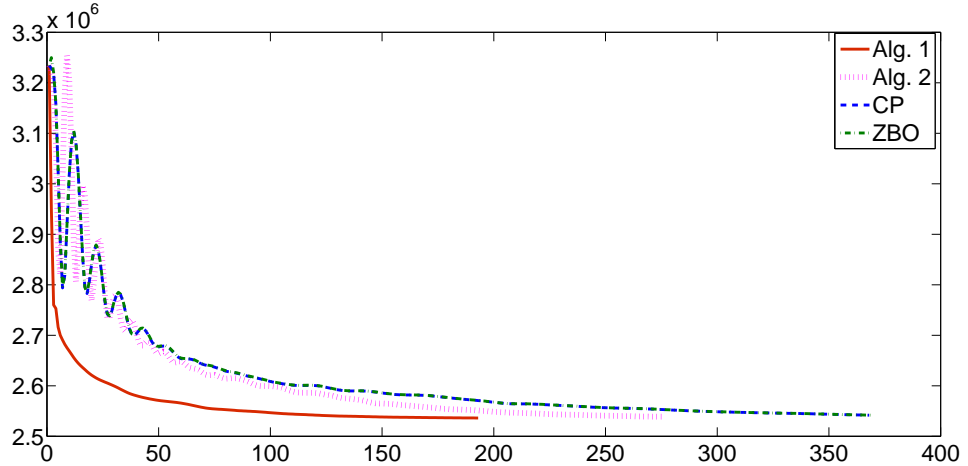
Figure 4.9: Evolution of function values for the ℓ_1-TV model for image "Cameraman" blurred by the $(21, 10)$-GBM.

ponents) x in our experiments, is generated in such a way that non-zero components are given by

$$\eta_1 10^\theta, \tag{4.35}$$

where $\eta_1 = \pm 1$ with probability $1/2$ and θ is uniformly distributed in $[0, 1]$. The locations of the nonzero components are randomly permuted. Clearly, the range of the magnitude of nonzero components of an s-sparse signal is $[1, 10]$. The sparsity s is chosen to be $0.01n$. The noisy observed signal $y \in \mathbb{R}^m$ is obtained by equation (4.1), where the entries in the noise vector η are i.i.d. from a Gaussian distribution with mean zero and standard variance σ. The standard deviation σ is chosen as 0.05.

The underlying sparse signal x to be recovered is formulated as a solution to the ℓ_p-regularized minimization problem (4.19), where $\epsilon = \sqrt{m}\sigma$ denotes the upper bound of noise power. The extension of an algorithm proposed in [20] to solve problem
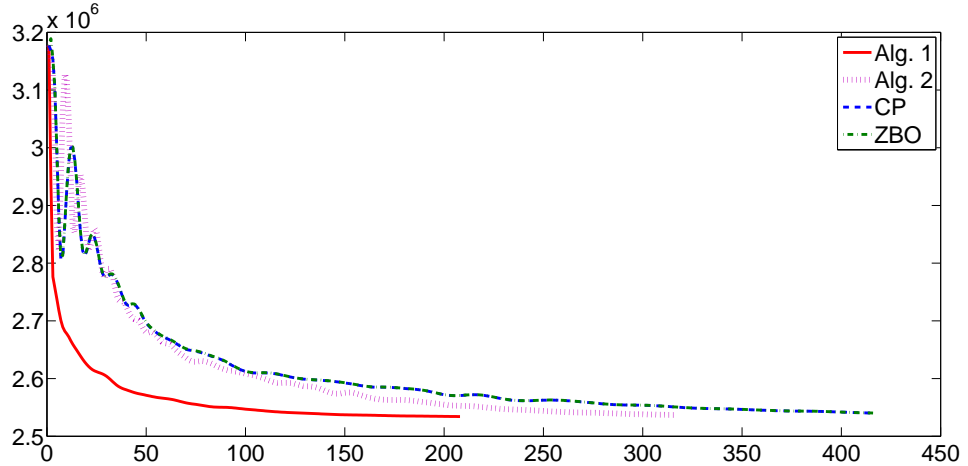
Figure 4.10: Evolution of function values for the ℓ_1-TV model for image "Peppers" blurred by the $(21, 10)$-GBM.

(4.19) with $p < 1$ is described in Algorithm 4. The key step in the implementation of Algorithm 4 is to evaluate the proximity operator of the ℓ_p-norm which can be efficiently computed by Algorithm 3. We remark that the convergence analysis of Algorithm 4 was already given in [20] for $p = 1$, but is unknown for $p < 1$ due to the difficulty caused by the non-convexity of the corresponding cost function of problem (4.19).

In our numerical experiments, we will investigate the performance of model (4.19) using Algorithm 4 for various values of $p \in \{0, 1/2, 2/3, 4/5, 1\}$. The maximum number of iterations of Algorithm 4 is set to be 1000. The accuracy of a solution obtained from Algorithm 4 with a specific value of p is quantified by the relative ℓ_2-error and the absolute ℓ_∞-error defined, respectively, as follows:

$$\|x - x_\diamond\|/\|x\| \text{ and } \|x - x_\diamond\|_\infty, \tag{4.36}$$

Algorithm 4: Algorithm for model (4.19)

Input: Initialization: $v^0 \in \mathbb{R}^m$, $x^0 \in \mathbb{R}^n$, $\epsilon > 0$, $\alpha > 0$, and $\beta > 0$ with

$\frac{\beta}{\alpha} < \frac{1}{\|M\|^2}$; set $v^{-1} = v^0 - (Ax^0 - y)$;

Result: x^∞

while *it is not convergent* **do**

Step 1:

$$x^{k+1} \leftarrow \mathcal{T}_{\frac{1}{\alpha}, p}\left(x^k - \frac{\beta}{\alpha}A^\top(2v^k - v^{k-1})\right)$$

Step 2: Denote $p^k := Ax^{k+1} + v^k - y$.

$$v^{k+1} \leftarrow \begin{cases} 0, & \text{if } \|p^k\|_2 < \epsilon; \\ \left(1 - \frac{\epsilon}{\|p^k\|_2}\right)(p^k), & \text{otherwise.} \end{cases}$$
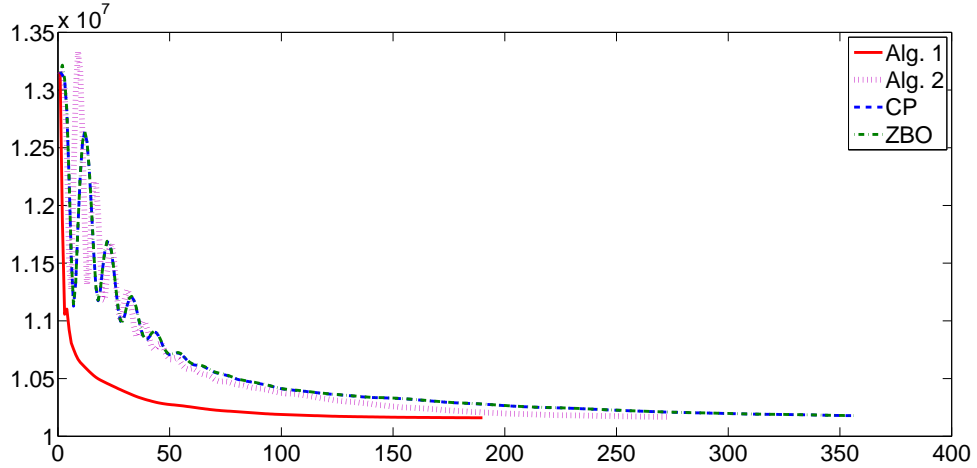
Figure 4.11: Evolution of function values for the ℓ_1-TV model for image "Lena" blurred by the $(21, 10)$-GBM.

where x is the true data and $x_\diamond$ is the restored data by Algorithm 4. All those errors reported in this section are the means and standard derivation of these relative errors from simulations that were performed 50 trials.

To use Algorithm 4, one needs to fix the parameters α and β such that $\beta/\alpha < \frac{1}{\|A\|^2}$. It has been demonstrated numerically in [20] that Algorithm 4 for $p = 1$ performs best in terms of the errors in (4.36) for a large ratio β/α. Therefore, we set $\beta = \frac{0.999}{\|A\|^2}\alpha$ in our numerical experiments. In such the way, α is essentially the only parameter that needs to be determined. The parameter α is chosen such that it would produce relatively optimal average error over the 50 trials.

The parameters used in our experiments are $n = 4096$, $m \in \{256, 512\}$ and $p \in \{0, 1/2, 2/3, 4/5, 1\}$. The numerical results over 50 trials are reported in Table 4.6 and Figure 4.28, 4.29. For $m = 512$, one can see that the performance of Algorithm
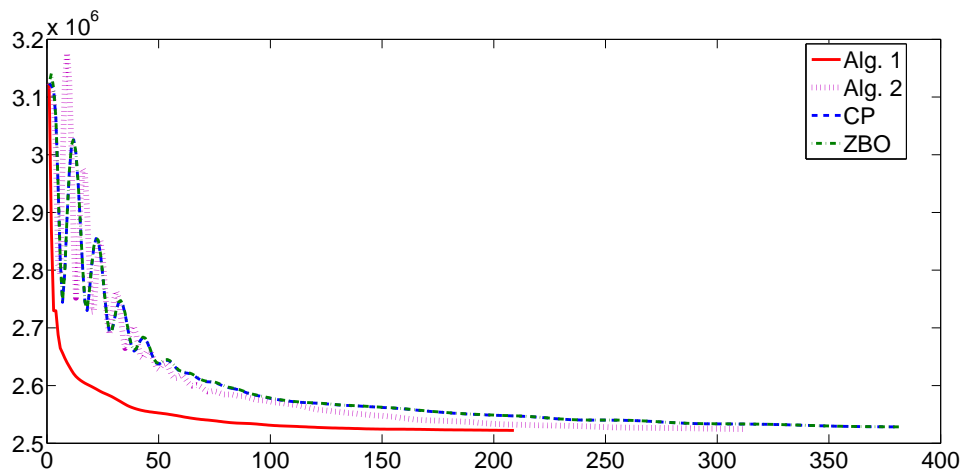
Figure 4.12: Evolution of function values for the ℓ_1-TV model for image "Goldhill" blurred by the $(21, 10)$-GBM.

4 with $p \in \{0, 1/2, 2/3, 4/5\}$ is comparable, but better than that with $p = 1$. For $m = 256$, the performance of Algorithm 4 with $p \in \{1/2, 2/3, 4/5\}$ is comparable, but better than that with $p \in \{0, 1\}$. We can conclude that Algorithm 4 with $0 < p < 1$ performs superiorly to that with $p = 0,\ 1$ in terms of accuracy and robustness, particularly, in the scenario of a small number of measurements.
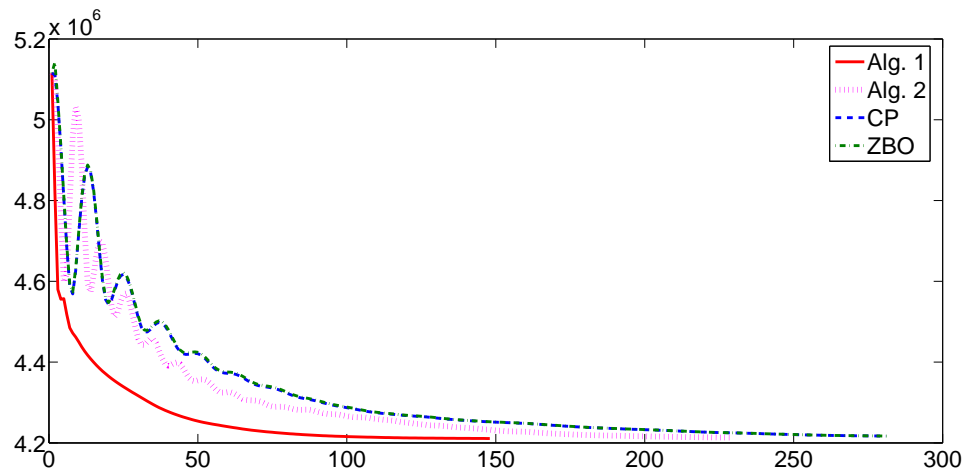
Figure 4.13: Evolution of function values for the ℓ_1-TV model for image "Cameraman" blurred by the $(15, 10)$-GBM.
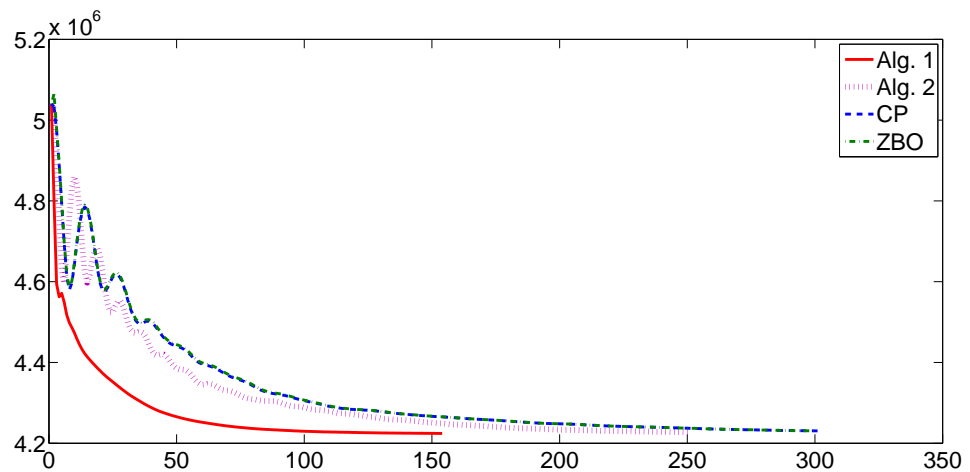
Figure 4.14: Evolution of function values for the ℓ_1-TV model for image "Peppers" blurred by the $(15, 10)$-GBM.
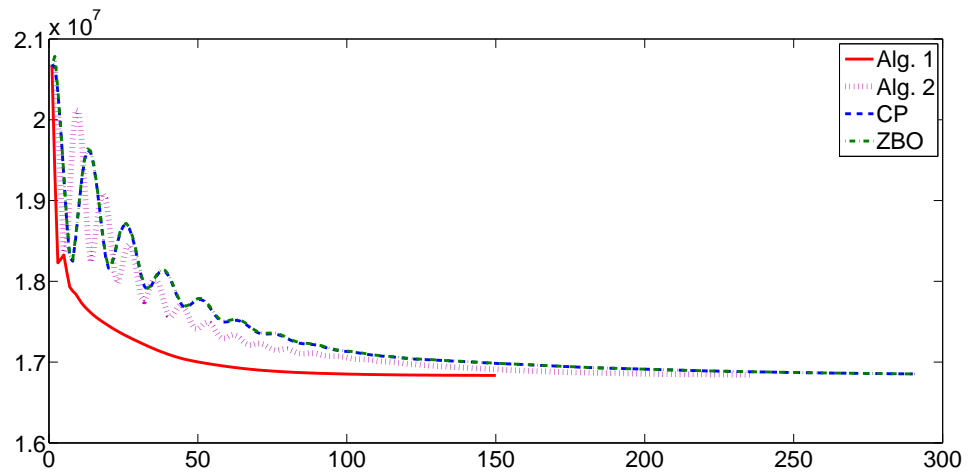
Figure 4.15: Evolution of function values for the ℓ_1-TV model for image "Lena" blurred by the $(15, 10)$-GBM.
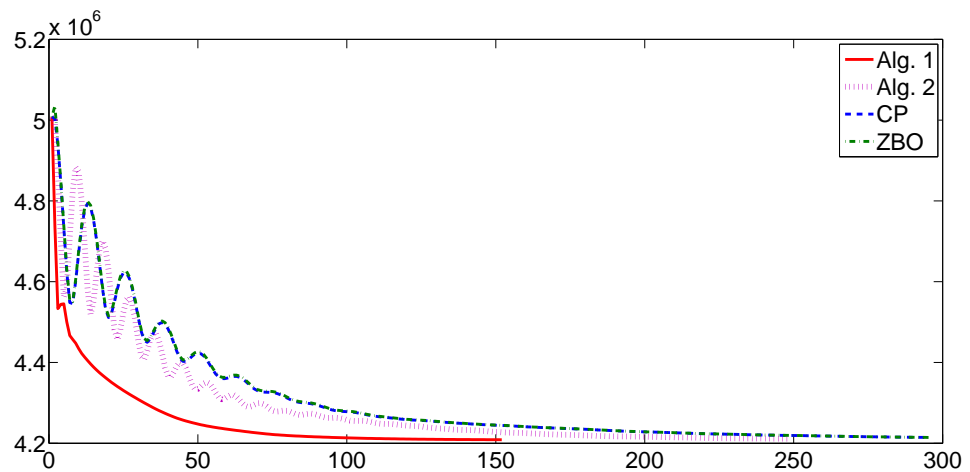
Figure 4.16: Evolution of function values for the ℓ_1-TV model for image "Goldhill" blurred by the $(15, 10)$-GBM.

Figure 4.17: Recovered images of "Cameraman", "Lena", "Peppers", and "Goldhill" (from top row to bottom row) with the ℓ_1-TV model for images blurred by the $(21, 10)$-GBM and corrupted by impulsive noise of level $p = 0.3$. Row 1: the CP; Row 2: ZBO; Row 3: Algorithm 2; Row 4: Algorithm 1.

Figure 4.18: Recovered images of "Cameraman", "Lena", "Peppers", and "Goldhill" (from top row to bottom row) with the ℓ_1-TV model for images blurred by the $(15, 10)$-GBM and corrupted by impulsive noise of level $p = 0.5$. Row 1: the CP; Row 2: the ZBO; Row 3: Algorithm 2; Row 4: Algorithm 1.
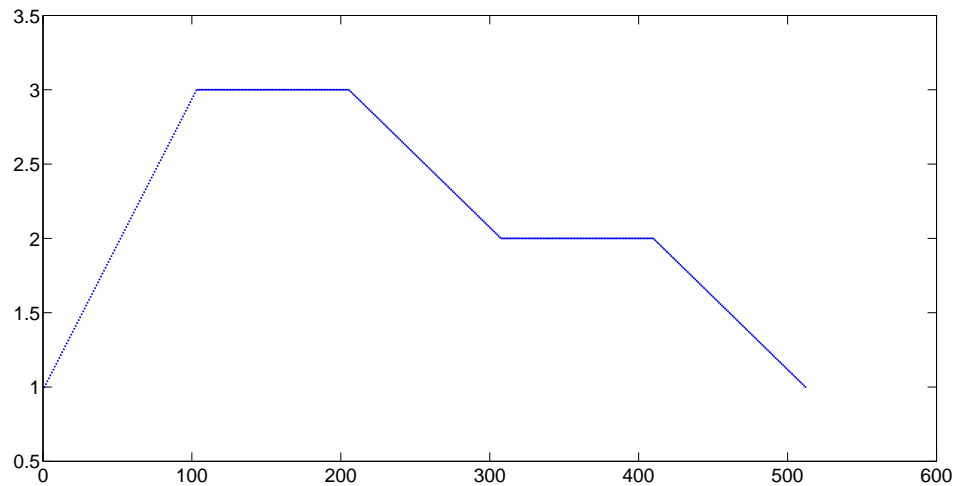
Figure 4.19: Original test signal for the ℓ_1-regularized compressed sensing.
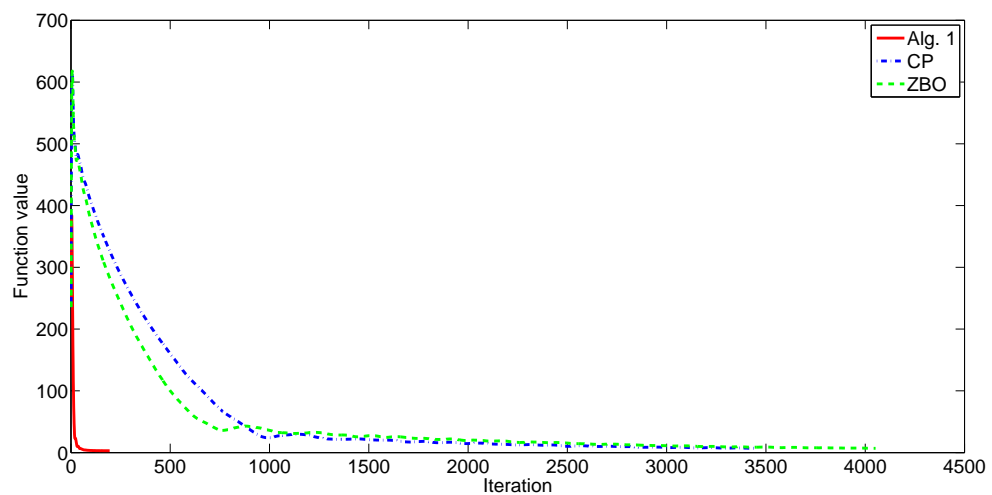
Figure 4.20: Evolution of function values for model (4.18) of compressed sensing with respect to iteration. $m_2 = n/2$, $\sigma = 0.05$.
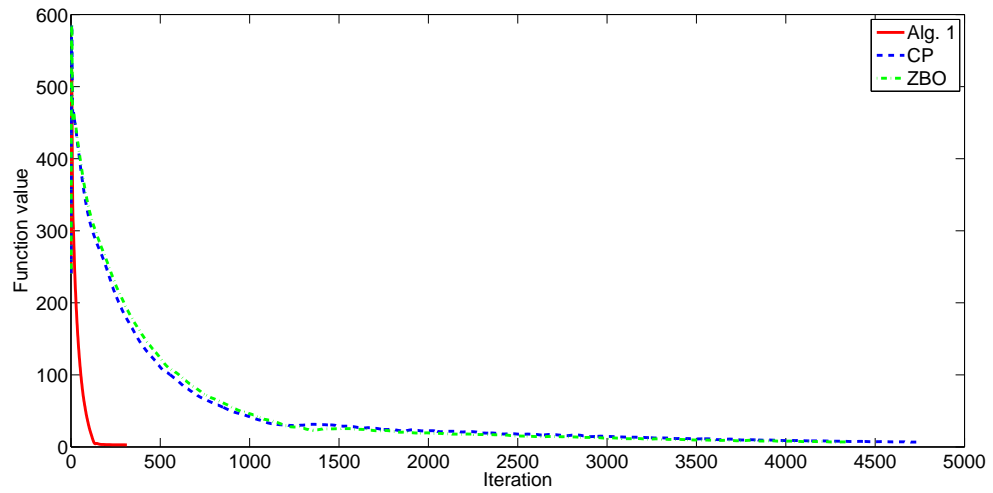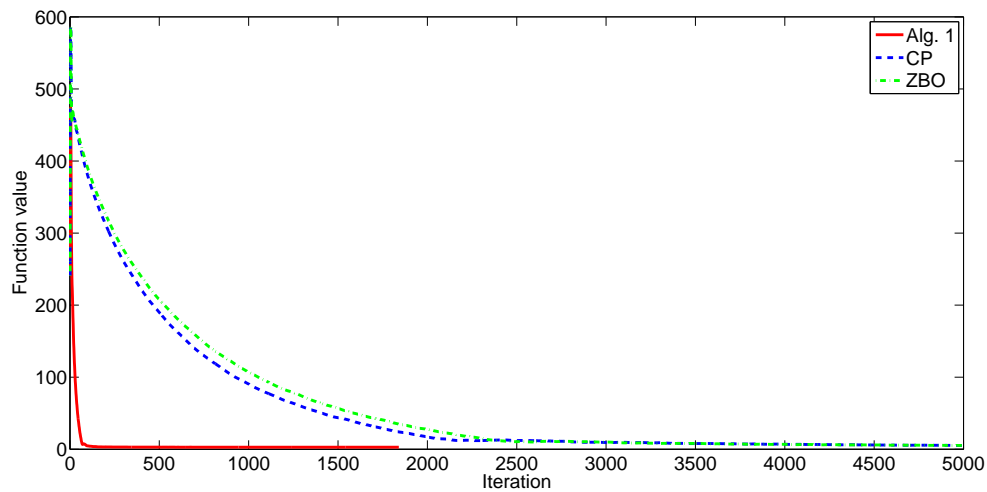
Figure 4.21: Evolution of function values for model (4.18) of compressed sensing with respect to iteration. $m_2 = n/4$, $\sigma = 0.05$.
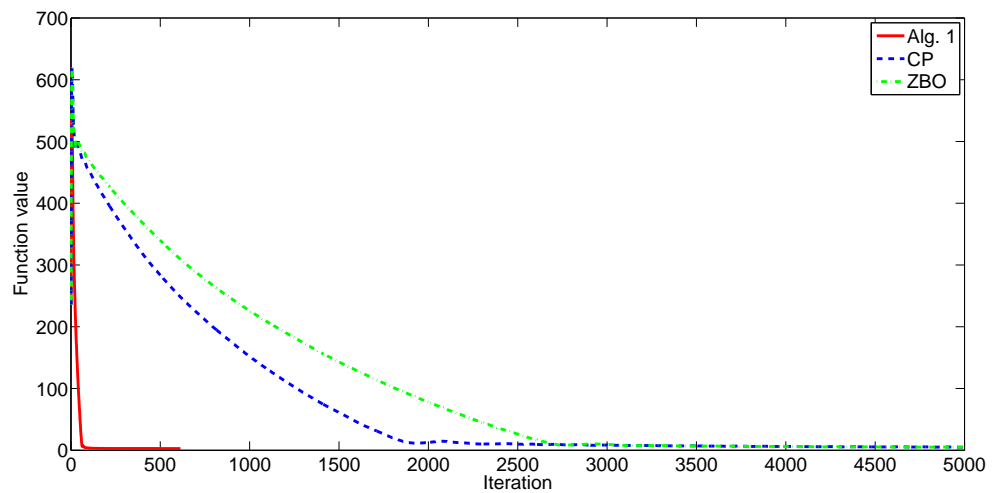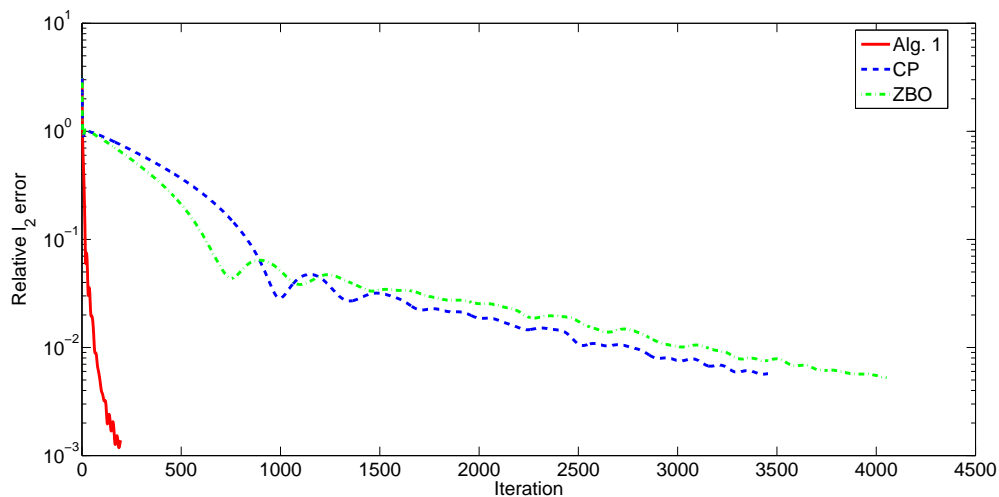

Figure 4.22: Evolution of function values for model (4.18) of compressed sensing with respect to iteration. $m_2 = n/2$, $\sigma = 0$.

Figure 4.23: Evolution of function values for model (4.18) of compressed sensing with respect to iteration. $m_2 = n/4, \ \sigma = 0$.
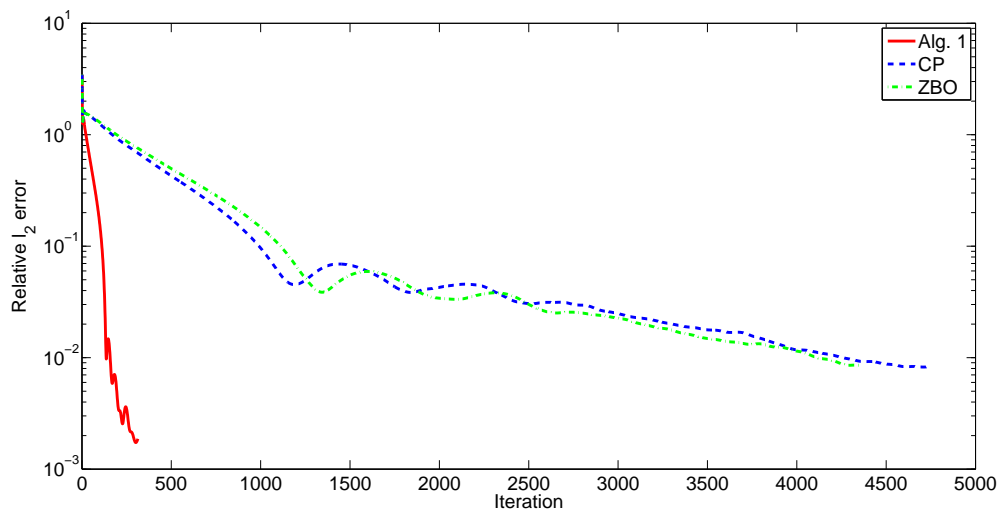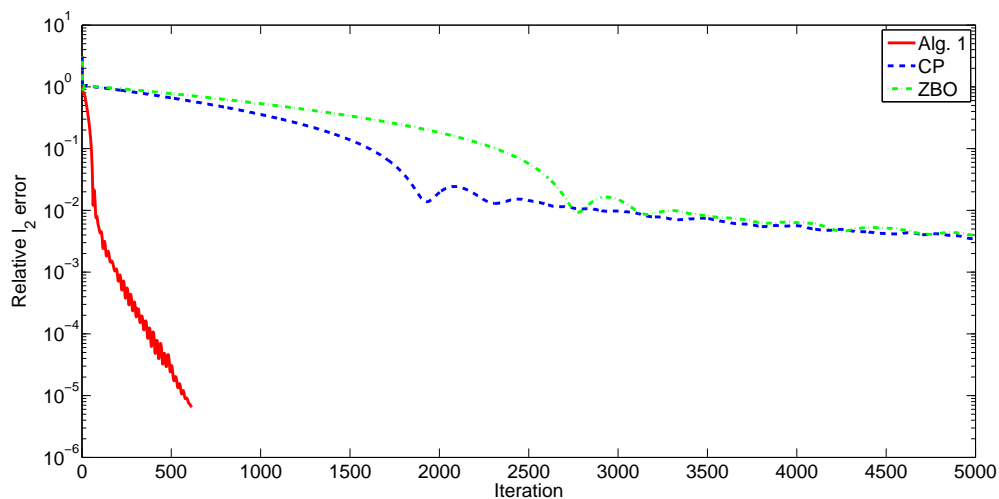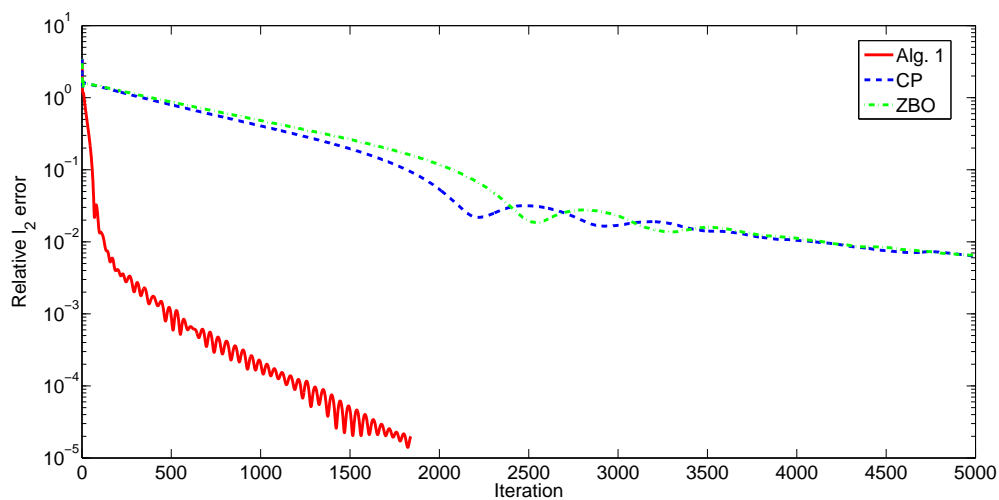

Figure 4.24: Evolution of relative ℓ_2-error of recovered signal with respect to iteration. $m_2 = n/2, \ \sigma = 0.05$

Figure 4.25: Evolution of relative ℓ_2-error of recovered signal with respect to iteration. $m_2 = n/4, \ \sigma = 0.05$.

Figure 4.26: Evolution of relative ℓ_2-error of recovered signal with respect to iteration. $m_2 = n/2, \ \sigma = 0$.

Figure 4.27: Evolution of relative ℓ_2-error of recovered signal with respect to iteration. $m_2 = n/4$, $\sigma = 0$.

p	$(m, n) = (256, 4096)$		$(m, n) = (512, 4096)$	
	ℓ_2-error	ℓ_∞-error	ℓ_2-error	ℓ_∞-error
0	(2.2978e-1, 1.5371e-1)	(2.5759e0, 9.5095e-1)	(5.0219e-4, 7.0712e-5)	(5.6873e-3, 1.0695e-3)
1/2	(3.2857e-3, 1.1173e-2)	(4.1458e-2, 1.6342e-1)	(5.5597e-4, 1.2796e-4)	(6.2438e-3, 1.3898e-3)
2/3	(1.1604e-3, 1.6500e-4)	(1.2177e-2, 2.3400e-3)	(6.6470e-4, 1.5286e-4)	(7.2339e-3, 1.4871e-3)
4/5	(1.3583e-3, 3.4781e-4)	(1.3723e-2, 3.8123e-3)	(7.4240e-4, 1.3873e-4)	(7.7716e-3, 1.4080e-3)
1	(1.0070e-1, 1.3429e-1)	(7.2380e-1, 9.5382e-1)	(1.7355e-3, 1.9504e-4)	(1.3659e-2, 1.5971e-3)

Table 4.6: The pairs of the means and standard derivation of the relative ℓ_2-error and the absolute ℓ_∞-error over 50 simulations are given for the recovery for each value of p.
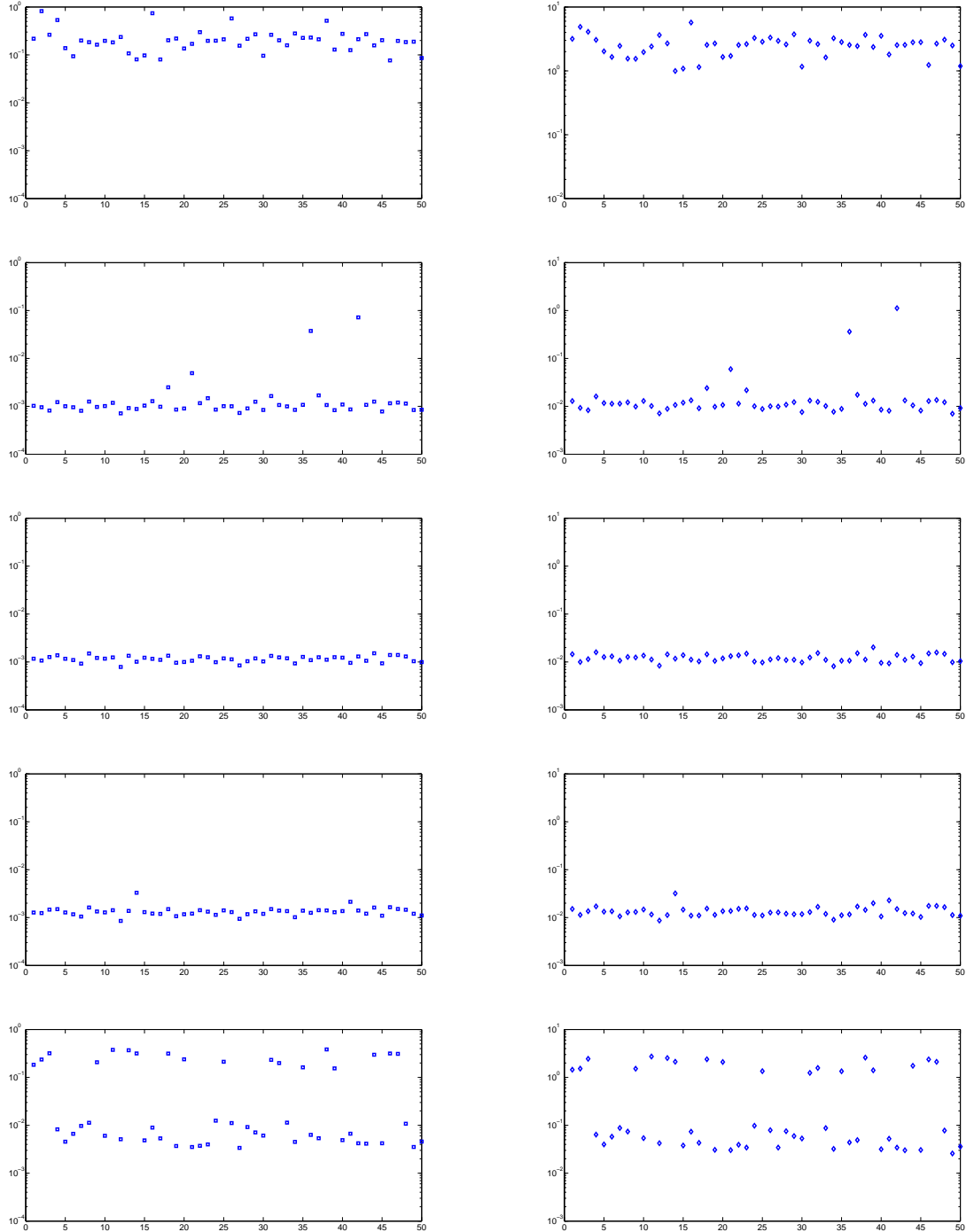
Figure 4.28: Errors of recovered data for each of 50 trials. Row 1-5 represents the performance of Algorithm 4 for $p = 0, 1/2, 2/3, 4/5, 1$ respectively. The first and second column represents the relatively ℓ_2-error, absolute ℓ_∞-error respectively. The setting for m, n is $n = 4096$, $m = 256$.
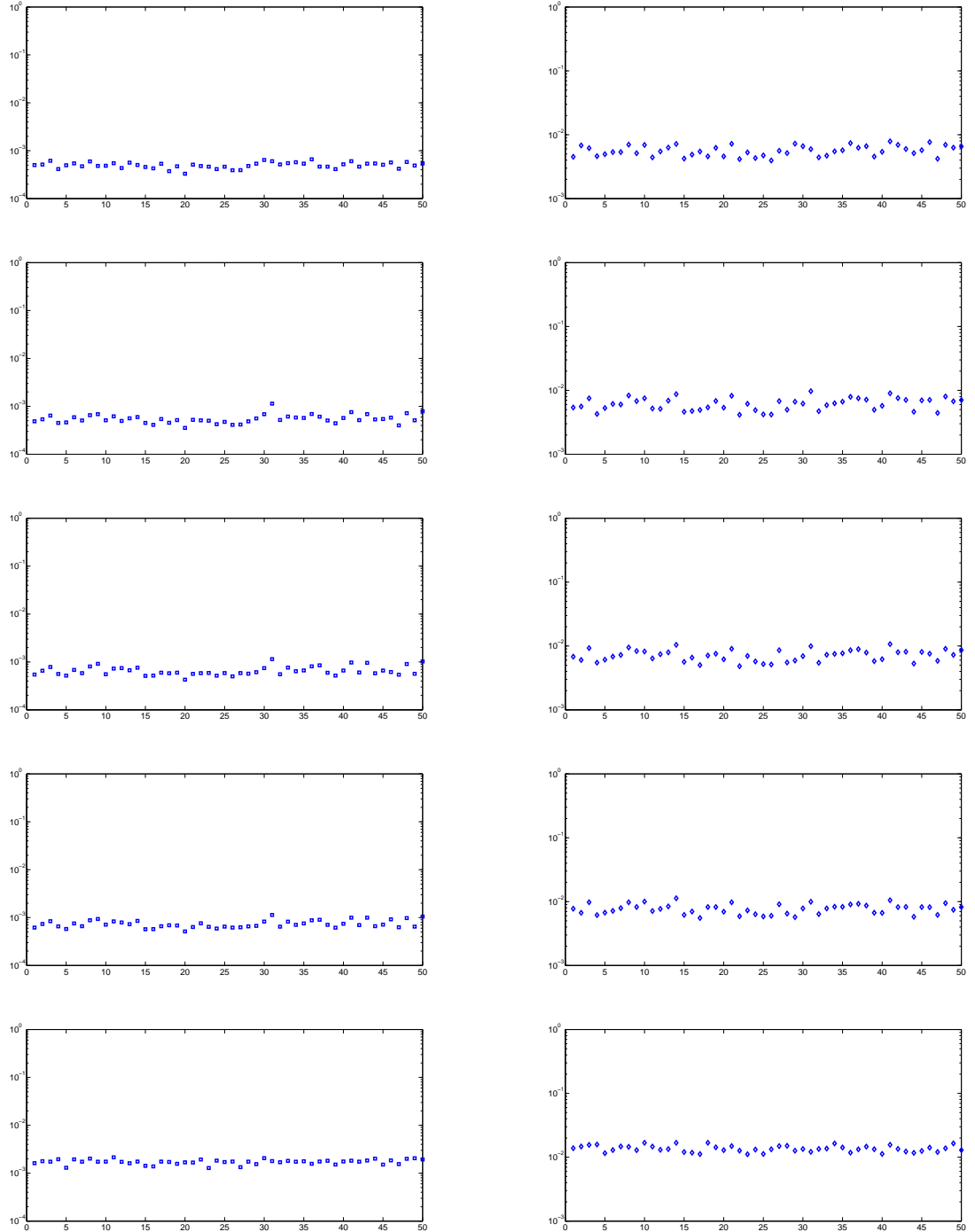
Figure 4.29: Errors of recovered data for each of 50 trials. Row 1-5 represents the performance of Algorithm 4 for $p = 0, 1/2, 2/3, 4/5, 1$ respectively. The first and second column represents the relatively ℓ_2-error, absolute ℓ_∞-error respectively. The setting for m, n is $n = 4094$, $m = 512$.

Chapter 5

Future Research

The following lines of research are proposed as ways of further advancing understanding of composite optimization problems and the ℓ_p-regularization:

1. *The rate of convergence of Algorithm 1.* In this thesis, the convergence analysis of Algorithm 1 has been studied. It is worthy to investigate in what rate the proposed algorithm will converge to a desirable solution. It is also interesting to know if the Nesterov acceleration technique can be adapted to Algorithm 1 with an improved rate of convergence.

2. *Composite convex optimization problems with three or more terms.* In our current study, we developed algorithms for composite convex optimization problems with two terms. This might limit its applications. For example, in compressed sensing MRI, the function to be minimized in [51, 52] is the sum of three terms, namely, a sparsity promoting term, a total variation regularization

term, and a fidelity term that describes the data consistency. Hence, there is a practical need to extend our current research to composite convex optimization problems with three or more terms.

3. *Convergence analysis for the ℓ_p-regularization.* In our current research, the convergence analysis of Algorithm 4 is missing due to the difficulty caused by the nonconvexity of the ℓ_p-norm with $0 \leq p < 1$, even though Algorithm 4 performs well in our numerical experiments. Therefore, convergence analysis of Algorithm 4 will provide theoretical guarantee of its numerical performance. Its impact may go beyond the current research context.

Chapter 6

Published and Completed

Research Work

Research Work Has Been Published

1. Feishe Chen, Lixin Shen, Bruce W. Suter, and Yuesheng Xu. *Nesterov's Algorithm Solving Dual Formulation for Compressed Sensing.* Journal of Computational and Applied Mathematics, vol. 260, pp. 1-17, 2014.

2. Feishe Chen, Lixin Shen, Yuesheng Xu, and Xueying Zeng. *The Moreau Envelope Approach for the L1/TV Image Denoising Model.* Inverse Problems and Imaging, vol. 8, pp. 53-77, 2014.

3. Feishe Chen, Lixin Shen, Bruce W. Suter, and Yuesheng Xu. *A Fast and Accurate Algorithm for ℓ_1 Minimization Problems in Compressive Sampling.* EURASIP Journal on Advances in Signal Processing, vol. 1, pp. 1-12, 2015.

4. Sijia Liu, Feishe Chen, Aditya Vempaty, Makan Fardad, Lixin Shen, and Pramod K. Varshney. *Sparsity Promoting Sensor Management for Estimation: An Energy Balance Point of View.* The 18th International Conference on Information Fusion, pp. 231-238, 2015.

Research Work Has Been Completed

1. Feishe Chen, Lixin Shen, and Bruce W. Suter. *Computing the Proximity Operator of the ℓ_p Norm with $0 < p < 1$.* submitted, 2015.

Bibliography

[1] Mariana S. C. Almeida and Mrio A. T. Figueiredo. Deconvolving images with unknown boundaries using the alternating direction method of multipliers. *IEEE Transactions on Image Processing*, 28:3074–3086, 2013.

[2] Heinz H. Bauschke and Patrick L. Combettes. *Convex Analysis and Monotone Operator Theory in Hilbert Spaces*. AMS Books in Mathematics. Springer, New York, 2011.

[3] Amir Beck and Marc Teboulle. Fast gradient-based algorithms for constrained total variation image denoising and deblurring problems. *IEEE Transaction on Image Processing*, 18:2419–2434, 2009.

[4] Stephen Becker, Jérôme Bobin, and Emmanuel J. Candès. NESTA: a fast and accurate first-order method for sparse recovery. *SIAM Jornal on Imaging Sciences*, 4(1):1–39, 2009.

[5] Dimitri Bertsekas. *Nonlinear Programming*. Athena Scientific, Belmont, Massachussets, 2003.

[6] Jérôme Bolte and Edouard Pauwels. Majorization-minimization procedures and convergence of sqp methods for semi-algebraic and tame programs. *arXiv*, 2014.

[7] Charles Bouman and Ken Saue. A generalized gaussian image model for edge-preserving map estimation. *IEEE Transactions on Image Processing*, 2:296–310, 1993.

[8] Stephen Boyd, Neal Parikh, Eric Chuh, Borja Peleato, and Jonathan Eckstein. Distributed optimization and statistical learning via alternating direction method of multipliers. *Foundations and Trends in Machine Learning*, 3, 2010.

[9] Jian-Feng Cai, Stanley Osher, and Zuowei Shen. Linearized Bregman iteration for frame based image deblurring. *SIAM Journal on Imaging Sciences*, 2:226–252, 2009.

[10] Jian-Feng Cai, Stanley Osher, and Zuowei Shen. Split Bregman methods and frame based image restoration. *Multiscale Modeling and Simulation: A SIAM Interdisciplinary Journal*, 2:337–369, 2009.

[11] Emmanuel J. Candès, Justin Romberg, and Terence Tao. Robust uncertainty principles: Exact signal reconstruction from highly incomplete frequency information. *IEEE Transactions on Information Theory*, 52(2):489–509, 2006.

[12] Emmanuel J. Candès and Terence Tao. Decoding by linear programming. *IEEE Transactions on Information Theory*, 51(12):4203–4215, 2005.

[13] Emmanuel J. Candès and Terence Tao. Near optimal signal recovery from random projections: Universal encoding strategies? *IEEE Transactions on Information Theory*, 52(12):5406–5425, 2006.

[14] Wenfei Cao, Jian Sun, and Zongben Xu. Fast image deconvolution using closed-form thresholding formulas of $L_q(q = \frac{1}{2}, \frac{2}{3})$ regularization. *Inverse Problems and Imaging*, 24:31–41, 2013.

[15] Antonin Chambolle and Thomas Pock. A first-order primal-dual algorithm for convex problems with applications to imaging. *Journal of Mathematical Imaging and Vision*, 40:120–145, 2011.

[16] Tony Chan, Gene H. Golub, and Pep Mulet. A nonlinear primal-dual method for total variation-based image restoration. *SIAM Journal on Scientific Computing*, 20(6):1964–1977, 1999.

[17] Rick Chartrand. Exact reconstruction of sparse signals via nonconvex minimization. *IEEE Signal Processing Letters*, 14:707?710, 2007.

[18] Rick Chartrand and Valentina Staneva. Restricted isometry properties and nonconvex compressive sensing. *Inverse Problem*, 24:1–14, 2008.

[19] Rick Chartrand and Valentina Staneva. Total variation regularization of images corrupted by nongaussian noise using a quasi-newton method. *IET Image Processing*, 2:295–303, 2008.

[20] Feishe Chen, Lixin Shen, Bruce W. Suter, and Yuesheng Xu. A fast and accurate algorithm for ℓ_1 minimization problems in compressive sampling. *EURASIP Journal on Advances in Signal Processing*, 1:1–12, 2015.

[21] Feishe Chen, Lixin Shen, Yuesheng Xu, and Xueying Zeng. The Moreau envelope approach for the L1/TV image denoising model. *Inverse Problems and Imaging*, 8(1):53–77, 2014.

[22] Peijun Chen, Jianguo Huang, and Xiaoqun Zhang. A primal-dual fixed point algorithm for convex separable minimization with applications to image restoration. *Inverse Problems*, 29(2):025011, 2013.

[23] Scott Shaobing Chen, David L. Donoho, and Michael A. Saunders. Atomic decomposition by basis pursuit. *SIAM Journal on Scientific Computing*, 20:33–61, 1998.

[24] Xiaojun Chen, Fengmin Xu, and Yinyu Ye. Lower bound theory of nonzero entries in solutions of $\ell_2 - \ell_p$ minimization. *SIAM Journal on Scientific Computing*, 32(5):2832–2852, 2010.

[25] Christian Clason, Bangti Jin, and Karl Kunisch. A duality-based splitting method for L1-TV image restoration with automatic regularization parameter choice. *SIAM Journal on Scientific Computing*, 32:1484–1505, 2010.

[26] Ronald Coifman and David Donoho. Translation-invariant de-noising. In *Wavelet and Statistics, Springer Lecture Notes in Statistics*, volume 103, pages 125–150, New York, 1994. Springer-Verlag.

[27] Corinna Cortes and Vladimir Vapnik. Support-vector networks. *Machine Learning*, 20(3):273–297, September 1995.

[28] Bruce Cox, Anatoli Juditsky, and Arkadi Nemirovski. Dual subgradient algorithms for large-scale nonsmooth learning problems. *Mathematical Programming*, 148:143–180, 2014.

[29] Dao-Qing Dai, Lixin Shen, Yuesheng Xu, and Na Zhang. Noisy 1-bit compressive sensing: models and algorithms. *Applied and Computational Harmonic Analysis*, in press, 2014.

[30] Ingrid Daubechies. *Ten Lectures on Wavelets*, volume 61 of *CBMS Conference Series in Applied Mathematics*. SIAM, Philadelphia, 1992.

[31] Ingrid Daubechies, Bin Han, Amos Ron, and Zuowei Shen. Framelets: MRA-based constructions of wavelet frames. *Applied and Computation Harmonic Analysis*, 14:1–46, 2003.

[32] Yiqiu Dong, Michael Hintermüller, and Marrick Neri. An efficient primal-dual method for L^1-TV image restoration. *SIAM Journal on Imaging Sciences*, 2:1168–1189, 2009.

[33] David L. Donoho. Compressed sensing. *IEEE Transactions on Information Theory*, 52(4):1289–1306, 2006.

[34] David L. Donoho and Yaakov Tsaig. Fast solution of ℓ_1-norm minimization problems when the solution may be sparse. *IEEE Transactions on Information Theory*, 54(11):4789–4812, 2008.

[35] Jonathan Eckstein and Dimitri P. Bertsekas. On the douglas-rachford splitting method and the proximal algorithm for maximal monotone operators. *Mathematical Programming*, 55:293–318, 1992.

[36] Ernie Esser, Xiaoqun Zhang, and Tony F. Chan. A general framework for a class of first order primal-dual algorithms for convex optimization in imaging science. *SIAM Journal on Imaging Sciences*, 3:1015–1046, 2010.

[37] Simon Foucarta and Ming-Jun Lai. Sparsest solutions of underdetermined linear systems via ℓ^p-minimization for $0 < q \leq 1$. *Applied Computational Harmonic Analysis*, 26:395–407, 2009.

[38] Daniel Gabay and Bertrand Mercier. A dual algorithm for the solution of nonlinear variational problems via finite-element approximations. *Computers and Mathematics with Applications*, 2:17–40, 1976.

[39] Roland Glonwinski and Patric Le Tallec. Augumented lagrangians and operator splitting methods in nonlinear mechanics. *SIAM, Philadephia*, 1989.

[40] Tom Goldstein and Stanley Osher. The split Bregman method for L_1-regularized problems. *SIAM Journal on Imaging Sciences*, 2:323–343, 2009.

[41] Xiaoxia Guo, Fang Li, and Michael K. Ng. A fast ℓ_1-TV algorithm for image restoration. *SIAM Journal on Scientific Computing*, 31:2322–2341, 2009.

[42] Bingsheng He and Xiaoming Yuan. Convergence analysis of primal-dual algorithms for a saddle-point problem: From contraction perspective. *SIAM Journal on Imaging Sciences*, 5(1):119–149, 2012.

[43] Magnus R. Hestenes. Multiplier and gradient methods. *Journal of Optimization Theory and Applications*, 4:303–320, 1969.

[44] Dilip Krishnan and Rob Fergus. Fast image deconvolution using hyper-laplacian priors. In *NIPS*, pages 1033–1041, 2009.

[45] Andrzej Krol, Si Li, Lixin Shen, and Yuesheng Xu. Preconditioned alternating projection algorithms for maximum a posteriori ect reconstruction. *Inverse Problems*, 28(11):115005, 2012.

[46] Ming-Jun Lai and Jingyue Wang. An unconstrained ℓ_q minimization with $0 < q \leq 1$ for sparse solution of under-determined linear systems. *SIAM Journal on Optimization*, 21(1):82–101, 2011.

[47] Qia Li, Charles A. Micchelli, Lixin Shen, and Yuesheng Xu. A proximity algorithm accelerated by gausscseidel iterations for L1/TV denoising models. *Inverse Problems*, 28(9):095003, 2012.

[48] Qia Li, Lixin Shen, Yuesheng Xu, and Na Zhang. Multi-step fixed-point proximity algorithms for solving a class of optimization problems arising from image processing. *Advances in Computational Mathematics*, 41:387–422, 2015.

[49] Yan-Ran Li, Lixin Shen, and Bruce W. Suter. Adaptive inpainting algorithm based on DCT induced wavelet regularization. *IEEE Transactions on Image Processing*, 22(2):752–763.

[50] Pierre-Louis Lions and Bertrand Mercier. Splitting algorithms for the sum of two nonlinear operators. *SIAM Journal on Numerical Analysis*, 16:964–979, 1979.

[51] Michael Lustig, David L. Donoho, and John M. Pauly. Sparse MRI: The application of compressed sensing for rapid MR imaging. *Magnetic Resonance in Medicine*, 58:1182–1195, 2007.

[52] Michael Lustig, David L. Donoho, Juan M. Santos, and John M. Pauly. Compressed sensing MRI. *IEEE Signal Processing Magazine*, 25:72–82, 2008.

[53] Stephane G. Mallat. A theory for multiresolution signal decomposition: the wavelet representation. *IEEE Transaction on Pattern Analysis and Machine Intelligence*, 11:674–693, 1989.

[54] Charles A. Micchelli, Lixin Shen, and Yuesheng Xu. Proximity algorithms for image models: Denoising. *Inverse Problems*, 27:045009(30pp), 2011.

[55] Charles A. Micchelli, Lixin Shen, Yuesheng Xu, and Xueying Zeng. Proximity algorithms for image models II: L1/TV denosing. *Advances in Computational Mathematics*, 38:401–426, 2013.

[56] Jean-Jacques Moreau. Fonctions convexes duales et points proximaux dans un espace hilbertien. *C.R. Acad. Sci. Paris Sér. A Math.*, 255:1897–2899, 1962.

[57] Pierre Moulin and Juan Liu. Analysis of multiresolution image denoising schemes using generalized-Gaussian and complexity prior. *IEEE transactions on Information Theory*, 45(4):909–919, April 1999.

[58] Mila Nikolova. A variational approach to remove outliers and impulse noise. *Journal of Mathematical Imaging and Vision*, 20:99–120, 2004.

[59] Stanley Osher, Martin Burger, Donald Goldfarb, Jinjun Xu, and Wotao Yin. An iterative regularization method for total variation-based image restoration. *Multiscale Modeling and Simulation: A SIAM Interdisciplinary Journal*, 4:460–489, 2005.

[60] M. J. D. Powell. A method for nonlinear constraints in minimization problems. *in Optimization, R. Fletcher, ed., Academic Press, New York*, pages 283–298, 1969.

[61] Ashley Prater and Lixin Shen. Separation of undersampled composite signals using the dantzig selector with overcomplete dictionaries. *IET Signal Processing*, 9:226–234, 2015.

[62] Ashley Prater, Lixin Shen, and Bruce W. Suter. Finding dantzig selectors with a proximity operator based fixed-point algorithm. *Computational Statistics and Data Analysis*, 90:36–46, 2015.

[63] R. Tyrrell Rockafellar. The multiplier method of Hestenes and Powell applied to convex programming. *Journal of Optimization Theory and Applications*, 12:555–562, 1973.

[64] R. Tyrrell Rockafellar and Roger J-B. Wets. *Variational Analysis*. Springer, 1998.

[65] Amos Ron and Zuowei Shen. Affine system in $L_2(R^d)$: the analysis of the analysis operator. *Journal of Functional Analysis*, 148:408–447, 1997.

[66] Leonid I. Rudin, Stanley Osher, and Emad Fatemi. Nonlinear total variation based noise removal algorithms. *Physica D*, 60:259–268, 1992.

[67] Lixin Shen, Yuesheng Xu, and Xueying Zeng. Wavelet inpainting with the ℓ_0 sparse regularization. *Applied and Computational Harmonic Analysis*, in press, 2015.

[68] Lixin Shen, Yuesheng Xu, and Na Zhang. An approximate sparsity model for inpainting. *Applied and Computational Harmonic Analysis*, 37:171–184, 2014.

[69] Eero P. Simoncelli and Edward H. Adelson. Noise removal via Bayesian wavelet coring. In *Third Int'l Conf on Image Proc*, volume I, pages 379–382, Lausanne, September 1996. IEEE Sig Proc Society.

[70] Min Tao and Junfeng Yang. Alternating direction algorithms for total variation deconvolution in image reconstruction. *available at Optimization Online*.

[71] Vladimir N. Vapnik. *The Nature of Statistical Learning Theory*. Springer, New York, 1995.

[72] Yilun Wang, Junfeng Yang, Wotao Yin, and Yin Zhang. A new alternating minimization algorithm for total variation image reconstruction. *SIAM Journal on Imaging Sciences*, 1:248–272, 2008.

[73] Pierre Weiss, Laure Blanc-Féraud, and Gilles Aubert. Efficient schemes for total variation minimization under constraints in image processing. *SIAM Journal on Scientific Computing*, 31(3):2047–2080, 2009.

[74] Chunlin Wu, Juyong Zhang, and Xue-Cheng Tai. Augmented lagrangian method for total variation restoration with non-quadratic fidelity. *Inverse Problems and Imaging*, 5:237–261, 2011.

[75] Zongben Xu, Xiangyu Chang, Fengmin Xu, and Hai Zhang. $L_{1/2}$ regularization: A thresholding representation theory and a fast solver. *IEEE Transactions On Neural Networks and Learning Systems*, 135:1013–1027, 2012.

[76] Junfeng Yang, Yin Zhang, and Wotao Yin. An efficient TVL1 algorithm for deblurring multichannel images corrupted by impulsive noise. *SIAM Journal on Scientific Computing*, 31:2842–2865, 2009.

[77] Xiaoqun Zhang, Martin Burger, and Stanley Osher. A unified primal-dual algorithm framework based on Bregman iteration. *Journal of Scientific Computing*, 46:20–46, 2011.

BIOGRAPHICAL DATA

NAME OF AUTHOR: Feishe Chen

PLACE OF BIRTH: Zhanjiang, China.

DATE OF BIRTH: March, 1984.

GRADUATE AND UNDERGRADUATE SCHOOLS ATTENDED:

Syracuse University, NY, USA

Sun Yat-sen University, Guangzhou, China

DEGREES AWARDED:

M.S., Sun Yat-sen University, 2009

B.S., Sun Yat-sen University, 2007